STATE OF THE ART REPORT FOR THE ANALYSIS METHODS FOR UNREINFORCED MASONRY HERITAGE STRUCTURES AND MONUMENTS

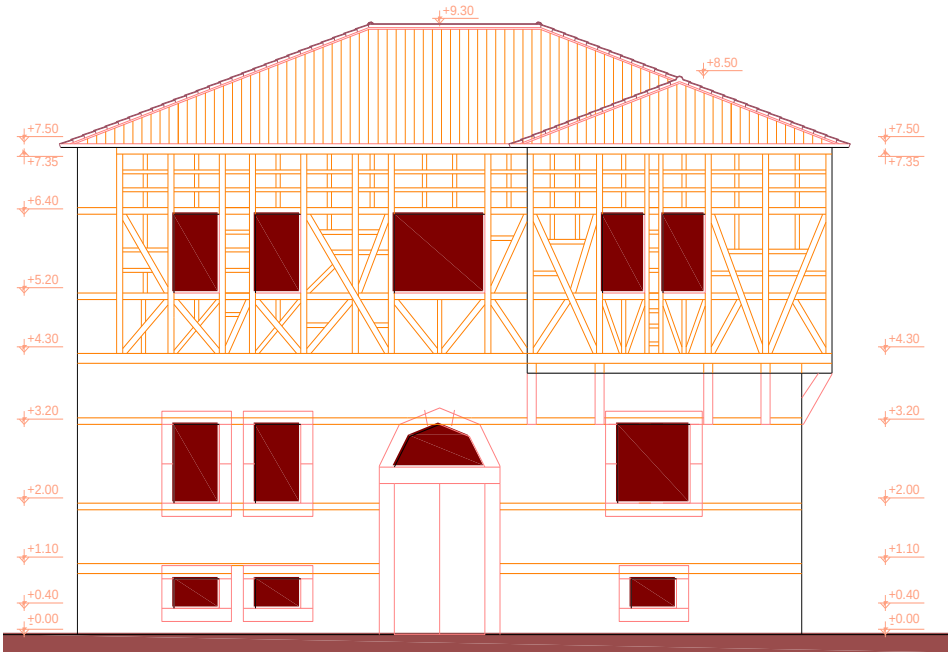

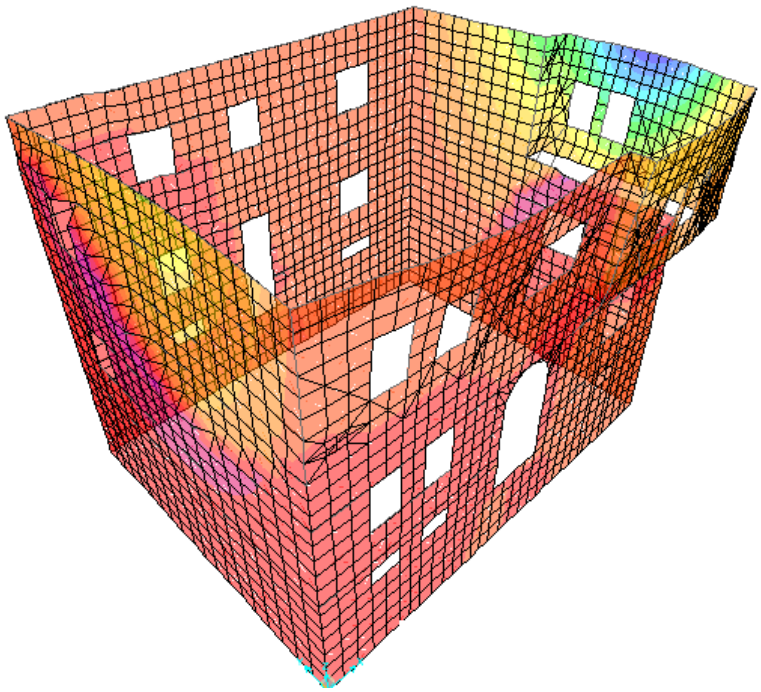

by

S. J. Pantazopoulou, PhD

Professor of Structural Engineering

October 2013

ABSTRACT

The proliferation of new materials and structural systems in urban construction highlight by contrast the heritage buildings of the past, conveying the signature of evolution of human achievement in architecture and engineering. These older structures comprise mostly unreinforced load-bearing masonry construction (URM), dating anywhere from antiquity to the 19th and early 20th Century. Ageing and being exposed to the elements, heritage buildings may be in various states of disrepair or degradation of the constituent materials. Disintegration of the essential components that secured in the original system continuity, resilience and robustness places the future of this cultural treasure at risk: response to a potential earthquake at some unknown moment in the years to come is unpredictable and the ensuing consequences in terms of cultural loss that a structural failure would entail are articulated without words in the picture of the failed L'Aquila dome (Fig. 1).

Figure 1: *Failure of monument after the 2009 L'Aquila Earthquake (S. Maria di Paganica: http:// www.diocesilaquila.it/laquila/allegati/24504/Maria%2520Paganica.jpg)*

Of course not all heritage structures are of equal significance. There is a great range of structures listed as monuments of cultural heritage not only in terms of their comparative value as historical samples of human achievement but also in terms of their structural complexity and size, the risk to human life effected by a potential collapse and their role in defining the ambiance and character of the urban space where they may belong. Thus, in complete analogy of the urgency of the condition, the risk and the overall significance of the structure, its seismic assessment may involve a range of analysis procedures that may vary in terms of complexity of implementation and modelling, computational demand and degree of simplification of the actual circumstance. In all cases the objective includes estimation of demands within an acceptable level of confidence and quantification of the resistances and mechanisms of behaviour of the structure in question, so as to establish the anticipated performance in the event of a seismic hazard scenario but also in order to guide rehabilitation and strengthening strategies.

Analysis procedures used to study this complicated problem are reviewed in this state of the art report with the objective to illustrate the available tools at the disposal of the assessor, also highlighting the limitations and difficulties of the underlying modelling approaches. It is always tempting to extend from the well documented field of seismic

assessment of reinforced concrete where volumes on performance based methods based on nonlinear models and analyses have been authored. But a note of caution is in order: extending current nonlinear analysis practices for seismic assessment of heritage buildings is neither straightforward, nor wise in most cases: in contrast with conventional frame structures, they are characterised by distributed stiffness and mass and poor diaphragm action. Interventions are often restricted by international treaties for non-invasiveness and reversibility of the intervention - given the practical requirements for the buildings' intended reuse. Poor understanding of the mechanics of masonry and the inherent brittleness of the material further compound the uncertainties in analytical methods used today for seismic assessment and rehabilitation.

TABLE OF CONTENTS

CHAPTER 1 - INTRODUCTION

1.1 Scope: The term Heritage structures refers to any type of construction that stands witness of past civilizations in that it coveys tractable information about technology, aesthetics, way of life, customs, religious practices, art, defense and governance in former times, and as such they are deemed inseparable components of historical evolution of the people. A great range of structures qualify as cultural heritage. They range from monumental edifices and fortresses to small dwellings, from stocky heavy structures to slender spires and towers, from utilitarian structures to triumphant ornamental constructions – being historical, the great majority have been there before our time and for this reason today they are considered an inextricable component of the greater environment where they belong, thereby defining its ambiance and identifying its global image (Fig. 1.1, Fig. 1.2).

Figure 1.1: Heritage URM buildings of the 20th Century located in the center of Thessaloniki, Greece.

Figure 1.2: Vernacular Architecture defines the Ambiance and Character of a City

Figure 1.3: (a) Timber-Laced Masonry House from Herculaneum dating from 78 A.D.), (b), (c) Timber Laced Walls Used Till Recently in URM Construction,

Historic and cultural buildings of the 19th and 20th Century are a significant part of the built environment in many cities across Europe. Having a lifetime of more than a hundred years, load-bearing masonry buildings of this class are a living part of the European history and as such, they are protected by international treaties and organizations. Over the several decades of their service life, most of those buildings have suffered from structural damages of different severity level, especially in countries of the Mediterranean basin with high seismicity. Yet, even today they remain in good condition, being operational in many cases (Fig. 1.1). Due to those buildings' historical importance and their significance as examples of an architectural school of thought, an increasing interest for their rehabilitation has recently emerged, often regulated by international treaties for noninvasiveness and reversibility of the intervention combined with the practical requirements for the buildings' modern day intended reuse.

Preserving heritage structures for the future generations is a priority deeply embedded in the conscience of developed societies. For this purpose treaties have been signed, guidelines and rules have been issued, aiming to secure that in the process of restoration and preservation, no irreversible alterations are made to those quintessential elements of cultural heritage that warrant the conservation in the first place. Such elements may be, the architectural form, the aesthetic aspects of decorations, the methods of construction, the original materials, the types of structural systems and remarkable techniques devised by our ancestors in order to tame the forces of nature, to mold the materials, to serve the needs of the users, and to inspire safety, convenience, awe, a notion of harmony, devotion, fear, familiarity or admiration through contact with the structural object.

Restoration under the constraints imposed by the objectives of preservation and reversibility of intervention outlined above can be a challenging engineering feat. For one, the structural systems concerned are often difficult to understand, their intricate workings being complicated by the contact of dissimilar materials and the complexity of multiple interfaces and undefined force paths through the continuous massive walls. These difficulties are compounded by disintegration of the materials due to ageing and corrosion, and by the inherent brittleness of the mortars and building blocks, by the great variety of material used (stone with a great range of strength and surface rendering, clay tiles, adobe, timber, lime-based or mud mortar, Fig. 1.3). Implications of this complexity affects both the

modeling assumptions regarding discretization of the continuous system into individual structural members, but also the constitutive models that may be employed to represent the mechanical behavior of the materials (Fig. 1.4, 1.5).

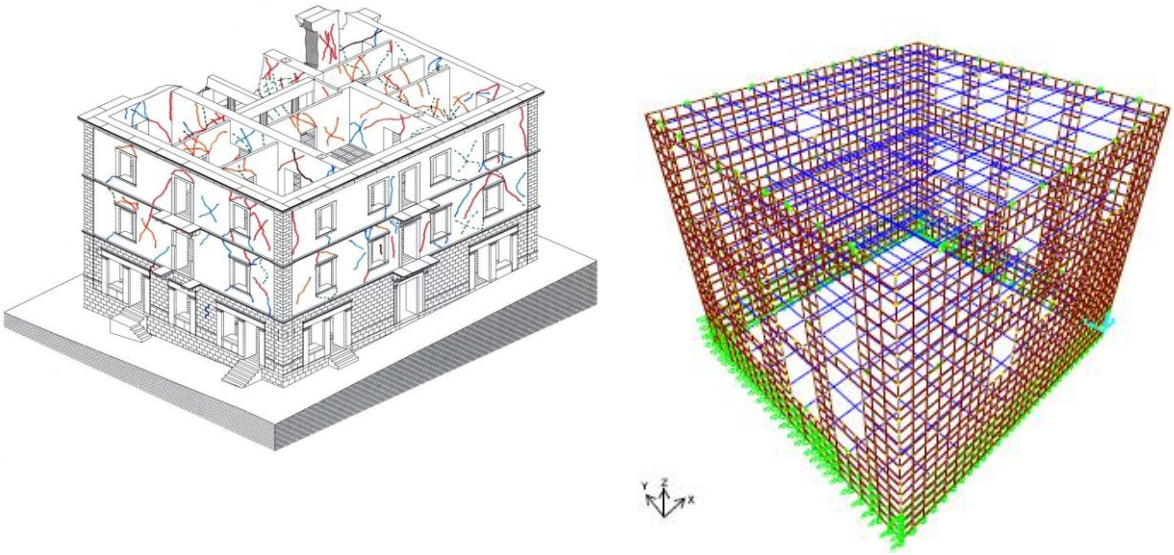

Figure 1.4: (a) Spatial Complexity, Vague Structural System and Continuity of Mass and Stiffness is a distinguishing characteristic of URM Buildings. (b) 3-D Idealization

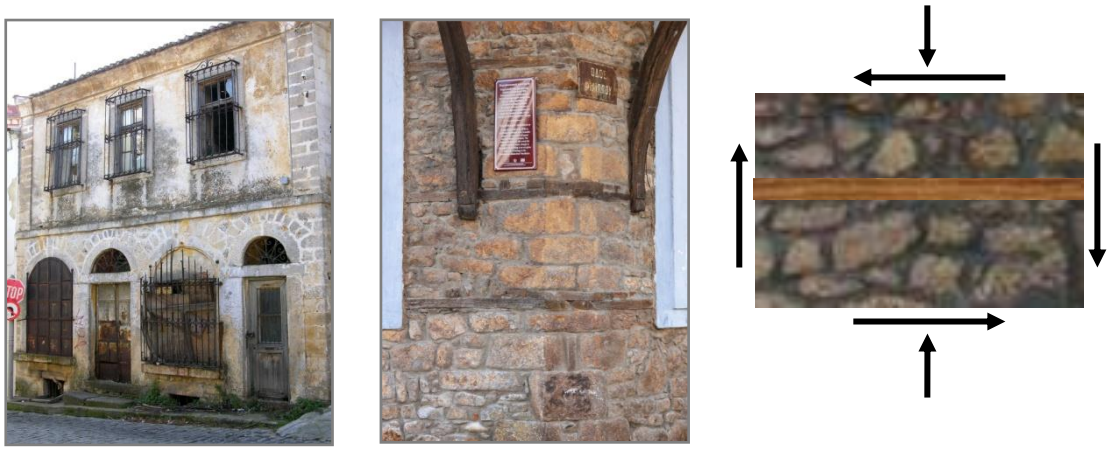

Figure 1.5: (a) Disintegration of the Material and Ageing and (b) Contact between the Building Blocks and Dissimilar Materials under plane stress (also Fig. 1.3(b))

Thus, in terms of analysis methods, heritage structures may exhaust the limits of the current state of the art in terms of computational simulation, particularly if this analysis consistently accounts for material nonlinearity and brittleness and for the system complexity. Analysis is prerequisite to structural assessment of the existing structure. Through assessment the demands in terms of stress or strain are determined in the critical elements of the structure; the analysis conducted ought to be able to faithfully identify locations of potential weakness, mechanisms of failure, and the associated resistance of the structure. If properly assembled, the analytical model may also be used to guide retrofit and rehabilitation strategies. Furthermore, the choice of the analytical modeling procedure need be commensurate to a number of other important considerations: the degree of knowledge available regarding the structural system and its materials, the uncertainty of the

future risks imposed by the continued use or by natural disasters to which the structure may be subjected to in its residual life, but also the importance of the monument itself that defines the available budget, the acceptable complexity of application of the recommended methods and the urgency for a definite result.

Clearly, of the many possible threats to survival of a well-cared for unreinforced masonry structure the most critical to the occupants but also to the integrity of the structure itself, is earthquake. Prolonging through restoration the service life of an old structure necessarily increases the possibility of occurrence of the design earthquake and beyond. Thus, seismic assessment is a priority objective.

1.2 Problem Statement

The problem statement is depicted in Fig. 1.6. The objective is to dependably estimate the level of structural performance of the URM structure to a prescribed seismic hazard, such as given by the design spectrum in the site of interest, or a representative recorded time history of ground acceleration. A natural first choice would be to extend the concepts of pushover static analysis which has been thoroughly developed in the last 20 years for seismic assessment of reinforced concrete and steel structures. In this framework the performance point (i.e. the force and displacement demand imposed by the earthquake in consideration) is sought on the resistance curve of the building. The resistance curve is obtained from the so-called pushover analysis of the building where a pattern of lateral forces or displacements that represent the earthquake effects is applied on the building with gradually increasing intensity. The vertical axis represents the base shear of the building whereas the horizontal axis is the displacement of the so-called control or "target" node. Here it should be noted that some debate exists regarding the applicability of this approach and the uniqueness of the obtained results, for the following reasons:

(a) In 3-dimensional idealizations of the structure it is necessary that horizontal forces are not only distributed height-wise but in the transverse direction of the building as well (i.e. a function of z and y). This is a significant departure from the analysis of structures with rigid diaphragms, where forces would be applied at the center of mass in the rigid diaphragms and would only depend on the position in height (z coordinate). The reason is, that in structures with flexible diaphragms and distributed masses the pattern of inertia forces that are attracted by the building (represented in the pushover analysis by the pattern of lateral forces) depends on the point-wise distribution of mass spatially, and on the magnitude of acceleration.

(b) A point of contention in pushover analysis of structures with flexible diaphragms is the selection of the so-called target or control node. Actually this is somewhat of a superficial point – all that is required by the method is:

-(b.1) Consistency in the choice of the point of reference, i.e. the same point of reference should be used throughout the derivation of the resistance curve.

-(b.2) The fundamental mode of vibration used in order to obtain the properties of the Equivalent Single Degree of Freedom (SDOF) and through which the performance point is interpreted, should be normalized with respect to the displacement coordinate of the chosen control node.

To overcome the difficulties presented in (a) above the use of Incremental Dynamic Analysis is a valid and dependable alternative to static pushover procedures, since the inertia forces are generated automatically in the discretized model of the structure through the consistent (nodal) mass matrices of the finite solid elements and the associated accelerations occurring at the degrees of the freedom of the finite element mesh. But the consistency gained through the step-by-step nonlinear analysis is counterbalanced by the simplicity of the static pushover alternative.

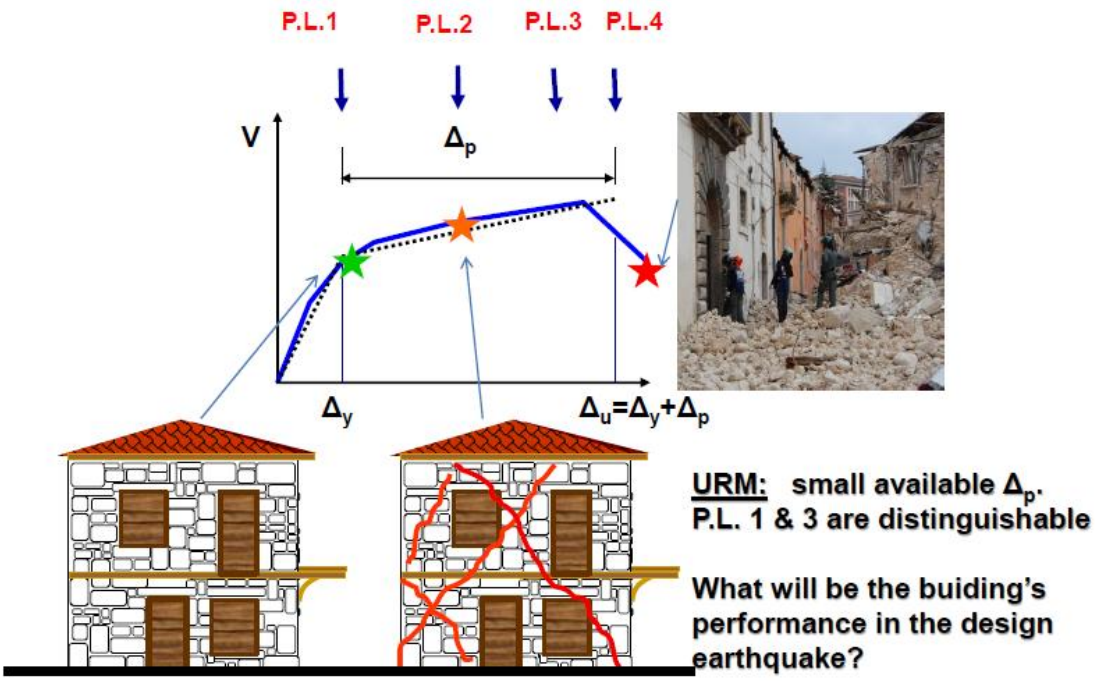

Figure 1.6: Definition of performance levels in the pushover curve of the URM masonry building.

Due to their inherent brittleness the plastic displacement capacity, marked by Δ_p in the pushover curve depicted in Fig. 1.6 is generally limited in URM structures. In this case the performance levels (P.L.) are closely spaced and therefore not easily distinguishable. In practical assessment it may suffice to evaluate the structure at P.L.s 1 and 3, i.e., at visible cracking and collapse prevention states; (note that for URM structures, visible cracking is taken as phenomenological yielding of the structure). Damage corresponding to attainment of the performance point is quantified by measures of strains since they pertain to material capacities. In the context of the present study damage is measured by the relative drift ratios occurring between any successive pair of reference points in the structure.

Relative drift is the angle forming between the final and the original chord of any deformed member and is calculated from the ratio of relative displacement divided by the

distance. For continuous systems such as the URM structure with flexible diaphragms, drift ratio is a meaningful index both height-wise and in the building plan (see Fig. 1.7). It may be the result of shear strain (in wall elements under plane stress) or curvature (most prevalent in wall elements under out of plane flexural action). Considering that shear cracking of URM structures is usually associated with a shear strain in the range of 0.1%-0.15%, it may be concluded that even very simple, practical assessment procedures may readily yield meaningful results:

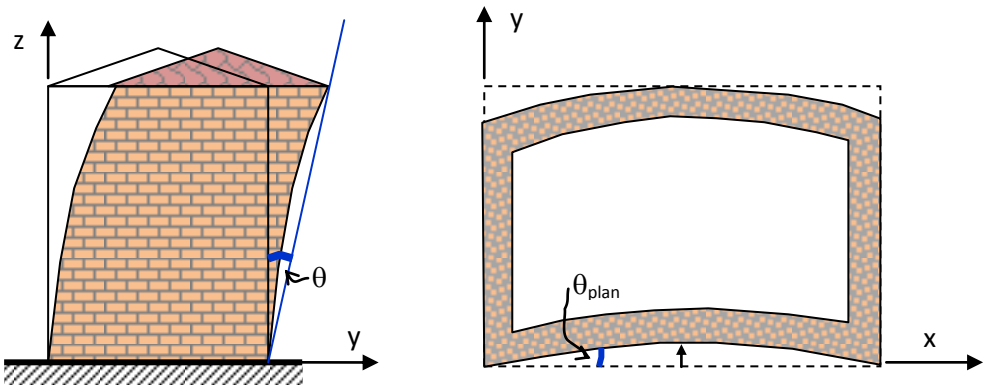

Figure 1.7: Definition of Relative Drift Ratios in height and in plan, for assessing the intensity of demand and supply as well as the associated damage level: θ, and θ_{plan}

Consider for example a simple two-storey URM structure such as the one shown schematically in Fig. 1.8, with a period of 0.3 sec, subjected to the design earthquake acting in the y-direction: For the sake of demonstration of concepts, let's assume that the seismic hazard is described by the Type-I EC-8-I (2004) spectrum with a peak ground acceleration a_g=0.16g (low seismicity) and soil class A (S=1). For a damping ratio of 5% the acceleration at the top of the structure is estimated as S_e =2.5 x 0.16g = 0.4g, whereas the relative displacement at the top relative to the base is $0.4gx0.3^2/4\pi^2$= 0.009 m. For a URM building height of 5.6 m, the relative drift ratio is, θ = 0.009/5.6m = 0.16% which corresponds to attainment of P.L. 1 (visible cracking or apparent yielding of masonry).

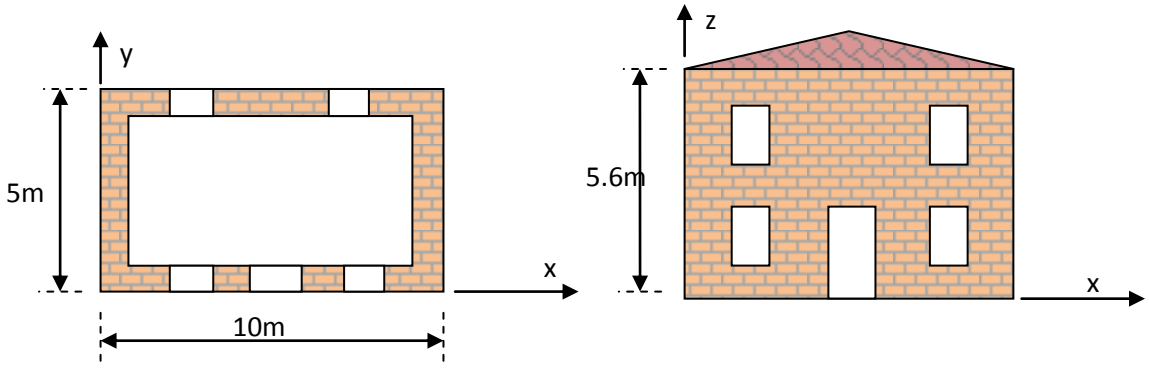

Figure 1.8: Sample Structure – Analysis for Rapid Assessment

The base shear force is equal to, $V_{base} = \lambda \cdot (W/g) \cdot S_e$, where W the weight of the structure and λ the correction factor prescribed by Eq. (4.5) of EC8-I, which is taken equal to 1; for a specific weight of masonry γ_w=20kN/m^3, and a roof weight in the order of 1.5 kN/m^2,

the estimated W is, W=2·(5m+10m)·0.5m·5.6m·20kN/m^3+1.5kN/m^2·5m·10m=1755kN, thus V_{base}=700kN. The overturning seismic moment is (2/3)x700*kN*-mx5.6m=2600kN-m, thus the eccentricity of the overbearing load at the base of the structure is 2600kN-m/1755kN=1.5m which exceeds the limiting dimension of the kern (=5m/6 = 0.8m); this means that about 1/3 of the length of the shear walls is in direct tension due to the overturn and therefore cannot contribute to shear resistance.

With this finding the average shear stress demand is estimated for the walls oriented parallel to the earthquake: 700kN/2/(2x5m/3)/0.5m = 210kN/m^2 = 0.21 MPa. Assuming that the shear strength of masonry is in the same order as its tensile strength (i.e. 0.15MPa), the above result implies a behavior factor q_{demand} of 1.4, which may be excessive for common URM, but may be within the realm of timber-laced masonry walls. The associated displacement ductility demand is estimated according with EC-8-I recommendations for low period systems as $\mu_{\Delta,demand}=1+(q_{demand}-1)(T_c/T)$, where T_c is the end of the plateau in the acceleration spectrum (for soil of type A, T_c=0.4), i.e., $\mu_{\Delta,demand}$ = 1+(1.4-1) ·(0.4/0.3) = 1.5, thus the revised values of displacement and corresponding relative drift ratio, experienced by the structure are actually a bit higher than the original estimate, at 0.01m and 0.17%, respectively (after multiplication with the ratio $\mu_{\Delta,demand}/q_{demand}$ = 1.5/1.4).

This is an example of the types of simple tools available that could be used for rapid assessment of demand versus supply in common URM structures. To further localize the damage and therefore assess its ramifications, it is further required that the shape assumed by the structure during peak ground motion response be known. Through this it would be possible to identify critical regions in the structure and the magnitudes of deformation in terms of normal or shear strain in the materials. This requires more detailed analysis, which, if the significant sources of nonlinearity in the structure are considered, can become very involved, due to the complex behavior of masonry materials.

In the following Chapters the available methods of analysis of unreinforced masonry structures for seismic assessment are reviewed, with particular emphasis on application to the commonest types of heritage unreinforced masonry structures, namely the simple family dwellings. Methods of differing degree of complexity are considered; practical issues, uncertainties and difficulties associated with their application are an essential focus of the presentation.

CHAPTER 2 - REVIEW OF BACKGROUND LITERATURE

2.1 Scope: Of all the identifying characteristics of URM structures the one that is decisive in determining the suitability of analysis methods is the spatial continuity of the structures. Thus, in most situations it is not feasible to use prismatic (linear) elements (beam-column elements) in the discretized model of the structure except in special cases of elements which may be considered prismatic (having small sectional dimensions as compared to their deformable length); in masonry structures, these include timber beams and joists, slender masonry piers, columns. The departure from the conventional frame analysis which has been the workhorse of Structural Engineering is also dictated by the absence of robust diaphragm action in several URM structures and monuments.

Eurocode 8-III (2005) provides guidance for assessment of existing structures, which rides on analytical estimations of seismic demand that are calculated from a number of analytical alternative representations of the structure. Those representations are ranging from equivalent single degree of freedom systems to detailed three-dimensional modeling of the geometrical details with consideration of the regions of nonlinearity; the seismic hazard may also be represented simply, through an acceleration spectrum or through an acceleration time history which requires step by step integration in time. The spectral representation of the seismic hazard lends itself to modal superposition, provided that the structural model is linearly elastic, or to "performance-point evaluation" if a "static" pushover curve may be independently established for the structural system. These two general options regarding choices of representation of the structural system and loading patterns, corresponding to differing degrees of complexity, when combined in all possible ways, yield an array of several different alternative methods that could be used for demand estimation, all more or less acceptable in practice. This variety rides on the assumptions that (a) where needed, available computer software supports nonlinear modeling of the individual member components and (b) no premature, brittle modes of failure that would macroscopically cause a post-peak softening branch identifiable trough a negative or zero pivot in the tangent stiffness matrix of a structure would occur over the range of calculated seismic response.

2.2 Background : Issues of Complexity in Analysis of URM Structures

The above assessment code builds on established computer modeling technologies for lumped systems, mostly frames, for which most commercial codes enable modeling of lumped or spread nonlinearity and detailed time history calculations. And because it calls on concepts that are general in principle, it is considered applicable and easily extendable to all types of structures, including URM buildings. However, when attempting to practically apply the above ideas to the simplest of these structures, a number of stumbling blocks may be encountered. For one, the state of the art in structural software today does not address the requirement (b) above: URM is brittle and thus, maintaining a positive definite stiffness of pier members after cracking is not possible particularly in tension-controlled modes of failure. Furthermore, most of the available commercial software packages today do not offer the option for 3-D analysis using nonlinear shell elements that are needed to model masonry wall behavior. So, accounting for nonlinearity in this class of structures is restricted to either one-dimensional elements (beams, trusses, springs and gap elements) that can be used to model secondary elements (such as timber beams in diaphragms and roof trusses) or points of contact (such as unilateral contact at the point of embedment of a timber beam in a masonry wall using gap

elements, contact between foundation masonry with the surrounding soil using springs with asymmetric properties, etc.). However, most commercial software packages today do not offer complete options for dynamic response estimations, except for combinations of modal response maxima (which, being based on the principle of superposition, precludes the option for even considering secondary sources of nonlinearity). An added difficulty emanates from the distributed character of URM structures. As the number of modes generated is proportional to the total number of degrees of freedom in the structure, there is no clearly prevalent "first" or "fundamental" mode. The mode with the highest period is oftentimes associated with vibration of a single secondary component (such as a diaphragm timber beam), with insignificant ratio of mobilized mass. Previous studies by the authors and co-workers [2, 3] have illustrated that in some cases with flexible diaphragms, several hundreds of modes need to be included in the calculation just so as to mobilize as much as 70% of the total mass in lateral translation. This numerical circumstance in practice nullifies the so called equivalent single degree of freedom representation of the structure, which, combined with the pushover analysis methods, forms the backbone of modern code methods for seismic assessment and design (see EC8-I, Appendix B [4]).

Special – research-oriented software may be used instead, to conduct detailed time history analysis of URM structures (e.g. ABAQUS, DIANA, 3DEC, etc.); as a rule of thumb, the effort required is disproportionately higher than the degree of confidence in the actual values of the input parameters concerning both the materials and the description of the seismic hazard thereby pushing the frontiers of applicability of this technology in URM structures to the limit. In the following sections a quick review of the various alternative options is presented.

2.3 Methods of Analysis for URM Structures

In the context of URM structures, the term "Analysis" is used to refer to two complementary attributes of the procedures used in assessment of the building response:

- (A): Methods of discretization and assembly of the structural model used in order to represent the actual building in the framework of a calculation algorithm.
- (B): Methods used to satisfy the governing equations and subsequently solving for the internal stress state generated in the structure in response to applied external disturbance (here, earthquake effects).

There are several alternative options classified under the two groups: in (A) different methods of idealization are concerned with accurately representing in a computational environment the physical world – namely the spatial, the geometric and material complexity of the structure. A critical decision is the selection of the typical elementary building component (a virtual "building bock") that is used to assemble the computer model of the structure. A virtual building block, termed "element" in the context of the analysis is defined by its volume, its material, and the defining nodes which are the reference points equipped with degrees of freedom. Nodes at the element boundary are the points of connection with adjacent elements – therefore they define the topology of the structural model. The function of the element is associated with its essential degrees of freedom (d.o.f), that is, those independent nodal movements that engage the element in deformation (to be distinguished from the rigid body motions). Proper selection of the element type to be used in URM idealization, ought to be based on the number of essential d.o.f. it is equipped with: for example, the difference between a

truss element and a beam element in one dimensional elements is that the former only stores strain energy in axial deformation, whereas the latter also stores strain energy in flexural deformation (rotations from the chord) as well. In 2-D this same difference distinguishes plane-stress from shell elements; the latter account for flexural deformation in addition to membrane forces, and therefore, between the two element types, they are the only elements appropriate for modeling URM behavior (e.g. in the out-of-plane bending of URM walls).

Establishing the governing equations and obtaining a solution for the response under the applied excitation is pursued using different alternative solution strategies; thus, (B) in the preceding classification of analysis methods encompasses a variety of solution algorithms used in order to calculate the dynamic response from the field equations of motion, namely:

$$\underline{M} \cdot \ddot{\underline{U}} + \underline{C} \cdot \dot{\underline{U}} + \underline{K} \cdot \underline{U} = -\underline{M} \cdot \underline{r} \cdot \ddot{u}_g \qquad (2.1)$$

This is a coupled system of equations where the vector $\underline{U}$ represents the nodal relative displacements along the degrees of freedom of the structure, $\ddot{\underline{U}}$ and $\dot{\underline{U}}$ are the time derivatives (acceleration and velocity vectors), $\underline{r}$ is the influence vector (i.e. the vector containing the displacements occurring in the degrees of freedom of the structure when a unit displacement occurs at the point of input of the ground motion (usually at the base), $\underline{M}$, $\underline{C}$ and $\underline{K}$ the mass, damping and stiffness matrices of the structure and $\ddot{u}_g$ the ground acceleration (a function of time).

Clearly, the freedom that the user may exercise in their selection of a method to solve Eq. (2.1) is not independent of their choices made in the process of idealization of the structure: for example, if the assembled stiffness matrix $\underline{K}$ depends on the magnitude of deformation ($\underline{U}$) due to material nonlinearity, then Eq. (2.1) need be reformulated at each time step for which the algorithm detects any changes in the element stiffness during state determination (i.e. evaluation of internal forces from element displacements). This, coupled with the fast increase in the number of operations (n.o.) required to obtain just one solution point (the n.o. grows with the cube of the total number of degrees of freedom), effected by the three dimensional nature of the structure, may prove very costly for the users attempting to opt for a full three dimensional, nonlinear time history analysis of the entire building. Thus, in the forthcoming sections, the choice of idealization procedure (section 2.4) coupled with a solution algorithm (section 2.5) defines a user-selected solution strategy that may be seen as a compromise between what one can and what one wishes to achieve within the framework of currently available analysis methods for the civil engineering practitioner.

2.4 Analysis in the context of structural modeling:

This part of analysis refers to the discretization of the structure into elements, and the proper selection of the element types, connectivity and material properties. Implementation is critical in that it determines the kind of mechanical function that may be supported by the components of the analytical model through the degrees of freedom by which the individual elements are equipped – e.g. frame elements, 3-D solids, shell elements, plane stress elements. Alternative approaches that qualify under this classification of methods are:

-A.1. Equivalent Frame Models, Strut and tie Models (e.g. Lagomarsino et al. 2013)

-A.2. Finite Element analysis (e.g. Lourenço et al. 2007)

-A.3. Discrete Element analysis (e.g. Van Mele et al. 2012)

-A.4. Simple Models

A.1 Equivalent Frame Analysis: Significant contributions in the direction of developing criteria guiding the choice of Modeling Methods have been made by Lagomarsino and his Co-workers in the recent EU-funded project known as "perpetuate" (www.perpetuate.eu). In this study, systems are separated according with their inherent robustness and function as candidates for the A.1 or the A.2 Methods of analysis. Note that in the method known as "Equivalent frame" analysis, the elements comprise orthogonal discs, which may represent piers or spandrel beams spanning over openings, and are actually deformable masonry panels. Each disc possesses degrees of freedom at the corner points for connectivity with adjacent elements and for derivation of stiffness properties; any nonlinearity in the response refers to these deformable components. Rigid portions are the remaining regions that connect the deformable parts together. Moreover the idealization as an equivalent frame easily allows the user to include in the model other structural elements, such as reinforced concrete beams or columns, together with the masonry ones. Thus, this method is also palatable in modeling mixed structures (where masonry and reinforced concrete subsystems exist in the buildings).

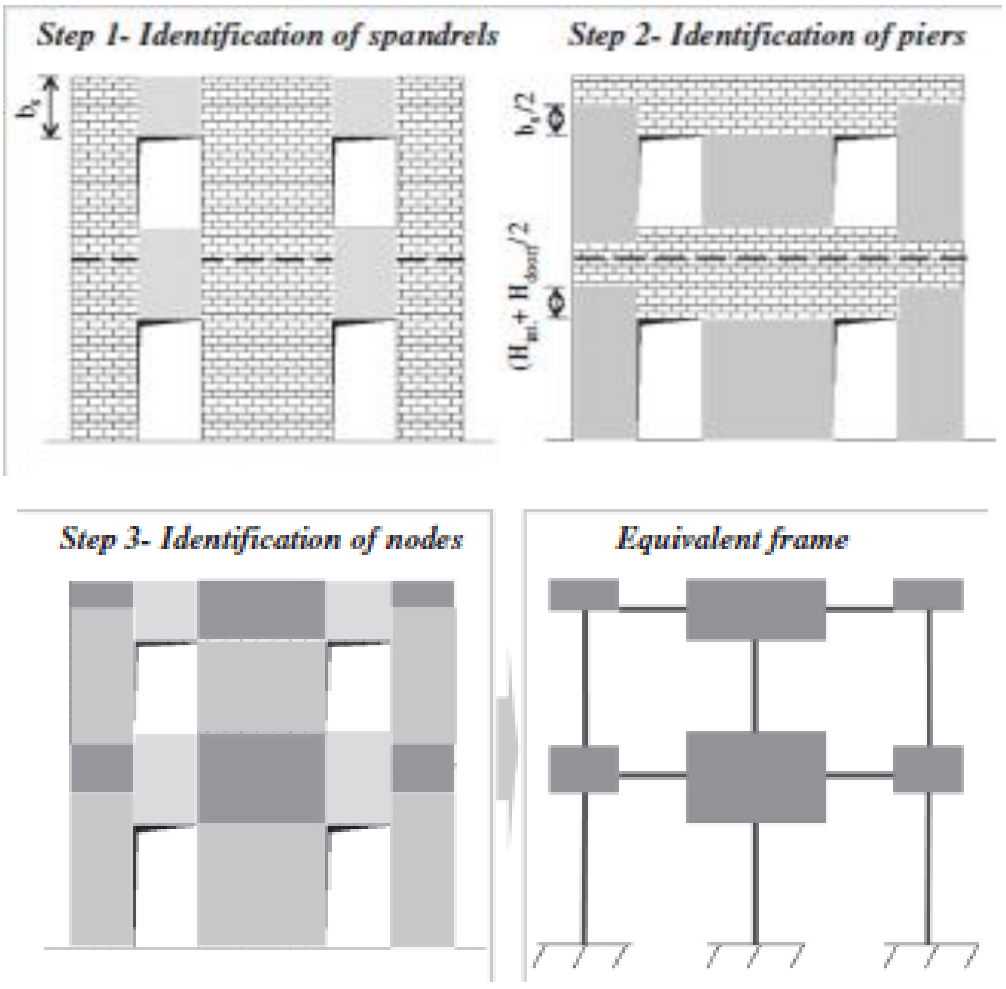

Figure 2.1: Idealization of a structural wall with openings for action in its own plane (*from Lagomarsino et al. 2013*)

Through the Equivalent Frame approach it is possible to analyze complete 3-D buildings without significant computational effort while accounting for nonlinearities in the response (Fig. 2.1, TREMURI Software, Lagomarsino et al. 2012, STADATA 2012). The authors claim the possibility of modeling complex three dimensional models of URM structures, obtained by assembling walls and floors, however *mainly referring to their in-plane strength and stiffness contributions*. This particular issue is considered a significant disadvantage of the method when applied to structures with flexible diaphragms, where the out-of-plane component is dominating the overall response. Specifically the authors state as criteria for assemblying a three dimensional model of the URM structure (from Lagomarsino et al. 2013):

> *" The 3-dimensional modeling of whole URM buildings starts from the following basic hypotheses: (a) the construction bearing structure, both referring to vertical and horizontal loads, is identified with walls and horizontal diaphragms (roofs, floors or vaults); (b) the walls are the bearing elements, while diaphragms are the elements governing the sharing of horizontal actions among the walls; (c) the flexural behavior of the diaphragms and the wall out-of-plane response are not computed because they are considered negligible with respect to the global building response, which is governed by their in-plane behavior. The global seismic response is possible only if vertical and horizontal elements are properly connected; then, if necessary, ''local'' out-of-plane mechanisms have to be verified separately through suitable analytical methods."*

Thus, in structures where the out of plane action in walls orthogonal to the earthquake motion is expected to prevail, this approach may place the emphasis elsewhere, outside of the failure zones. For this reason in many codes the use of equivalent frame analysis is permitted only if stiff diaphragms are available in the structure.

The Stiffness formulation of classical beam-column frame elements accounting for shear deformation and rigid end zones and also including lumped plasticity at the ends are the basic element model used in this approach (Fig. 2.2).

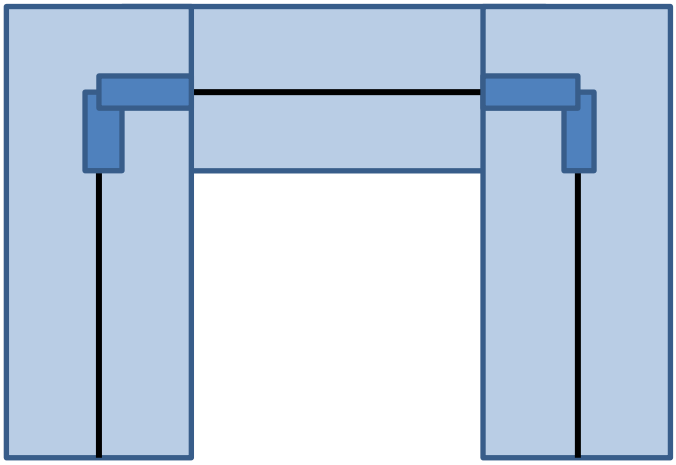

Figure 2.2: Definition of Beam-Column Elements connected with rigid end zones, modeling piers and spandrel.

<u>*A.2: Finite Element Analysis:*</u> This method is clearly a general procedure that enables the user through the element library to represent in the computer model the geometric, spatial and material complexity

of the structure with significant accuracy. However, material constitutive modeling has undergone a slower evolution than the overall Finite Element framework (Lourenço, 2001, Roca, et al., 2010) and detailed material parameters for the various types of constituent materials composing unreinforced masonry, are fragmented and non-standardized. Masonry is by construction anisotropic (the response being biased by the orientation of the joints), exhibiting quite a complex mechanical behavior owing to the composite nature of the material (mortar and blocks). Behavior in tension is rather brittle to the extent that the assumption of tension cutoff may be reasonable in constitutive characterization of the material. Compressive strength is dependable and considered high, although it is actually one quarter the value of normal concrete. Frictional response is governed by shear. Describing this complex mechanical behavior usually requires very sophisticated constitutive formulations, equipped with elastic and plastic response, failure surfaces and flow potential functions (non-associated plasticity, Fig. 2.3). For this reason, masonry in most finite element formulations is treated as a homogenized continuum (Zucchini 2007), having mechanical properties that are a weighted mean between mortar and block characteristics (e.g. the characteristic compressive strength of homogenized masonry is taken $f_{mk} = kf_b^a f_m^d$ where f_b is the compressive strength of the blocks and f_m the compressive strength of the mortar material, whereas the exponents are empirical constants).

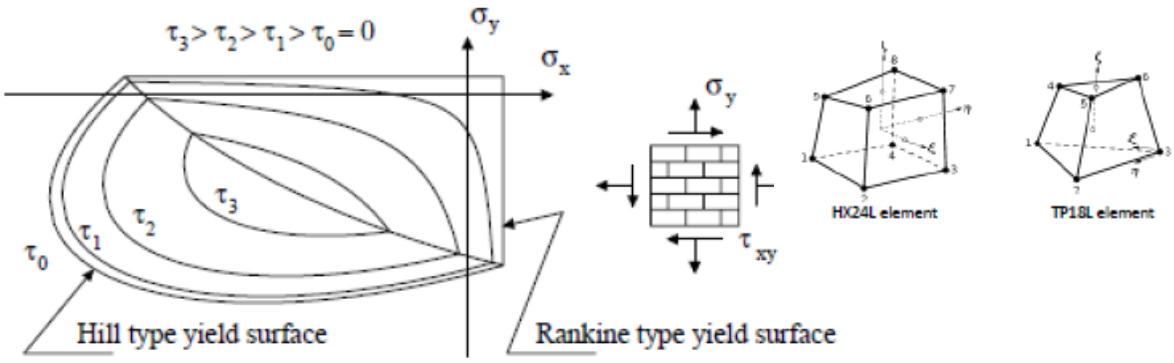

Figure 2.3a: Composite yield surface with iso-shear stress lines proposed by Lourenco (Lourenco 1996). Different strength values for tension and compression along each material axis. Solid elements available in the DIANA software for 3-D modeling of masonry; nodes have 3 translational degrees of freedom (TNO DIANA BV, 2010) (From E. Scheibmeir, 2012).

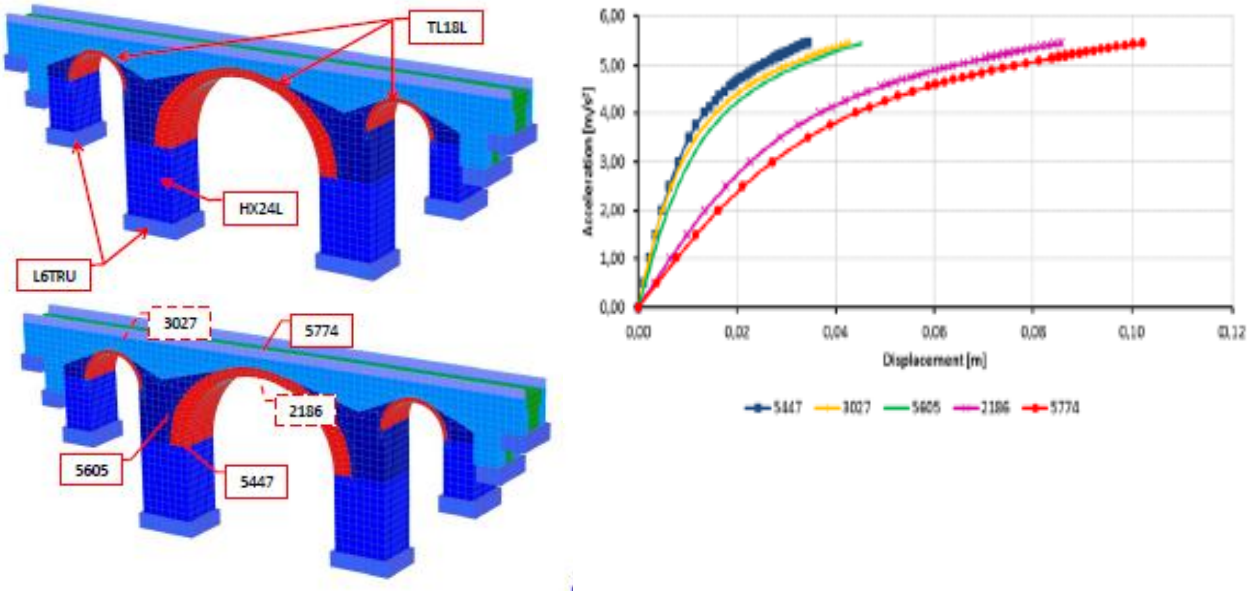

Figure 2.3b: Example Case study obtained using Sophisticated Finite Element Simulation of Masonry

Structures: Stone bridge analyzed using the elements of Fig. 2.3a and a Drucker-Prager plasticity constitutive law for homogenized material behavior: (i) Types of elements used to model different regions of the bridge; (ii) Reference node identities that are referred to in the pushover curves plotted in (iii). (From E. Scheibmeir, 2012)

Clearly, nonlinear Finite Element Solutions are still hampered today by the convergence and algorithmic stability problems instigated by the tension cutoff after cracking in URM, (where the tensile strength is insignificant), combined with the absence of the stabilizing participation of reinforcement which is available in the case of concrete structures. Thus, once failure is detected, the process of several revisions of the stiffness matrix slows down considerably the rate of convergence of the solution, to the extent that dynamic nonlinear time history analysis becomes quickly non-feasible. So in these cases conducting nonlinear pushover analysis in simple masonry elements is the limit of current nonlinear F.E. technologies.

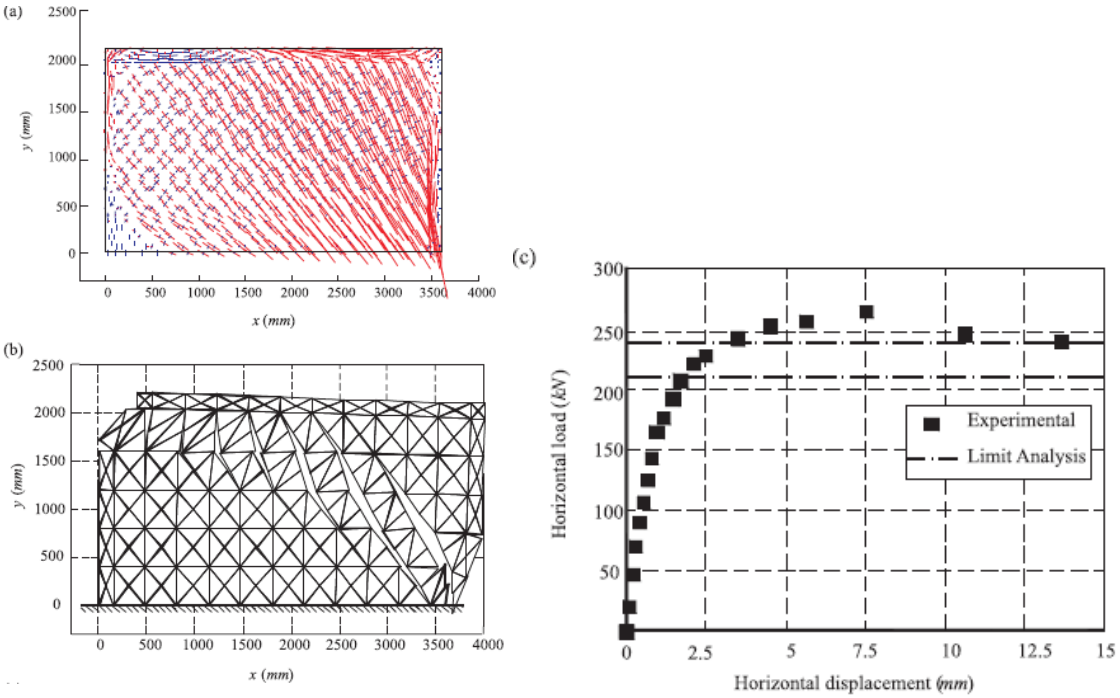

Figure 2.4: Progressive re-meshing of new boundaries to reflect crack formation and propagation. The analytical model is linear elastic. The increasing compliance (nonlinearity) is owing to the loss of connectivity (From Lourenço et al. 2007).

Alternative methods for achieving reproduction of the nonlinear characteristics of the response, while taking advantage of the stability of elastic models have been sought. An effective option is re-meshing of the structure while considering the creation of new boundaries of discontinuity in the continuum along the paths of cracks, as these form and propagate (e.g. wherever the principal tensile stress exceeds the tensile strength of the homogenized material). Each time a new boundary is created (by the incremental propagation of a crack) re-meshing is followed by restructuring of the elastic stiffness matrix of the structure, which however, becomes more compliant as the connectivity between adjacent nodes is lost due to opening of a crack. This progressively increasing compliance imparts the characteristic of nonlinearity on the global resistance curve of the structure. Again, as in the case of F.E. simulations with advanced nonlinear/plasticity models for masonry, pushover analysis of simple structures appears to be the upper limit of applicability of current software capabilities.

A.3 Discrete Element Modelling (DEM) & Analysis: This idealization technique appears to hold significant promise for nonlinear simulation of brittle structures, as it does not present the types of convergence instabilities associated with the occurrence of a postpeak descending branch after tensile fracture. Here the structure is subdivided to discrete volumes with a polygonal surface, and either rigid or elastic constitutive properties. Inelasticity occurs at the points of contact between discrete volumes, which are modeled through one dimensional (axial or shear) springs, with predetermined force – displacement relationships. In this context masonry blocks are treated as separate units. DEM methods may use 'compliant contacts' or 'unilateral contacts'. In the former, contact forces are obtained from the contact springs, whereas in the later contact formulations are used to prevent penetration between adjacent discrete elements. Several studies have been conducted modeling a variety of URM structures to loads including seismic (Lemos 1998, Çaktı et al. 2013). Example cases such as that in Fig. 2.5 illustrate the capability of the model to mimic the observed collapse modes well beyond the limits of applicability of nonlinear FEM analysis.

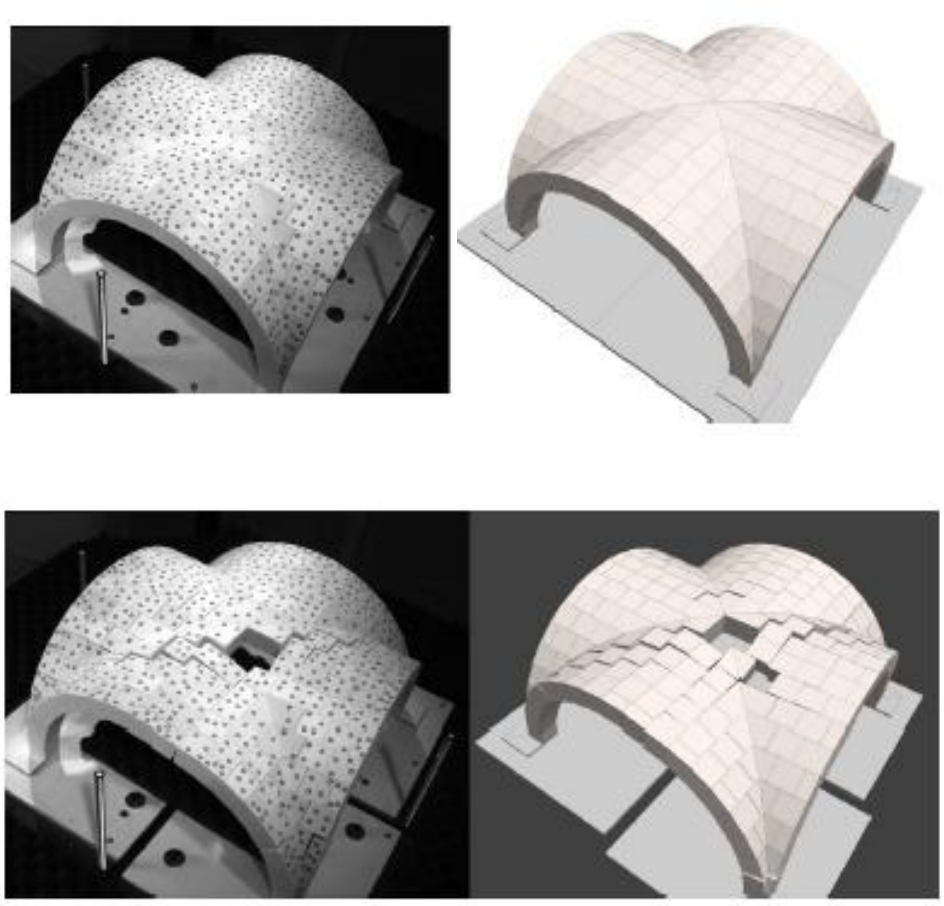

Figure 2.5: Physical Model of a Vault structure, DEM (computational) Model, and comparison of observed and computed modes of failure (from Van Mele et al. 2012).

A.4 Simple Models: In this type of analysis, a variety of simplifications have been tried with the objective to exploit the capabilities of commercially available, easy to use software, or in order to achieve a hands on, mechanistic model that may evade numerical simulation altogether. The wide range of possibilities cannot be treated with fairness in the summary presented herein; some key points are highlighted for the benefit of appreciation of the practical issues involved:

- ***Three Dimensional Elastic Finite Element Analysis:*** A favored approach among engineers that have access to the use of common engineering software (such as SAP 2000 or ACORD) is to develop a finite element model of the URM building, using shells as a basic unit for discretization and elastic material properties. Analyses of this type can be used to identify the force path through the structure, and those regions of high deformation demand (regions where sharp sharp strain gradients identify strain and stress concentrations). Of course, such models may not be taken literally to quantify URM behavior under seismic loads, but they may prove very useful in highlighting the regions of anticipated damage, but also in demonstrating in a qualitative sense, the effectiveness of retrofit measures in moderating the intensity of stress localization throughout the structure (i.e. results are to be used as relative indicators of the parametric dependencies of the response and not as quantifiers of the response). Some marginal nonlinearity may be introduced in this class of models without risking overall convergence failure: this refers to uniaxial nonlinear springs or gap elements that are necessary in order to account for imperfect contact between components, particularly in the case of dissimilar materials. Such cases include but are not limited to:

- Unilateral contact of masonry walls with the surrounding soil when the structure has a basement

- Unilateral contact of timber diaphragm beam penetrating into a wall

- Partial Bonding of timber laces embedded in masonry.

- Contact between parts of the structure that are not integrally connected.

Properties for such springs may be derived from basic mechanics of the problem idealized and the tributary area of the contact joint that is represented by the springs/gap elements.

- ***Mechanistic Models:*** Simple hand calculation tools for rapid assessment of masonry have been developed ranging from simple strut and tie equilibrium models, to distributed mass/stiffness single degree of freedom idealizations of the URM building. Such approaches are outlined in the forthcoming chapters, as these are considered today the most palatable by practicing engineers. An added advantage of these models is that they provide the user with a crisp, transparent understanding of the mechanics of failure and seismic response of the buildings without the obscuring complexity occasionally imparted by simulation.

2.5 Analysis in the Context of Response Calculation (Solution of the Equations of Motion)

It was stated earlier that there are two general attributes implied under the term “Analysis” of URM Buildings; Section 2.4 was dedicated to issues of idealization of the structural system and properties, which defines the property matrices $\underline{M}$, $\underline{K}$, and $\underline{C}$ in Eq. (2.1), but also the nature and topology of the degrees of freedom that enter the response vector, $\underline{U}$. The present section is concerned with alternative procedures and solution strategies that may be used in order to solve the equations of Motion (Eq. 2.1). Thus, (B) in the preceding classification of analysis methods encompasses a variety of solution algorithms used in order to calculate the dynamic response from the field equations of motion, namely:

-B.1. Nonlinear Step – by – Step Time History Analysis

-B.2. Nonlinear Static Analysis (Pushover)

-B.3. Linear Elastic Modal Analysis, using either Modal Spectral Response, or Modal Time History Response with mode superposition

-B.4. Static Analysis

The solution algorithms above are ordered with decreasing degree of complexity and computational demand. In all cases there is a significant degree of interaction with the choice of mechanical model – the more complex the idealization strategy chosen in the context of methods (A), the more restrictions will be imposed on the choice of a solution strategy under (B). Certainly, the most general but complicated option is the so-called step-by-step nonlinear time history analysis in which case the solution algorithm marches in time satisfying at each time step the conditions of dynamic equilibrium. This means that complete constitutive relationships must be provided with the input, which include rules by which full deformation reversals may be modeled; through these, the secant or tangent stiffness of the various elements that compose the structure will be updated at each step accounting for the stiffness changes that occur due to accumulation of residual (permanent) inelastic deformation.

A comprehensive description of the methods of analysis (solution strategies) has been presented by Clough and Penzien (1976) and Chopra (1995). Spectral Analysis where the seismic hazard is specified in the form of an acceleration and displacement spectrum eliminates the need for detailed time-history analysis and thus alleviates the requirement for using constitutive models that are endowed with complete unloading rules; this is the basis for many popular analysis methods including the so-called N2 Approach that is featured as “Nonlinear Static Analysis” in EC8-I (Appendix B). Linear Elastic Modal Analysis may be used with both spectral and time history definitions of the seismic hazard, but is nevertheless restricted to the use of linear-elastic idealizations of the structure, as the underlying premise of this method is the principle of superposition. Of the two alternatives of linear elastic analysis, clearly the option of time history analysis of modal response and real time superposition of modal contributions is the only accurate option. Despite this, most commercial popular software that could be used for analysis of URM structures only offer the possibility of combination of the Modal Maxima either through the Complete Quadratic Combination (CQC) or the Square - Root - of the - Sum- of the - Squares (SRSS) options. These approaches combine maximum responses of different modal contributions which, in time history records, are not concurrent. The danger from these approaches is that overly conservative estimates may be obtained from such an analysis, in light of the fact that several modes need be accounted for before 70% of the total URM building mass may be said to be engaged in elastic F.E. modal analysis since in the absence of diaphragms several hundreds of subordinate modes are excited in such computer models. These modes are occasionally spurious and bear no relevance to the actual behavior. Overly conservative estimates of response emanating from SRSS may lead to excessively invasive (nonreversible) interventions in URM buildings during rehabilitation, and as such they should be always treated with particular caution.

CHAPTER 3 –SIMPLE ANALYSIS METHODS

*3.1 Scope:*Given the inherent brittleness of URM construction, simple methods of analysis are particularly valuable in preliminary assessment as they may be used for quick identification of systematic pathologies, but also for singling out those buildings that are the more likely candidates for collapse in a future seismic hazard. To keep things simple, the earthquake spectral characteristics and intensity may be taken to correspond to the values used in practical seismic design, although any type of spectrum from a real earthquake may be used as an alternative. Important performance criteria in the process of quick assessment are (a) the eccentricity of gravity load required to resist the overturning moment as this determines the fraction of the plan area which is under direct tension – this may be used to quantify the maximum tolerable ground acceleration prior to excessive damage. (b) The intensity of out of plane differential translation and in plane shear distortion of masonry walls oriented orthogonal to and parallel with the seismic action, respectively, (c) The magnitude of axial tension transferred at the corners of the structure, which may be responsible for localized failure modes as depicted in Fig. 3.1.

Figure 3.1: Failure at the corners and out of plane due to transfer of tension (Photos: courtesy Dr. F. Karantoni).

The same concepts of analysis may be used to guide retrofit through measures that reduce the intensity of (b) and (c) since these two phenomena are most critical in determining the likelihood, extent and localization of damage. Example case studies (Karantoni and Pantazopoulou (2013), Papadopoulos

and Pantazopoulou (2011)) are used for demonstration of concepts: The effectiveness of each intervention scenario is evaluated by the effected improvement of measurable response indices. In this regard, characteristic Balkan types of traditional construction are used in the study as model structures for illustration.

3.2 Simple Methods and Models of Analysis of URM Buildings

In URM structures lateral load resistance is imparted by interface friction between layers of laid stone/mortar; frictional resistance is supported by the clamping action of the overbearing pressure provided by gravity loads. Occasionally, URM is reinforced in shear by horizontally oriented timber laces or tiers of different size bricks, and, in several cases, iron clamps are used as cross ties between orthogonal walls. A basic characteristic of URM construction is the relatively large area ratio of exterior and interior walls combined with relatively flexible diaphragms. In this regard, a paradoxical aspect of the seismic behavior of this class of structures is that weight is the underlying cause of both demand (inertia forces increase with the mass) and supply (since lateral strength at any level is also secured by the overbearing gravity loads through friction).

Based on post-earthquake reconnaissance of URM, it is generally recognized that the primary modes of failure of such structures comprise diagonal cracking, out-of-plain bending and detachment of perpendicular connected walls, particularly in the absence of stiff diaphragms but also due to the cumulative implications of long term phenomena (creep, corrosion/erosion and soil settlement). Furthermore, masonry walls with large or several openings appear to be most vulnerable regardless of the direction of action of the earthquake (either in-plane or out of plane) as they represent the point of concentration of deformation demand in the structure. This is why the primary measures of retrofit in such situations are targeted towards reducing the relative drift between points in the plan of the structure, particularly at floor and roof levels, through the addition of a non-visible ring-beam at roof level and/orenhancing the diaphragm stiffness and connection at the floor levels and at the roof.

Following the axiom that the intensity of the effort required to obtain a result, at least in the initial phase, should be compatible with the level of confidence associated with the input data and information, simple alternative assessment procedures are required, lying between the two extreme options, namely rapid visual screening on one hand, and detailed F.E. or D.E. analysis as reviewed in Chapter 2 on the other. Analysis procedures presented in this chapter are intended to address the need for simplicity of approach; they concern buildings that have a favorable morphology for lateral load resistance: i.e. (a) buildings that have a fundamental natural translational period T in both principal directions of the floor plan that falls below the value of $2T_c$, where $T_c$is the characteristic period value at the of the plateau of the design acceleration spectrum (EC8-1, 2004), (b) that may also be considered regular in plan and in height (building plan approximately rectangular so that torsional effects may be considered negligible, continuous walls along the height, adjacent floors on opposite sides of a single wall are at the same height).

An estimation of the fundamental translational period of the building is required in order to obtain the seismic demands from the spectrum. For common buildings which are adequately robust to support the assumption that $T \leq T_c$, demands may be estimated directly from the acceleration and displacement values associated with T_c in the design spectrum. Alternatively, in order to eliminate the need of detailed computational idealization of the building, *T* may be approximated in each of the principal directions of the plan according with the empirical approximations included in EC8-I (2004) and modified to match the characteristics of the URM construction features:

$$T = C_t \cdot H^{3/4} (sec) \quad but \quad T \geq 0.05 H^{3/4} (sec) \tag{3.1}$$

Where, *H*is the total building height, in m, measured from the level of foundation or the level of rigid basement and $C_t$is a constant given by the relationship:

$$C_t = \mathbf{0.075} / \sqrt{A_w} \tag{3.2}$$

In Eq. (3.2), A_w represents the total area of load-bearing walls in the ground floor of the building (in m^2) and is calculated from:

$$A_w = \sum \left[A_i \cdot \left(\mathbf{0.2} + (l_{wi} / H) \right)^2 \right] \tag{3.3}$$

A_i is the active cross section of the i-th wall in the direction of seismic action considered in m^2, and l_{wi} is the length of the i-th wall in the direction of seismic action, in m.

3.3 Base Shear Demand Estimation

Owing to their robust morphology, URM buildings carry relatively low levels of axial stress due to self weight, and present significant stiffness to lateral and vertical loads. Thus, they implicitly satisfy serviceability limit states, and therefore need to be evaluated primarily at the ultimate limit state for seismic assessment. Note that for masonry walls, lateral drift at cracking is in the range of 0.15%±0.05% whereas drift ductility at failure is usually less than 2.5 (i.e., failure drift is in the order of 0.5%). (On the other hand, in very tall and slender URM structures such as towers and spires, long term behavior may be catastrophic due to the relatively high levels of overbearing pressure.)

The objective in seismic analysis is the dependable estimate of the terms in the basic acceptance criteria used in order to verify structural adequacy:

$$V_{sd} \leq V_{Rd} \tag{3.4}$$

The two terms, base shear demand, V_{Sd}, and base shear strength, V_{Rd}, both depend on structural properties and the seismic loading. As the structure's weight appears in both terms of the design inequality, higher gravity loads tend to enhance both the shear strength of the building and the seismic forces. Oc-

currence of normal tensile stresses in any part of the shear resisting walls is used in the context of this report, to identify wall failure.

Based on Type I earthquake spectra (EC8-I (2004)) and with the period estimate of the structure described in the preceding, T, the total acceleration demand at the top of the structure in the fundamental mode of vibration, $S_e(T)$, is obtained from Eq. (3.5)using as input the value of peak ground acceleration a_g for the site in consideration given from seismicity maps in m.s^{-2}, and the soil type coefficient, S, (=1 for stiff or rocky soil and it may be increased to 1.2 for more compliant soil)

$$\mathbf{0} \le T < T_B: \quad S_e(T) = a_g \cdot S \cdot \left[\mathbf{1} + \frac{T}{T_B}\left(\eta \cdot \beta_o - \mathbf{1}\right) \right] \tag{3.5a}$$

$$T_B \le T \le T_C: \quad S_e(T) = a_g \cdot S \cdot \eta \cdot \beta_o \tag{3.5b}$$

$$T_C \le T \le T_D: \quad S_e(T) = a_g \cdot S \cdot \ \eta \cdot \beta_o \cdot \left(\frac{T_C}{T} \right) \tag{3.5c}$$

$$T_D \le T: \qquad S_e(T) = a_g \cdot S \cdot \eta \cdot \beta_o \cdot \left(\frac{T_C \cdot T_D}{T^2} \right) \tag{3.5d}$$

where T_B, T_C are the corner period values (i.e. for firm soil of type A it is T_B=0.15sec and T_C=0.40sec), η is the damping coefficient depending on the viscous damping ratio, ζ: ($\eta=(7/(2+\zeta)^{0.5} \ge 0.7$; for tier-type masonry it is assumed that ζ=5%). Parameter β_o=2.5 is the spectral amplification. This term is divided by the response coefficient q when nonlinear response is considered. Factor q is linked to the mode of construction (for masonry structures with horizontal tiers q=1.5, with both horizontal and vertical tiers q=2 and for reinforced masonry q=2). The associated relative displacement demands are obtained from the total acceleration values according with ($S_d=S_e \cdot T^2/40$):

$$\mathbf{0} \le T < T_B: \qquad S_d(T) = a_g \cdot S \cdot \left[\mathbf{1} + \frac{T}{T_B}\left(\mathbf{2.5}\eta - \mathbf{1}\right) \right] \cdot \frac{T^2}{\mathbf{40}} \tag{3.6a}$$

$$T_B \le T \le T_C: \qquad S_d(T) = a_g \cdot S \cdot \eta \cdot \mathbf{2.5} \cdot \frac{T^2}{\mathbf{40}} \tag{3.6b}$$

$$T_C \le T \le T_D: \qquad S_d(T) = a_g \cdot S \cdot \eta \cdot \mathbf{2.5} \cdot \left(\frac{T_C \cdot T}{\mathbf{40}} \right) \tag{3.6c}$$

$$T_D \le T \le \mathbf{4}\,sec: \quad S_d(T) = a_g \cdot S \cdot \eta \cdot \mathbf{2.5} \cdot \left(\frac{T_C \cdot T_D}{\mathbf{40}} \right) \tag{3.6d}$$

If, instead of a period estimate, the T_c value is used to determine the demands (as suggested in Section 3.2 considering that URM buildings are relatively stocky structures seldom higher than two storeys so that the fundamental period falls in the constant acceleration range of the spectrum), total acceleration and relative displacement values are given by:

$$S_e = \mathbf{2.5}\, a_g \cdot S \cdot \eta / q; \quad S_d(T_1) = \mathbf{0.0625} \cdot a_g \cdot S \cdot \eta \cdot T_c^2 \ \text{(in m·s}^{-1}\text{ and m)} \tag{3.7}$$

In the framework of simplified analysis the URM building is treated as a cantilever structure, having a cross section defined by the plan of the structure. Here, the occasional position of openings is neglected in considering the overall response, so that the building is idealized as a hollow tubular beam having a wall thickness *t* equal to the actual thickness of the perimeter walls of the building. Lateral forces*v(z)*occur over the entire height of the structure owing to the spatial distribution of the wall mass. The total inertia force is equilibrated by the base shear V_o, the magnitude of which is defined by,

$$V_o = C_1 \cdot C_m \cdot S_e(T) \cdot (W / g) \quad \text{(kN)} \tag{3.8}$$

where $S_e(T)$ is the spectral acceleration in $m \cdot s^{-2}$, C_1 isthe inelastic amplification (≥1) that relates the anticipated peak inelastic displacement of the structure to the displacement value of a perfectly elasto-plastic system of equal initial stiffness (here this is taken =1, but the symbol is kept explicitly in the calculations, nevertheless, for the sake of generality) and $C_m$is the mass participation coefficient, equal to (Clough and Penzien, 1993):

$$C_m = \frac{L_e^2}{m}; \quad L_e = \int \Phi(x,y,z) \cdot \overline{m}\ dxdydz + \sum_i m_i \cdot \Phi_i$$
$$m = \int \Phi(x,y,z)^2 \cdot \overline{m}\ dxdydz + \sum_i M_i \cdot \Phi_i^2 \qquad (tn) \tag{3.9}$$

where, $\Phi(x,y,z)$ is the fundamental shape of vibration, and $\overline{m}$ the distributed mass of the structure (weight per unit volume of masonry, around 20 kN/m^3). M_i are lumped masses wherever they exist (e.g. at the floor and roof levels). Generally, for lumped systems, C_m is around 1 for distributed mass systems, 0.8 for higher structures; for distributed mass systems, C_m in the fundamental mode is far less, around 0.6.For example, in the case of a tower with uniformly distributed mass, excited at the base, the mass participation coefficient is 0.58. In the remainder of the present chapter, C_m is taken equal to 0.6 to avoid detailed calculation.

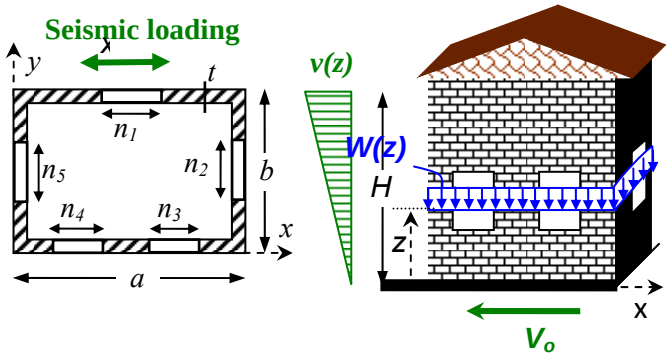

Figure 3.2. Seismic loading on a traditional masonry structure

The distributed lateral forces acting at a distance z from the base, v(z) , result in internal shear and flexural moment resultants at any building cross section. A linear distribution is assumed, for simplicity, although a uniform distribution of lateral force may be equally plausible for this class of structures. Thus, at distance z from the base, the lateral force *v(z)* is related to the total base shear, V_o, from: $v(z) = v(z|_H)\cdot(z/H)$, with $v(z|_H)=v(H)=2V_o/H$. From equilibrium requirements it follows:

$$V(z) = (H-z)\cdot\left[v(z)+v(H)\right]/2 \quad \text{(kN)} \tag{3.10}$$

$$M(z) = v(z)\frac{(H-z)^2}{6} + v(H)\frac{(H-z)^2}{3} \quad \text{(kN-m)} \tag{3.11}$$

The most critical level is the ground level *(z=0)*; Equations (3.10) and (3.11) yield the base shear value, V_o and overturning moment, M_o, of the building:

$$V_o = C_1 \cdot C_m \cdot S_e(T)\cdot W/g = H\cdot v(H)/2 \Rightarrow v(H) = 2\cdot C_1\cdot C_m\cdot S_e(T)\cdot W/g/H \tag{3.12}$$

$$M_o = v(H)\frac{H^2}{3} = \frac{2}{3}\cdot C_1\cdot C_m\cdot S_e(T)\cdot\frac{W}{g}\cdot H \tag{3.13}$$

To quickly evaluate the building against the implications of the stress resultants defined above, the plane sections assumption is invoked for the idealized cantilever in order to determine normal and shear stresses through the wall thickness of the building. Considering the two ends of the plan in the dimension parallel to the ground motion, P_1 and P_2, A_w the cross sectional area of the walls in the plan, and Ω_w the flexural modulus of the buildings' cross section (i.e., plan), normal stresses are calculated at the two extremes of the building's plan, as follows (Karantoni and Pantazopoulou 2013, Tastani et al. 2009):

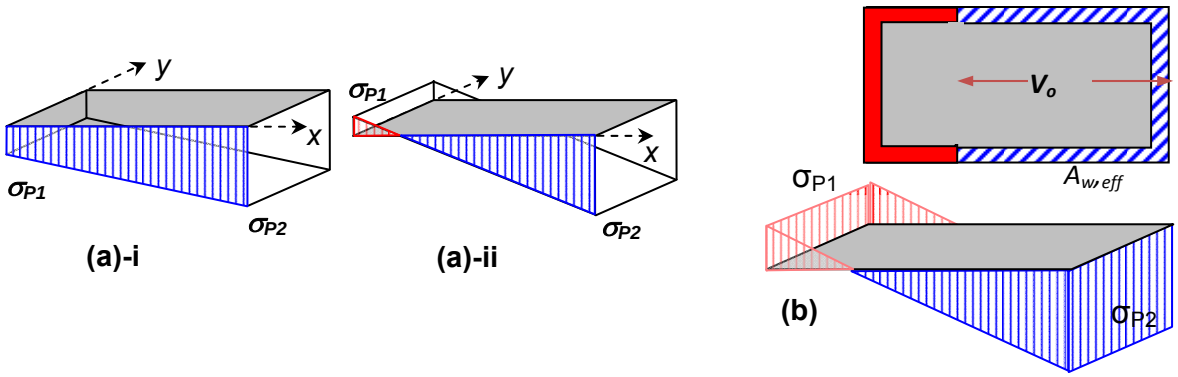

Figure 3.3: The plane stress assumption for the plan of the structure. (a) Distribution of normal stresses over the plan section (direction *x-x*) when stress $\sigma_{P1}$is (a-i) compressive and (a-ii) tensile. (b) The part of the structure in normal tension is considered inactive in resisting shear forces (red area). The effective area, $A_{w,eff}$ is the part of the wall cross section under normal compression.

$$\sigma_{P1} = -\frac{W}{A_w} + \frac{M_o}{\Omega_w} \quad \& \quad \sigma_{P2} = -\frac{W}{A_w} - \frac{M_o}{\Omega_w} \text{ (MPa)} \tag{3.14}$$

In the above, *W(z=0)* is the overbearing self-weight of the structure, at the level considered (ground level), A_w is the total area of the walls, and Ω_w is the resistance of the "tubular" cross section (=*I/a/2*). Term *W(z)* (in *kN*) is the total overbearing gravity load composed by the roof weight W_r and the weight of the walls W_w from the top down to level *z*: $W(z) = W_w(z) + W_r$, where W_r is taken as $\gamma_r \cdot A_r$; A_r is the roof area, and γ_r is the unit area weight of the roof, ranging from γ_r =160-180 Kg/m^2 for stone tiles, to γ_r =110-150 Kg/m^2 for roman-type and byzantine-type ceramic tiles. These values include the self weight of timber trusses, sheathing and insulation. The tributary roof weight is transferred to the supporting walls according to the geometry of the roof (two-way or four-way). Similarly, the unit weight of the walls is obtained from the wall thickness and the specific gravity of the stone blocks, γ_w (ranging between γ_w = 20 to 27 kN/m^3). Thus, $W_w(z) = \gamma_w \cdot A_w \cdot (H-z)$ whereas the total axial load at level z above the ground is $W(z)=\gamma_w \cdot A_w \cdot (H-z) + \gamma_r \cdot A_r$ and increases linearly towards the base of the structure. Note that the wall cross sectional area, A_w, may be altered with *z* due to the presence of openings. Here, for simplicity and with no loss of generality, A_w is assumed constant with regards to the definition of the axial load.

From the assumed normal stress distribution it is possible to determine the position of the neutral axis in the building's plan. If the axial compression load due to overbearing pressure is very large, the neutral axis will be located outside of the building's plan, and thus the entire cross section of the building will be active in carrying lateral load, including the shear stresses required to equilibrate V_o. If on the other hand, the neutral axis is located within the boundaries of the structure's plan at ground level, then the part of the wall that is estimated to be subjected in direct (vertical) tensile stress will be considered inactive in resisting shear; actually in that situation a criterion limiting the magnitude of the earthquake acceleration, a_g, that may be tolerated by the building without local failure will be related to the magnitude of the nominal tensile strength of masonry, f_{tm}, as follows:

$$\sigma_{P1} = f_{tm} = W\left(-\frac{\mathbf{1}}{A_w} + C_1 C_m \frac{S_e(T)}{\Omega_w g} \cdot \frac{\mathbf{2}}{\mathbf{3}} H \right) = W\left(-\frac{\mathbf{1}}{A_w} + C_1 \cdot C_m \cdot a_g \cdot \frac{\mathbf{2.5}\eta S}{\Omega_w g} \cdot \frac{\mathbf{2}}{\mathbf{3}} H \right) \qquad (3.15a)$$

$$\sigma_{P2} = -W\left(\frac{\mathbf{1}}{A_w} + C_1 C_m \frac{S_e(T)}{\Omega_w g} \cdot \frac{\mathbf{2}}{\mathbf{3}} H \right) = -W\left(\frac{\mathbf{1}}{A_w} + C_1 \cdot C_m \cdot a_g \cdot \frac{\mathbf{2.5}\eta S}{\Omega_w g} \cdot \frac{\mathbf{2}}{\mathbf{3}} H \right) \qquad (3.15b)$$

Equation (3.15a) defines a limit for the level of ground earthquake acceleration, a_g, beyond which there will be inactive regions due to direct tension at the base of the structure is defined by,

$$a_g \le \mathbf{0.6} \cdot \frac{\Omega_w \cdot g}{C_1 \cdot C_m \cdot \eta \cdot S \cdot H} \cdot \left[\frac{f_{tm}}{W} + \frac{\mathbf{1}}{A_w} \right] \qquad (\mathrm{m \cdot s^{-2}}) \qquad (3.16)$$

An alternative assessment test is definition of the eccentricity of the vertical load (structural weight) at any critical level of the structure, z. In the context of seismic assessment, the eccentricity of the load combination defined by (*M(z), W(z)*) is, *e=M/W.* Barring any severe discontinuities of mass and geometry, the most likely critical cross section is at z=0 (base of the structure, where $e=M_o/W$). Setting limits so as to eliminate tension ($\sigma_{P1}=0$) results in the limiting value of eccentricity below which the entire wall

cross section at the level considered is effective in resisting shear. For example, consider a structure with a rectangular plan of dimensions ℓ_x and ℓ_y and a wall thickness t, subjected to ground shaking in the x-direction. In order to eliminate tension at the wall base for earthquake parallel to the x direction it is required that $e \le e_{lim}$:

$$-\frac{W}{A_w}+\frac{M_o}{\Omega_w}=0 \Rightarrow e_{lim}=\frac{M_o}{W}=\frac{\Omega_w}{A_w}\approx\frac{1+3\left(\frac{\ell_y}{\ell_x}-2\frac{t}{\ell_x}\right)\cdot\left(1-\frac{t}{\ell_x}\right)^2}{6\cdot\left(1-\frac{t}{\ell_x}\right)\cdot\left(1+\frac{\ell_y}{\ell_x}-2\frac{t}{\ell_x}\right)}\cdot\ell_x \quad \text{(m)} \qquad (3.17a)$$

Where

$$e=a_g\cdot\frac{5}{3}\cdot C_1\cdot C_m\cdot S\cdot\eta\cdot\frac{H}{g}\,\text{(m)} \qquad (3.17b)$$

For usual wall thickness values and plan aspect ratio values (ℓ_y/ℓ_x), Eq. (3.17) yields the values shown for easy reference in Table 3.1, where the limiting eccentricity is given as a fraction of the respective dimension of the structure in the direction of seismic action. With these values for for e_{lim}/ℓ_x, the acceleration limit beyond which a part of the building will suffer from direct tension is obtained by replacing in Eq. (3.17b):

$$\frac{e_{lim}}{\ell_x}=\frac{a_g}{g}\cdot\frac{5}{3}\cdot C_1\cdot C_m\cdot S\cdot\eta\cdot\frac{H}{\ell_x}\Rightarrow\frac{a_g}{g}=\frac{0.6}{\eta C_1 C_m S}\cdot\underbrace{\frac{e_{lim}}{\ell_x}}_{\substack{\text{From}\\ \text{Table 3.1}}}\cdot\overbrace{\frac{\ell_x}{H}}^{\substack{\text{aspect ratio}\\ \text{of building}}} \qquad (3.18)$$

Table 3.1: Calculated limits for e_{lim}/ℓ_x

$t/\ell_x \rightarrow$ $\ell_y/\ell_x \downarrow$	0.05	0.1	0.15	0.2
0.5	0.261	0.246	0.234	0.226
1	0.317	0.303	0.290	0.280
2	0.372	0.355	0.340	0.326

Results for the limiting eccentricity and maximum tolerable ground acceleration are plotted in the form of simple design charts in the appendix (end of the chapter). Note that the peak tolerable ground acceleration reduces with increasing slenderness of the structure (H/ℓ_x ratio).

The same has been examined for the URM structure shown in Fig. 3.4, which represents a two storey URM structure in the city of Xanthi (Tastani et al. 2009).Parametric performance of Eq. (3.16) is

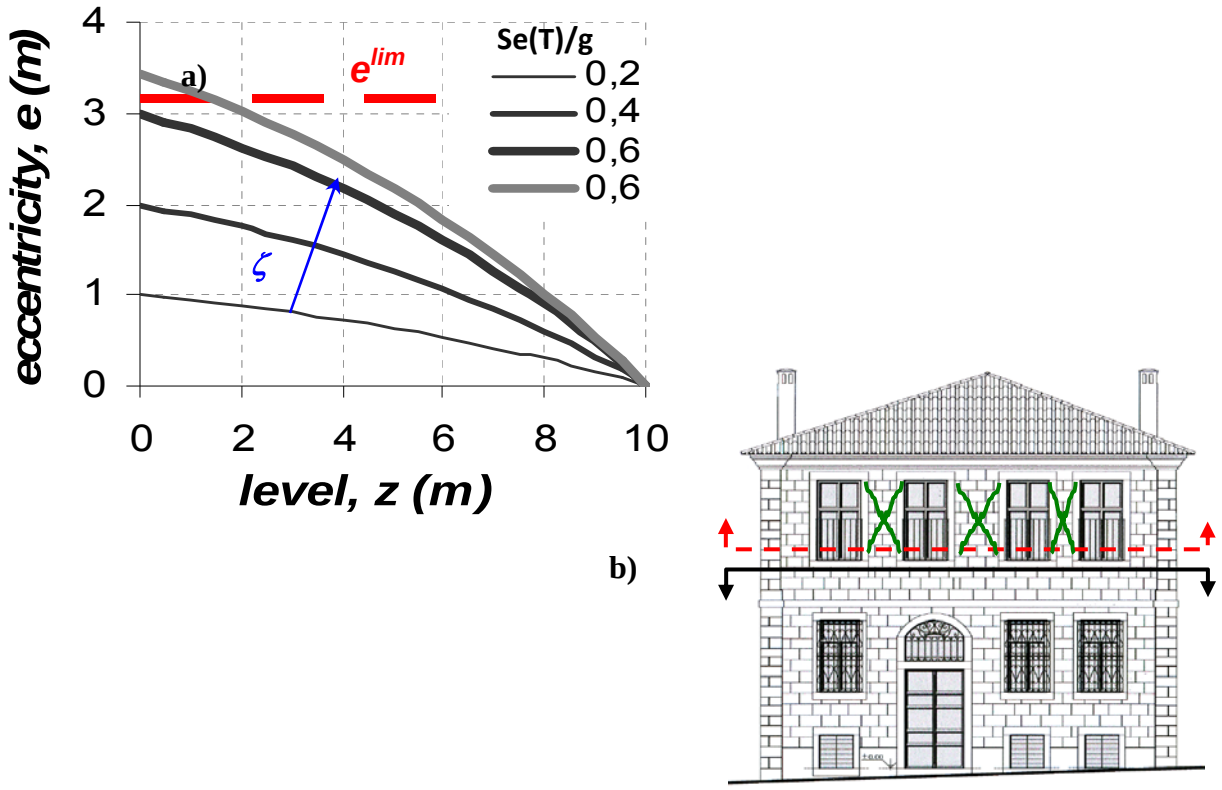

Figure 3.4.a) Eccentricity distribution along the height of a structure with variables being terms $S_e(T)/g$ and ζ. **b)** Levels with different wall areas due to presence of openings (Ratio ζ represents the roof weight expressed as a fraction of the total weight of the structure).

investigated, assuming $H=10m$, $C_m=0.67$, $\zeta=0.1$, $\ell_x=10\ m$ and $\ell_y=8m$ (ζ is ratio of the roof weight divided by the weight of the structure). Figure 3.4(a) depicts the distribution of e along the height of the structure for several values of the ratio $S_e(T)/g$ (i.e. *0.2, 0.4* and *0.6*). It is concluded that increasing the spectral acceleration the structure develops greater levels of eccentricity e. The same trend is obtained by increasing the roof weight. The red dashed line refers to the upper threshold of eccentricity e^{lim} (Eq. (3.17a)). If an eccentricity curve intersects this limit, then plan sections (defined by the level z from the ground, given in the horizontal axis) that are above the line for e^{lim} are susceptible for developing tensile stresses. For these plan sections more detailed evaluation is needed, particularly in the neighborhood of openings. Figure 3.4(a) was drawn for $\zeta=0.1$, without such incident. For $\zeta=0.3$ and $S_e(T)/g=0.6$ (grey curve) normal tension occurs up to the building section *1.5m* from the base of the structure (local wall failure in anticipated in that location, precipitating failure of the structure).

3.4 Acceptance criteria: Base shear strength

The estimated shear demand is compared with the masonry wall shear strength. Here, for the sake of simplicity, masonry is treated as a homogenized material with average mechanical properties, obtained as the weighted mean of mortar and masonry block compressive strengths using empirical, calibrated expressions. Shear strength is supported through frictional and cohesion mechanisms, in the presence of the clamping action of overbearing compression (if it exists). Thus, with reference to Fig. 3.3(b), only the part of the wall cross section in the compressed zone, $A_{w,eff}$, is considered active in resisting the shear force, V_o. Note here that the position of the neutral axis depth varies along the building height, since both the axial load and overturning moment at level z depend on the lateral forces and gravity load of the overbearing part of the structure. Thus, Eq. (3.15) may actually be used to identify complete inactive areas of walls over the entire structure. For example, at the wall base (z=0) the average shear stress demand within the $A_{w.eff}$ wall area is obtained from:

$$\tau_{ave} = \varepsilon \cdot \frac{V_o}{A_{w,eff}} \tag{3.19a}$$

Or, more generally,

$$\tau_{ave}(z) = \varepsilon(z) \cdot \frac{V(z)}{A_{w,eff}(z)} \tag{3.19b}$$

In Eq. (3.19) coefficient $\varepsilon(z)$is an amplification factor, accounting for the reduction in the actual, rather than the gross shear area, $A_{w,eff}$, effected by the presence of openings; thus, ε is the ratio of $A_{w,eff}$ to the minimum effective wall area, $A_{w,eff}^{min}$ in the critical storey. Window openings in the building's facades reduce locally the effective shear-resisting area of the wall cross section at locations where these occur. Referring by $A_{w,eff}^{\min}$ to the cross sectional area of the perforated walls at the level of openings (red dashed line in Fig. 3.4(b)), and considering that the total shear force resisted by two adjacent cross sections is the same (i.e., one section through the openings and one lying just below the openings, marked in Fig. 3.4(b) by red and black dashed-lines, respectively) it follows that the amplified shear demand is $\tau_{ave,amp} = (V/A_{w,eff}) \cdot A_{w,eff} / A_{w,eff}^{min} \geq V/A_{w,eff}$. The magnitude of $\tau_{ave,amp}$ should be less than the shear strength v_{Rd} else failure occurs by diagonal cracking of the adjacent piers. Similar checks may be made with reference to the storey shear at higher floors of the structure. This check is expected to be critical in tall, slender URM buildings with several openings and in structures with stiff diaphragms.

In the absence of diaphragm action, the effective wall area resisting shear may be further reduced by neglecting walls orthogonal to the direction of the ground motion. These walls would only be considered effective in contributing to the shear resistance (i.e. accounted for in $A_{w,eff}$), if they lie within the active area of the plan cross section (with reference to Fig. 3.3) and the diaphragm at the level above the one considered is rigid, so as to ensure equal lateral displacements for all points in its perimeter.

Acceptance criterion is that shear demand should not exceed the shear strength of unreinforced masonry (MPa), v_{Rd}, which is estimated according with a Mohr-Coulomb type frictional law:

$$v_{Rd} = c + 0.4 \cdot \sigma_N \leq 0.065 f_{m,b} \tag{3.20}$$

where, c isthe mean value of cohesion (it is a general practice to take $c=0.5\sqrt{f_{wt} \cdot f_{wc}}$ (MPa), i.e., the weighted mean of the homogenized masonry's compressive and tensile strength. In the examples considered in the present work, it was taken equal to*0.20* MPa), $\sigma_N$is the average normal compressive stress owing to overbearing loads only; $f_{m,b}$ is the mean compressive strength of the masonry units. These values should be obtained from field tests if such are available; otherwise, code-prescribed characteristic values could be used instead. Calibrated expressions for calculating the homogenized compressive and tensile strength as well as the modulus of elasticity of masonry are as follows: the characteristic homogenized strength of masonry $f_{wc}$is estimated from: $f_{wc}=Kf_{mb}^{0.65}f_m^{0.25}$ where f_{mb} is the compressive strength of the bricks, f_m is the mean compressive strength of the mortar (assuming $f_m<min\{20MPa; 2f_b\}$). Parameter K depends on the brick material: $K=0.4\Psi$with $\Psi = (15/f_{mb})^{0.33} <1.5$ for $f_b<15MPa$. Based on these definitions, the associated modulus of elasticity of the material is estimated from, $E=1000f_{wc}$; Table 3.2 contains nominal masonry strength values for mortar with $f_m=5MPa$ (Tomazevic 2006).

Table 3.2.*Homogenized Compressive strength of masonry as a function of the mortar and the brick material (according to Tomazevic, 2006)*

Brick material	f_b **(MPa)**	**Mortar type**	f_m **(MPa)**	f_k **(MPa)**
Clay	2.5	M2	2.5	**1.6**
Silica calcium	5	M5	**5**	**2.5**
Manuf. bricks	15	M10	10	**3.5**

In the case of tier-laced type of masonry, shear strength is enhanced by the contribution of the horizontal tiers (timber or reinforced concrete) intersecting the diagonal plane of failure, v_b, as per Eq. (3.21):

$$v_{Rd}^{tot} = v_{Rd} + v_b \tag{3.21}$$

Consider a tier-reinforced masonry pier under lateral shear deformation (Fig. 3.5). Before development of diagonal cracking owing to the tensile normal stresses σ_{P1} (Fig. 3.3(b)), the tensile force of tiers is small with negligible contribution to the wall's resistance. After initiation of cracking and prior to disintegration of the wall at failure, the bulk masonry and the tiers both contribute to the lateral load resistance, the former degrading with the intensity of imposed lateral drift and number of cycles thereby the latter becoming the prevalent source of shear strength. Assuming a diagonally cracked wall under lateral

loading (Fig. 3.5(b)), it follows from force equilibrium that the shear contribution of tiers V_b (in kN) is,

$$V_b = \sum_{i=1}^{n} A_b f_i \tag{3.22}$$

Where n is the number of tiers intersected by a diagonal crack (i.e. $n = \ell / s$ for 45°inclination) in walls parallel to the seismic action, A_b and f_i are the area and the axial tensile stress in the material that acts as reinforcement in the body of the tier (for steel this is limited by f_{yd} and for timber by f_{wd}). Timber tiers or reinforcing bars in R.C. tiers have a development capacity, f_i, which is controlled by bond stresses developing over the reinforcement-mortar interface, and by the available anchorage length L_{bi} (taken as the least value to the left or to the right of the point of intersection with the crack, to the end of the tier). Thus Eq. (3.22) is rewritten as:

$$v_b = \sum_{i=1}^{n} A_b f_i \quad \Rightarrow \quad v_b = u_b P_{tier} \sum_{i=1}^{n} L_{bi} \tag{3.23}$$

where u_b is the shear strength of the mortar (for simplicity, u_b is taken equal to the cohesion c between bricks and mortar, i.e. $u_b = 0.5(f_t' f_c')^{0.5}$). P_{tier} is the contact perimeter of the tier's cross section ($=2b$ for 2-sided contact of timber tiers with a cross sectional width $=b$). The shear strength of a tier-type masonry pier is estimated (in kN/m^2 after dividing the shear strength with the area of the pier's cross section A_w) from combination of Eqs. (3.20), (3.21) and (3.23):

$$v_{Rd}^{tot} = c + 0.4 \cdot \sigma_N + \frac{u_b P_{tier}}{A_w} \sum_{i=1}^{n} L_{bi} \tag{3.23}$$

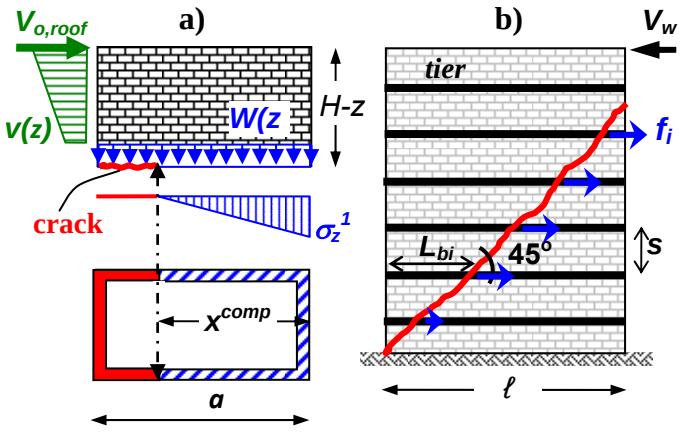

Figure 3.5.a) Free body diagram at level z: areas in tension (red) and compression (blue-hatched) in the plan section. **b)** Cracking of reinforced with horizontal tiers masonry: shear undertaken by the anchorage forces of the tiers.

3.5 Additional Acceptance Criteria: Out of Plane Action

In the works of Karantoni and Pantazopoulou (2013) and Vamvatsikos and Pantazopoulou (2009), acceptance criteria were formulated by which to determine the likelihood of local failure modes of URM structures with flexible diaphragms. Note that in the absence of the kinematic restraint provided by stiff diaphragms, URM structures are much more vulnerable to failure due to out of plane action, i.e., when responding to ground motions that occur normal to their orientation. For such structures, the walls bend out of plane under the influence of normal pressure the magnitude of which is, $p(z) = (z/H)\cdot S_e(T_1)\cdot t\cdot w/g$ (kN/m^2) acting throughout the wall surface from the base to the roof level where w the self-weight per unit volume of the walls (in kN/m^3).

Karantoni and Pantazopoulou (2013) proposed an approximate solution of the state of stress of the walls under the $p(z)$ pressure, obtained by treating the orthogonal walls as vertical plates in the structural model, using simple analysis procedures such as the method of strips. This approach is more consistent with the observed field performance of such structures, even in the presence of openings, as compared to procedures that subdivide the plate to smaller homogenous sub-plates, because in this manner the global boundary conditions of the wall are allowed to play a determining role in the manner by which the system responds; openings may be accounted for by proper amplification of the calculated moments in the strips that contain them.

To simplify the analysis, the walls may be considered fixed or partially restrained to rotation along the vertical boundaries at the corners of the building and at the base (the degree of fixity between orthogonal walls may be considered a parameter of epistemic uncertainty for this problem, in the event of fragility type analysis of this class of structures). The boundary at the roof level is unrestrained in the absence of a continuous confining ring beam tying the perimeter of the roof, or the wall may be considered simply supported at that level (unrestrained against rotation) if a ring beam exists or is added during retrofit. As in the case of plates the direction of load transfer is determined from tributary areas, depending on the boundary conditions on the perimeter of the wall.

Examples of this type of distribution and the ensuing loading pattern of the associated strips are depicted in Fig.3.6for several alternative cases. Note that the static model for strips oriented along z for an unrestrained top boundary lies between the cantilever and the fixed-simply supported case; it is fair to assume that z-strips are closer to the cantilever example if $L_y>L_z$, the reverse if $L_y<L_z$. (In case of densely spaced openings as seen in neoclassical buildings of the European urban centers of the 19th century, the walls in out of plane action could be alternatively solved when assuming the yield line formation which would lead the wall-plate to failure).The degree of fixity at the ends of strips 1 and 3 is reflected through λ: a value of $\lambda=0$ implies no restraint to rotation, $\lambda=0.7$ corresponds to noncompliant fixed supports, $\lambda<0.5$ refers to partial restraint against rotation. $\bar{g}_3$ is an equivalent uniform load for the load case of strip 3.

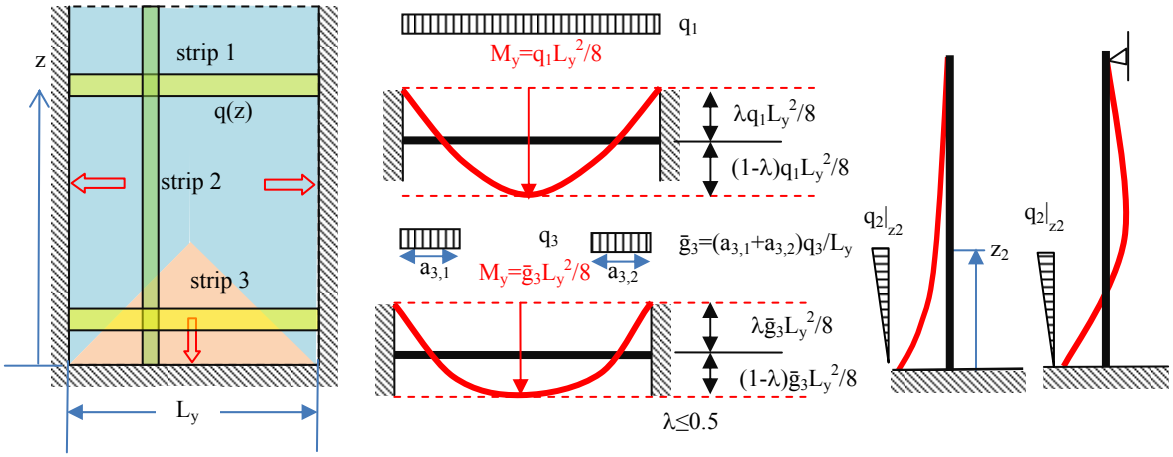

Figure 3.6: Influence Areas and Application of the Strip Method for Estimation of the State of Stress in walls transverse to the Earthquake Action

Acceptance criteria for this problem are related to the moments M_y and M_z (the subscript corresponds to the orientation of the strip considered) which are compared with the cracking moments of the wall; the peak ground acceleration tolerated prior to cracking may be estimated by setting the peak moment equal to the cracking strength. Using the same concept, higher values of peak ground acceleration that may lead to cracking over prescribed fractions of the total wall area may be determined in the process of assessment. By the same token, modifications to the boundary conditions of the walls, as possible rehabilitation measures, may be gauged by the amount of peak tolerable ground acceleration increase they may be able to secure for the building, enabling the structure to sustain a higher magnitude design earthquake through these measures. The cracking moment is estimated from:

$$M_{z,cr} = \left(f_{x1} + w \cdot (H - z)\right) \cdot \frac{t^2}{6} \tag{3.24}$$

and $$M_{y,cr} = f_{x2} \cdot \frac{t^2}{6} \tag{3.25}$$

where f_{x1} and f_{x2} is the flexural strength for failure plane parallel and normal to joints, respectively.

At any level, the moments in the z-strips should be amplified locally by the ratio L_y/ℓ_y, where ℓ_y is the dimension of the plan minus the breadth of the openings. If the strength of the orthogonal walls suffices to support a lower pressure, $p'(z)<p(z)$ than what would be estimated for the applied design value of a_g, then it follows that the assessed base shear strength of the building should be scaled down to the reduced ground acceleration thus estimated.

3.6 Performance Evaluation

The various assessment criteria encompassed by comparisons of Strength Demand vs available Capacity eventually allow for the possibility that earlier modes of failure such as out-of-plane bending of walls oriented orthogonal to the earthquake action may limit the magnitude of the earthquake intensity that may be supported through elastic response. For structures with diaphragms that provide at least a partial degree of restraint against out-of-plane deflections of transverse walls, it is even possible that the in-plane cracking or shear strength of walls parallel to the ground motion may be exhausted at acceleration levels lower than what is prescribed by the seismic hazard (i.e., Eq. 3.8). In these cases, the notion of a behaviour factor, q, may be established, exactly in the same manner as with conventional reinforced concrete structures. Its value, is used to determine the displacement ductility demand of the structure, and eventually the actual inelastic displacement attained at the top of the structure (at the monitored point), which in turn enables assessment of the extent and intensity of the anticipated damage. The procedure by which to perform these steps is as follows:

Lets' assume that in the process of assessment of the structure it is found that the apparent base shear strength at yielding (i.e., at the occurrence of visible cracking in the structure, whether this occurs in the out-of-plane or in the in-plane walls first), is V_y, occurring at a displacement at the point of reference, Δ_y. Beyond that point the resistance curve of the structure is assumed to follow a perfectly plastic branch up until the displacement associated with collapse, Δ_u. Thus,

$$q = \frac{V_o}{V_y} = \frac{C_1 \cdot C_m \cdot S_e \cdot (W/g)}{V_y} \tag{3.26}$$

If the structure had not yielded, then its elastic displacement demand would be $\Delta=(L_e/m)\cdot S_d(T) = \Gamma \cdot S_d(T)$ where L_e the excitation factor and m the effective mass of the equivalent SDOF system representing the structure (from Eq. 3.8), and $\Gamma=L_e/m$. For low period structures such as the common URM stone masonry systems, the equal energy assumption may be used to relate the displacement of the inelastic system, Δ_{inel}, with those of the elastic structure, and therefore, the ductility demand is estimated from,

$$\mu = \frac{q^2+1}{2}, \text{ whereas } \Delta_{inel} = \frac{\mu}{q} \cdot \Gamma \cdot S_d(T) = \frac{q^2+1}{2q} \cdot \Gamma \cdot S_d(T) \tag{3.27}$$

For systems with continuous mass distribution such as the masonry structures, the coefficient Γ is generally >1, and can for all practical purposes be approximated by the value of 1.5.

The estimation of the displacement demand and associated ductility may be used to anticipate the extent of damage in the structure, since, for brittle construction such as that of the URM, demands of $q>2.5$ and $\mu>3$ can hardly be sustained even in the best circumstances when inherent "system" ductility can be relied upon.

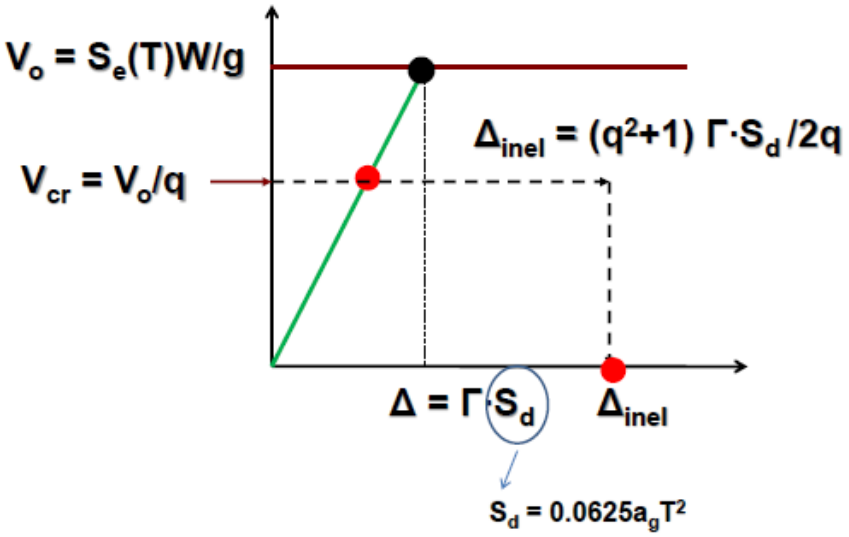

Figure 3.7: Methodology for determining displacement ductility demand and peak inelastic displacement

3.7Numerical Application (Example developed by Karantoni and Pantazopoulou, 2013)

The simplified procedure described in the preceding is meant to be used in rapid seismic assessment of URM structures, so as to determine whether the structure considered can withstand the design earthquake, or alternatively, to determine the magnitude of the ground acceleration that may be sustained without failure. To demonstrate the relevance of the method with more detailed calculations, a typical building was analyzed using a 3-D finite element model (see Karantoni and Pantazopoulou 2013), comprising shell elements for the wall elements of the structure and truss members for the connecting components, the diaphragm and roof elements using the program code ACORD-CP. The general layout of the structure and corresponding F.E. model are depicted in Fig. 3.8(a) and 3.8(b), respectively. Results were correlated with those obtained from the practical procedures described. Comparisons are done along the sections 1-1 and 2-2 in wall T1, and along the sections 3-3 and 4-4 in wall T2. The necessary input data for application of the simplified assessment methods are listed in Table 3.3.

The ground motion was prescribed using the EC8-I design spectrum with peak ground acceleration of 0.16g (in the constant acceleration range the design value of the acceleration at the top of the structure for $S=1$ and $\eta=1$ is, $S_e(T_1)=0.40g$) along each of the principal directions of the building in combination with the self-weight of walls, diaphragms and roof.

A separate additional comparison is made between the values for the out of plane action estimated according with the proposed simplified procedure and those obtained from finite element analysis of the transverse wall. The wall was solved assuming fixed boundaries along the vertical edges and the base, and free edge at the top, under normal pressure acting over its surface. The normal pressure

was varied linearly along the height of the building from zero value at the base, to a peak pressure at roof level (at *z=H*) obtained from:

$$p(z=H) = 2.5 \times 0.16 \times S(=1) \times \eta(=1 \text{ for } \xi=5\%) \times t(0.6m) \times 22kN/m^3 = 5.28\ kN/m^2 \qquad (3.28)$$

Masonry was modeled using $E=0.50E_{el}$where $E_{el}$the modulus of elasticity of the uncracked material state which was estimated from the relationship $E_{el}=1000f_w$, where $f_w=3.5MPa$the mean compressive strength of masonry.

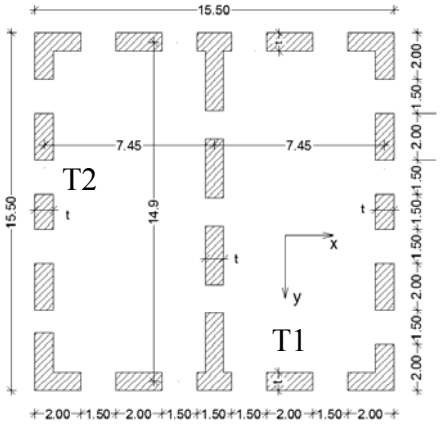

Figure 3.8(a): Plan View of the Structure

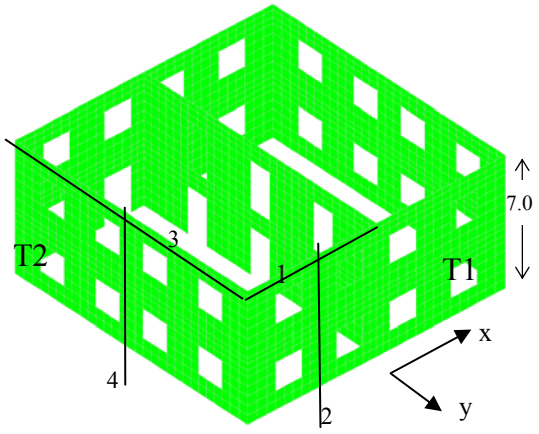

Figure 3.8(b): FE model and reference sections used for comparison with Simple Analysis

Table3.3: Parameter Values Used in Numerical Example

	symbol	value	unit	source
plan dimensions	L1, L2	15.5, 15.5	m	input data
Height	H	7.0	m	input data
Wall surface area in the plan	Ax, Ay	18.6, 27,9	m^2	calculated
Flexural Resistance	Ωx, Ωy	216.29, 192.3	m^3	calculated
Effective cross section	A_{cx}, A_{cy}	2.83, 3.61	m^2	Eq. 3.3
Constant	C_{tx}, C_{ty}	0.044, 0.039		Eq. 3.2
Fundamental period	T_{1x}, T_{1y}	0.191, 0.169	sec	Eq. 3.1
Weight	W	6916.54	KN	calculated
Ground acceleration	a_g	0.16g	m/sec^2	input data
Design spectral acceleration	$S_e(T_1)$	0.40g	m/sec^2	Input data
Weight per unit volume	w	22	KN/m^3	input data
Base shear	V_o	2856.27	KN	Eq. 3.12
Overturning moment	M_o	13329.26	KN	Eq. 3.13
Stresses along x	σ_{P1}, σ_{P2}	-84.25, -222.87	KN/m^2	Eq. 3.14

Stresses along y	σ_{P1}, σ_{P2}	-91.94,-215.19	KN/m^2	Eq. 3.14
Incremental factor for shear	ε_x, ε_y	1.55, 1.43		calculated
Mean shear stress	τ_{ox}, τ_{oy}	0.24, 0.14	MPa	Eq. 3.19
Uniform load	q_1, q_2,	5.28, 2.81	KN/m	Fig.3.28
Uniform load	q_3, $\overline{q_3}$, q_4	5.28,4.96,5.28	KN/m	Fig.3.28

3.7.1 Evaluation under in- plane earthquake action

Figure 3.9 depicts the distribution of axial forces obtained from the seismic combinations $G+E_x$ and $G+E_y$ calculated at the wall thickness midpoint, where G denotes the gravity loads and E_x, E_y the seismic action along x and y axes, respectively. In the example considered it is evident that normal compression is acting in all the perimeter walls at the base of the structure, therefore the entire wall cross section parallel to the earthquake action is actively engaged in shear resistance. This is consistent with the results of the approximate solution where it was found that shear stress demand in all cases was less than the value obtained from Eq. (3.20), not exceeding the value of 0.26 MPa.

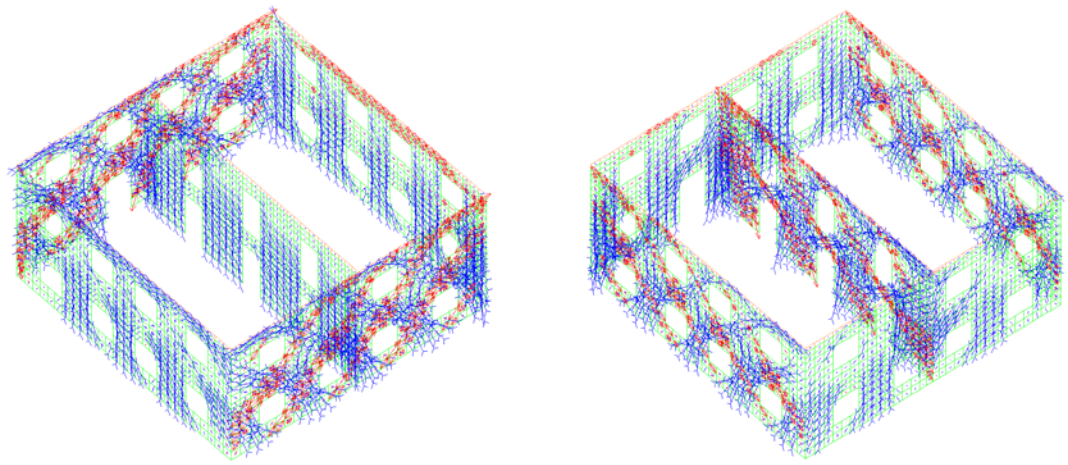

a) **b)**

Figure3.9: Axial Forces N for Load Combination: a) G+Ex and b) G+Ey

3.7.2 Evaluation of out-of-plane response

For the out of plane action moments were compared for the locations in the structure corresponding to strips 1-4 in Fig. 3.6. Table 3.4 presents peak values for flexural stress resultants (moments M_y, M_z per unit width of strip) obtained from: (a) detailed F.E. analysis of the entire structure (spectral analysis), (b) F.E. analysis of the transverse wall under normal pressure that varies linearly height-wise simulating earthquake effects, (c) the proposed simplified assessment method (for earthquake action along y, it was assumed that λ=0.40 and λ=0.60 for the edge and intermediate supports of the transverse wall, to account for the different rotational restraint). All analysis models considered identify consistently as being most critical the case of earthquake action along the x axis (longer unsupported wall in out-of-plane

action). The peak flexural moment occurring at the base of the longer wall bending out of plane is M_z =86.24 KNm; this is compared with the cracking moment $M_{z,cr}$ =12.24 KNm, from Eq. (3.24). Similarly, the maximum midspan moment at roof level, M_y=68.84 is compared with flexural strength $M_{y,cr}$= 6KNm from Eq. (3.25).

Table3.4. Bending Moments

	Ground motion along Y					Ground motion along X				
	Line 1			Line 2		Line 3			Line 4	
model	left	mid-dle	right	Bot-tom z=0.0	Middle z=3.5	left	mid-dle	right	Bottom z=0.0	Mid-dle z=3.5
FE, acc	13.65	-18.56	38.99	16.32	-9.64	56.24	-39.4	56.39	62.11	-13.83
FE, pres	12.07	-7.22	13.58	2.85	-3.72	42.59	-19.14	42.57	23.24	-6.96
Simplified	5.95	-22.35	8.92	12.99	0	68.84	-68.84	68.84	86.24	-26.95

Evidently, out of plane action is the controlling mode leading to failure at a much lower level of earthquake action as compared with the design ground acceleration of 0.16g. The peak spectral acceleration, $S_{ult}(T)$that may be supported by the building without any form of cracking may be estimated from the proposed methodology by setting the critical moment value $M_{y,cr}$equal with that produced by the limiting acceleration value. From solution of strips no. 3 and 4 the limiting value of acceleration was estimated at 0.037g. This acceleration value, $S_{ult}(T)$, is a limit for the so called performance level 1 in the established framework of EC8-I (2004), "Continued Operation". The extent of tolerable damage in the transverse walls, which could be associated to more damage-tolerant performance levels, such as "Reparable Damage" and "Collapse Prevention" ought to be defined with reference to the fact that some degree of ductility is imparted by the membrane forces developed in the masonry walls due to their thickness, which give rise to residual flexural strength in the cracked walls.

3.7.3 Strengthening Strategies

The procedure described was also used to assess the effectiveness of two of the usual rehabilitation schemes used frequently with TURM structures, namely: (a) construction of a ring or tie perimeter beam at roof level, (b) addition of a reinforced concrete plate at roof level to secure diaphragm action. Both techniques are easy to implement, almost concealable in the final project and low cost. Note that the addition of diaphragm plates in intermediate floors is less advisable as it is generally more costly, presents technical difficulties and has little effect in mitigating the out of plane action of the top floor. Implementation procedures are as follows:

3.7.3(i) Addition of a tie beam: Construction of tie beams contributes greatly to the seismic strength of a TURM building. Previous studies have shown that construction of tie beams at the roof level of such structures may reduce by as much as 50% the intensity at the critical upper level against out of plane action, even after removal of internal bearing walls. In the proposed method addition of a tie beam is

reflected by the addition of a support at the top end of the vertical strips, which is important for the longer walls that did not satisfy this criterion based on aspect ratio alone. Furthermore, the influence areas are modified to the more favorable distribution shown in Fig. 3.10 with the critical horizontal strip being located now further down at *z=4.45m*. Peak flexural moments are reduced to M_{y3}*=43.70 KN-m* both at mid-span and at the edges whereas, M_{z4}*=2.15KN-m* at *z=0* and $maxM_{z4}$*=10.96 KN-m* at*z=4.70m*. Again critical is the horizontal strip (#3) from which it is shown that peak tolerable spectral acceleration without cracking (Performance level 1) is *0.055g* corresponding to 48% increase in the strength of the building, consistent with the results from F.E. analysis of traditional unreinforced masonry buildings after rehabilitation with this procedure (Karantoni 2013).

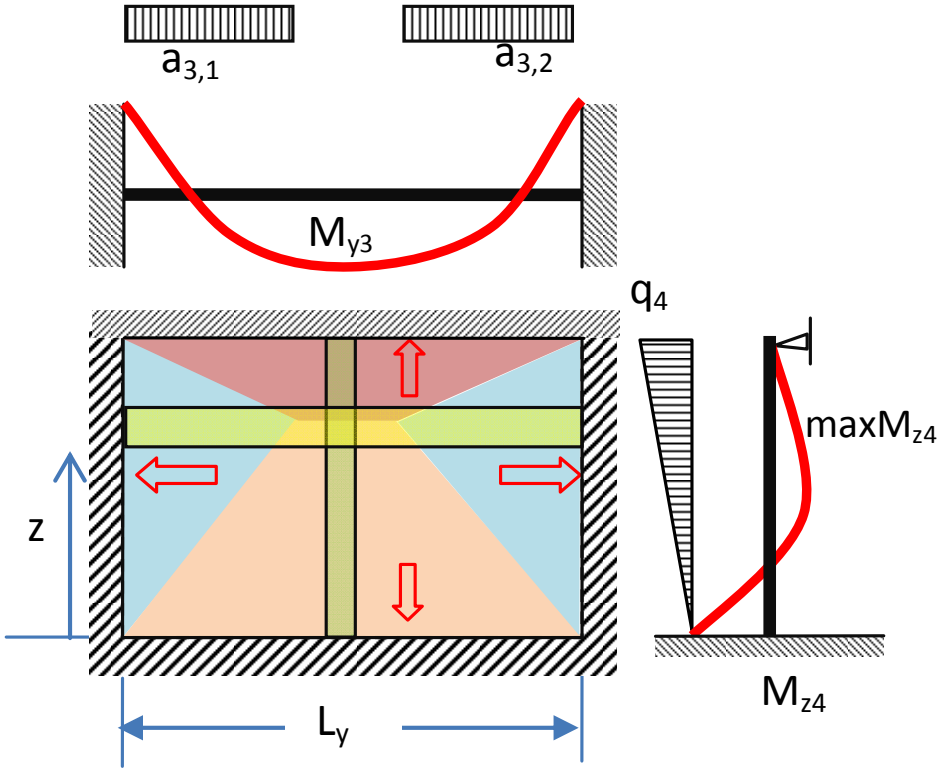

Figure 3.10: Tributary areas and Strip Boundary Conditions: Case with tie-beams

3.7.3(ii) ***Addition of Inextensible Diaphragm at Roof Level :*** Prerequisite for this intervention is the favorable layout of the load bearing walls at the top floor level. In the example structure it is assumed that two continuous plates offering diaphragm action to the floors (each having a theoretical span of 7.45 m, Fig. 3.11) will be constructed. The boundary conditions of the standing walls examined in the preceding will now be re-established to fixed supports on the entire perimeter. The layout of the influence zones and corresponding location of the critical strips are illustrated in the Figure 3.11. Flexural moments in strip 3 at *z=3.5m* are M_{y3}*=34.42 KN-m* both at mid-span and at the ends, whereas the corresponding values in strip 4 are *4* M_{z4}*=2.15KN-m* at *z=0* and $maxM_{z4}$*=12.93 KN-m* at *z=7.0m*. From the

critical strip #3 it follows that the peak spectral acceleration associated with Performance level 1 (onset of first cracking) is *0.07g*, therefore, the building strength is increased by twofold over its initial condition (i.e., 100% strength increase).

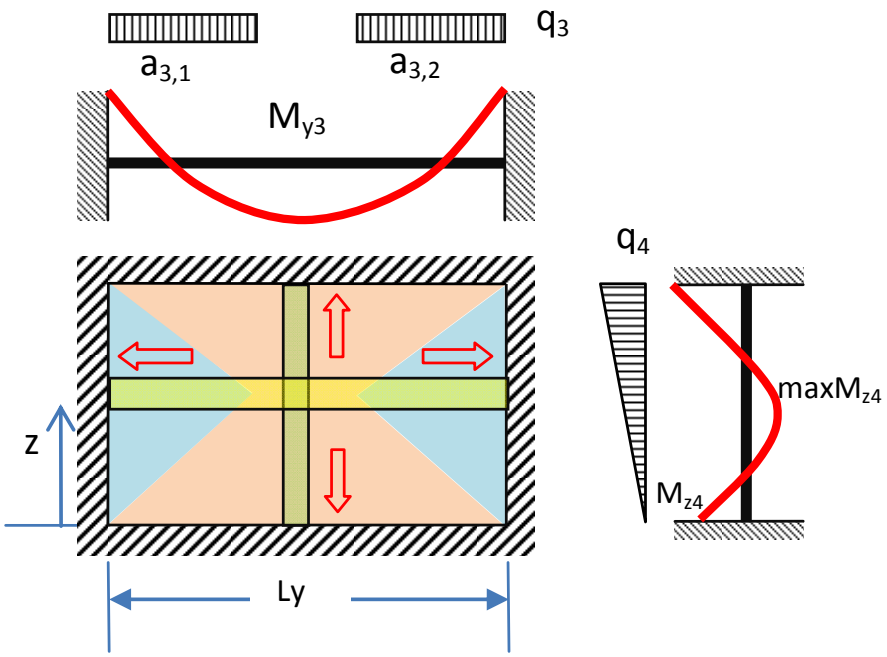

Figure 3.11: Tributary areas and Strip Boundary Conditions: Case with Rigid Roof

3.8 Conclusions

This chapter summarizes the steps of a simple seismic assessment method intended for a first level evaluation of traditional masonry structures. The Mohr - Coulomb frictional model is used to quantify base shear strength owing to the clamping action of the wall's pre-compression. Two indices controlling the adequacy of shear strength as compared to shear demand are determined, one owing to the restoring influence of gravity axial load, and one owing to the influence of overturning seismic moments. Both strength and demand depend simultaneously on the structure's weight whereas shear strength also depends on the mechanical properties of the masonry piers and the contribution of timber tiers. Unfavorable conditions for shear strength are associated with the loss of the clamping action imparted by normal pressures (loss of gravity pre-compression owing to the overturning effect). For direct assessment of this situation a limiting value of eccentricity is proposed as a simple criterion. Amplification of shear demand in perforated walls (with openings) is also estimated for rapid evaluation of the seismic vulnerability of captive piers.

Objective of the chapter was to demonstrate that simple methods of analysis are feasible for URM buildings, particularly the so-called box-type structure with flexible diaphragms. The performance of the mechanistic arguments established herein are proof tested, through comparison with detailed

finite element analysis, a simple, easy to implement, rapid assessment procedure for traditional, unreinforced masonry buildings, which populate the historical regions of old towns and cities in the Mediterranean region. The typical URM structure considered is built of stone or clay-brick masonry, and despite the architectural details that vary throughout the major region in consideration, it typically has flexible diaphragms and inadequately-tied roof perimeter beams. These structures are particularly vulnerable to seismic effects particularly in light of the large mass of the vertical walls, and the controlling mode of failure is out of plane bending. It is shown that the proposed methodology consistently estimates the mode of failure in the original structure, but also after rehabilitation, underscoring the salient characteristics of URM buildings that may cause their demise in an earthquake, and how by changing these characteristics an improved performance may be anticipated, as quantified herein by the increased level of ground acceleration that the structure may support with no cracking.

APPENDIX TO CHAPTER 3: Design Charts

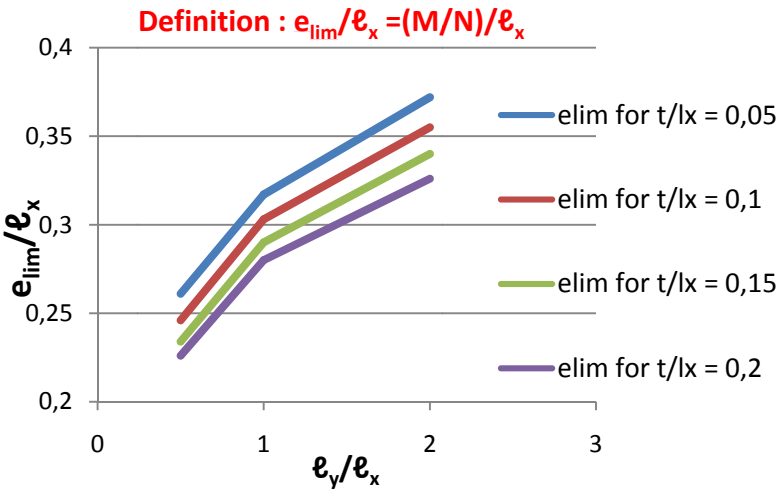

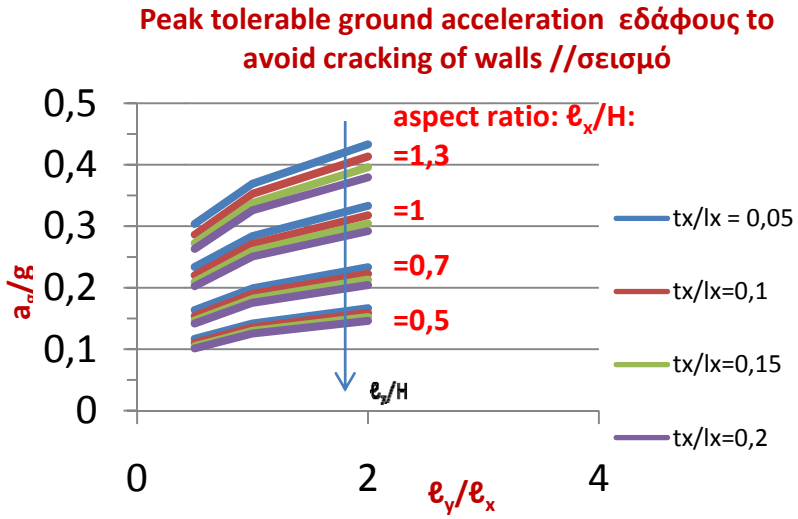

CHAPTER 4 – SIMPLIFIED MECHANICAL MODEL FOR EVALUATION OF THE DYNAMIC RESPONSE OF MASONRY

Co-authored with D. Vamvatsikos, Lecturer at NTUA, Greece

4.1 Scope: Although global indices of URM building response such as base shear demand, and stress-related acceptance criteria may be established in a relatively straightforward manner using the simplified analysis procedures described in Chapter 3, localization of demands and damage assessment is not possible unless deformation measures may be estimated in the critical locations throughout the structure. To enable a performance-based assessment, where damage may be quantified from the intensity of deformation demand it is important to also have information of the displaced shape assumed by the structure during the excitation, particularly at points of peak response. Furthermore, this would enable specific estimation of the important dynamic characteristics of the equivalent single degree of freedom representation of the structure (Period, Mass Participation, lateral drift in the horizontal and vertical plane of action), by parametrically accounting for the partial restraint provided by flexible diaphragms. Note that due to the low percentage of mass participation in the fundamental mode of structures with distributed masses, the lateral shape of vibration at peak response may comprise participation of more than just the fundamental mode. To address this need, consistent 3D shape functions are formulated in this chapter, in order to approximate the lateral shape of vibration considering both in-plane and out-plane wall bending as a result of insufficient diaphragm action. Parametric expressions for the dynamic properties are derived in terms of the important geometric, material, and system characteristics, and are used to express local demand from global estimates. Acceptance criteria are established in terms of deformation (both demand and supply in the critical locations of the structure), through transformation of global response quantities to local measures. An application example of the proposed assessment methodology is included, to demonstrate the ability of the model to reproduce the essential features of traditional masonry buildings under seismic action.

4.2 Mechanical Model

4.2.1 Extending the concepts of Pushover Analysis

The framework of performance-based seismic assessment methodologies for moment-resisting reinforced concrete frames which has been developed in the past twenty years forms the natural background for development of similar methods geared towards masonry structures. The commonest and most palatable of the available options are spectrum-based approaches where the structure is considered in its fundamental mode of vibration through the Equivalent Single Degree of Freedom (ESDOF) idealization (EC 8-I (2004), Appendix B). The associated resistance (pushover) curve is obtained considering load patterns that follow the height-wise profile of the translational mode.

However, a significant difference between RC moment resisting frames and URM structures exists, that renders direct applicability of the established procedures to masonry buildings rather improper: Reinforced concrete frame structures are for the most part lumped systems with stiff diaphragms, whereas traditional masonry buildings are distributed mass and stiffness systems and, having for the most part flexible diaphragms, they do not allow for kinematic interdependence between the translational degrees of freedom at any floor level. The consequence of this characteristic is that the fundamental mode of vibration engages a disproportionately low fraction of the building mass, well below the 75% cutoff value for mass participation which is a pre-requisite for the application of the simple ESDOF-based methods.

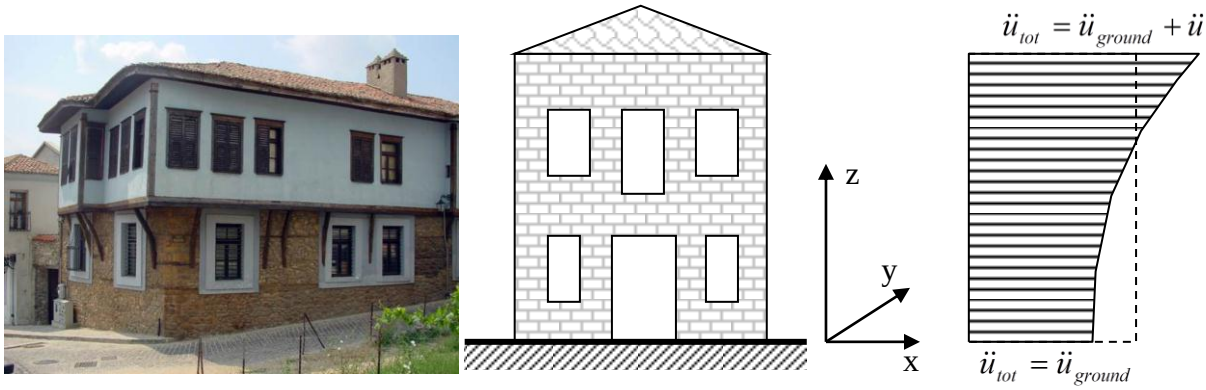

Figure 4.1. (a) Typical example of timber laced stone-masonry dwelling in Xanthi. (b) Idealized Building Model (c) Variation of *total* translational accelerations throughout the building height.

The alternative option of multimodal pushover analysis can only be realistically applied in practice strictly with elastic finite element analysis of masonry (Paraskeva and Kappos 2009, Elnashai 2001). A reason is, that realistic representation of the 3-D behavior of masonry walls requires shell element modeling in order to accurately represent both the in plane and out-of-plane action, whereas the various contacts between different materials in masonry structures (timber to stone, stone to soil, etc.) are usually unilateral or inelastic. In most cases the effort required to obtain dependable results coupled with the degree of uncertainty regarding the actual model properties render this approach beyond the scope of preliminary assessment for special monumental structures and beyond the realm of practitioners for assessment of usual URM structures. Equivalent frame models (Lagomarsino 2013) can be useful in reproducing local modes of failure in some cases, but they may not take into account the effect of global modes of failure on the dynamic characteristics of the structure.

In order to extend the concepts of classical pushover analysis to masonry structures the translational displacement shape is required, $\Phi(x,y,z)$, which is assumed by the structure at the peak of its dynamic response to horizontal ground motion. Through this shape it is also possible to identify and localize the likely points of concentration of anticipated damage from the resulting distribution of deformation implicit in $\Phi(x,y,z)$, while at the same time identifying locations where lack of stiffness may occur and the relative significance of possible mass or stiffness discontinuities.

The shape of lateral translation, $\Phi(x,y,z)$, at the peak of earthquake response, most likely comprises contributions of several modes and mechanisms of deformation, and must necessarily

engage a significant fraction of the system's mass during vibration as usually occurs with a random motion such as the ground excitation. In the present study, in order to establish its form, the structure is subjected to a horizontal gravitational field that acts in the direction of the earthquake considered. This approach is based on the observation that pointwise throughout the structure, the earthquake loading *p(x,y,z,t)* is proportional to the systems' mass, *m(x,y,z)*, as follows:

$$p(x,y,z,t) = m(x,y,z) \times \ddot{u}_{tot}(x,y,z,t) = w_d(x,y,z) \cdot \frac{\ddot{u}_{tot}(x,y,z,t)}{g}; \quad g = 9.81 m/s^2 \tag{4.1}$$

where, $w_d(x,y,z)$ is the associated value of the weight, and $\ddot{u}_{tot}$ is the distribution of total acceleration throughout the structure; this starts from the value of peak ground acceleration, $\ddot{u}_{ground}$, at ground level, and increases to the total acceleration of the system at the crest of the roof, $\ddot{u}_{tot} = \ddot{u}_{ground} + \ddot{u}$, where *u* is the relative displacement of the structure with reference to its base support (i.e., the distribution of total accelerations in Eq. (4.1) follows a trapezoidal-like distribution, as shown in Fig. 4.1(c)). From Eq. (4.1) it follows that the earthquake forces have the same spatial distribution as the mass, naturally increasing with height along with the lateral acceleration. In the proposed approach for finding the shape of lateral translation, whereby a lateral gravitational field is used to simulate the pattern of the earthquake forces, the increase in intensity which is owing to the variation of accelerations is essentially neglected. This is equivalent to assuming a uniform pattern of acceleration along the height of the structure (as shown by the dashed line in Fig. 4.1(c)).

The resulting lateral displacement of the structure, $u_d(x,y,z)$, owing to the application of the pointwise value of the weight in the direction of seismic action, has the advantage of satisfying all the essential and natural boundary conditions of the structural vibration problem. For example, the restoring forces that resist the applied gravitational field in the direction of the earthquake satisfy the associated dynamic equilibrium equation since:

$$k \cdot u(x,y,z) = m(x,y,z) \frac{\ddot{u}_{tot}(x,y,z,t)}{g} \tag{4.2}$$

and,

$$k \cdot u_d(x,y,z) = w_d(x,y,z) = m(x,y,z) \cdot g \tag{4.3}$$

It may be shown easily through calculation that the translational shape of vibration, obtained by normalizing the shape of u_d according with: $\Phi(x,y,z) = u_d(x,y,z)/u_{d,max}$, results in a mass participation factor in the direction of earthquake action, in the range of 90% or more (see Pardalopoulos et al. 2013). This procedure has the practical advantage that it enables the use of the familiar features of classical shell analysis software that are used routinely for gravity load analysis of distributed mass systems with sole input modification over conventional gravity load analysis being the direction of acting gravitational field selected by the user (e.g. SAP 2000).

Using the translational shape of vibration, the natural frequency of vibration of the system may be approximated with sufficient accuracy using the Rayleigh quotient as follows:

$$\omega^2 = g \cdot \frac{\int_{\Omega} m \cdot u_d \cdot d\Omega}{\int_{\Omega} m \cdot u_d^2 \cdot d\Omega} \tag{4.4}$$

Therefore, seismic demands may be determined in terms of total acceleration and displacement of the associated single degree of freedom system (EC8-I 2005, Appendix B or ASCE-41/06). It was stated in Chapter 3 that the design lateral forces (seismic demand and supply) for load-bearing unreinforced masonry structures, V_{Sd} and V_{Rd}, both depend on the distribution of mass of the URM building (the force demand increases with the system's mass, whereas the frictional resistance at any horizontal plane of sliding increases with the overbearing weight of the structure which is also proportional to the mass (Tastani et al. 2009)). For example, higher gravity loads attract a higher seismic base shear (greater mass), but the lateral shear resistance of the walls also increases through enhanced friction. Thus the two terms in the design inequality

$$V_{Sd} < V_{Rd} \tag{4.5}$$

interact, to the extent that structural safety may only be assessed for a specific seismic hazard spectrum. In light of the uncertainties in the input and the complexity of the mechanical problem, determination of the performance point for a given ground motion is estimated based on elastic analysis, making allowance for ductility in moderation the force demands and in magnifying the displacement demands. To further simplify the process, the important step of the calculation of the shape of translational vibration, $\Phi(x,y,z)$, and the associated characteristics of an equivalent SDOF (ESDOF) approximation of the load-bearing masonry structure are estimated through simplifying assumptions in the following sections so as to obtain closed form solutions that may provide the basis for easily applicable assessment tools. The essential derivations are listed in the following sections.

4.2.2 Estimation of the ESDOF system displaced shape under lateral translation

Consider a box-shaped rectangular-plan building having external plan dimensions a_{ext}, b_{ext}, with perimeter walls of uniform thickness t and height H (Fig. 4.2a, b) The corresponding midline dimensions (in the centerline of the walls) are $a = a_{ext} - t$, $b = b_{ext} - t$. Henceforth, without any loss of generality, the earthquake loading is assumed to act along the *longitudinal* wall of length a, and perpendicular to the *transverse* wall of length b. In order to approximate the deformed shape assumed by the building at peak lateral translation in response to the earthquake, the structure is considered under the action of an assumed field of uniform horizontal acceleration acting in the direction of interest. For simplicity the magnitude of the applied acceleration is that of the acceleration of gravity (i.e. 10m/s^2). Through this approach the structure may be analyzed by essentially subjecting it to its own gravity, only this time it is taken to act in the direction of the earthquake (Fig. 4.2c). The resulting load on the perimeter walls corresponds to a uniform field force $q(z)$ defined by:

$$q(z) = q = 2\rho_w t(a+b)g, \quad z \in [0, H] \tag{4.6}$$

where, ρ_w is the mass density of the wall masonry and g the acceleration of gravity.

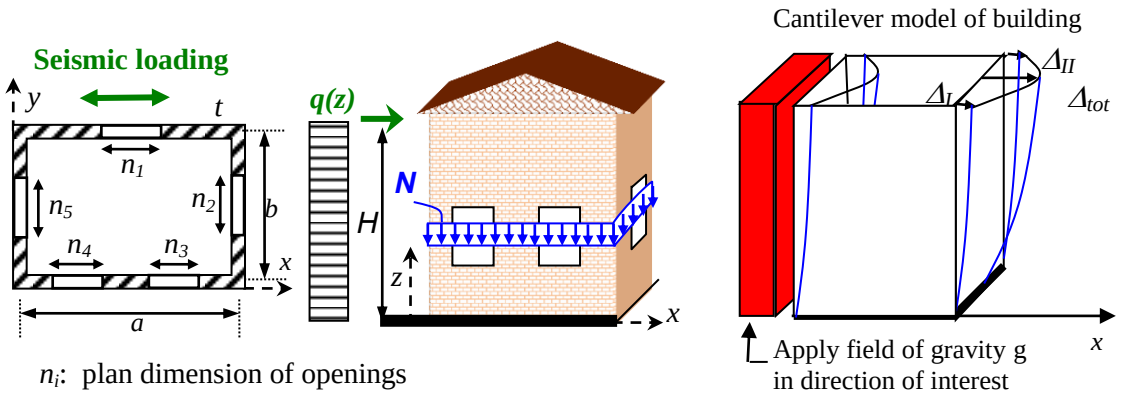

Figure 4.2. (a) Typical plan of traditional masonry structure, (b) seismic loading, and (c) method used to approximate fundamental lateral translational mode of vibration.

As illustrated in Fig. 4.2(c), the displaced shape assumed by the structure, in the absence of diaphragms, comprises contributions that result from deformation of walls oriented parallel to the seismic action, and walls orthogonal to the direction of the excitation. Walls parallel to the earthquake action are loaded in their plane of action, so that they deform *in-plane*. Walls orthogonal to the direction of excitation are loaded normal to their plane of action deforming *out-of-plane*. The in-plane components of deformation are referred to for brevity as type-I components. These collectively account for (a) the shear distortion occurring in walls parallel to the load, (b) the amplification of lateral distortion at the level of openings due to the increased lateral compliance of the structure at that level, and (c) for the flexural drift caused in the structure by the overturning moment of the distributed lateral pressure. The value of the type I components only depends upon the vertical coordinate z, but not on the in-plan coordinates x or y.

The out-of-plane components primarily comprise lateral deflections experienced by the transversal walls which are bent in flexure about their weak axis and they are referred to in the remainder as type-II components. Their magnitude represents relative displacements of points in the building plan – i.e., within the horizontal plane. They depend on the position of the points considered, (i.e., on x and y pointwise coordinates). The effect of diaphragms becomes a factor on the flexure-only terms of the deformation patterns (i.e., on type I and II components), modulating their contribution to the total.

By combining these contributions the deformation of the structure at any point are defined. Of particular interest is the peak lateral translation (usually at some point in the crest of the building), as it will be used to normalize the displacement profile so as the determine a shape, $\Phi(x,y,z)$. The point where the displacement shape after normalization is equal to 1.0 defines the control node of the structure, in pushover terms. In symmetric structures this usually occurs at the midcrest of a transverse wall that is bending out of plane (see Figure 4.2c), and the estimation of its displacement for a given level of seismic loading is the goal of the following subsections.

4.2.3 In-Plane Contributions to Lateral Translation: Type I components

If the building is seen as a cantilever structure fixed at ground level and free at the roof, having a box-type cross section as defined by the plan of the building, then the walls parallel to the direction of the load serve as the web of the cantilever. At any level z from the fixed end, the shear force $V(z)$ and associated shear strain $\gamma_s(z)$ along the building height in the web become:

$$V(z) = \int_z^H q(\zeta)\,\mathrm{d}\zeta = q\left(H - z\right) \tag{4.7}$$

$$\gamma_s(z) = \frac{V(z)}{G_w A_w} = \frac{q\left(H - z\right)}{A_w G_w} \tag{4.8}$$

where the shear modulus of the walls is G_w and the wall shear area is taken to be equal to their plan area $A_w = 2t\cdot(a+b)$. The resulting horizontal displacement along the loading direction x becomes

$$d_s(z) = \int_0^z \gamma_s(\zeta)\,\mathrm{d}\zeta = \frac{qz\left(2H - z\right)}{2A_w G_w} \tag{4.9}$$

And the maximum displacement due to shear at the top of the walls is

$$\Delta_s = d_s(H) = \frac{qH^2}{2A_w G_w} \tag{4.10}$$

Similarly, the moment $M(z)$ and curvature $\phi(z)$ along the height become:

$$M(z) = \int_z^H V(\zeta)\,\mathrm{d}\zeta = \frac{q\left(H - z\right)^2}{2} \tag{4.11}$$

$$\phi(z) = \frac{M(z)}{EI_{plan}} = \frac{q\left(H - z\right)^2}{2EI_{plan}} \tag{4.12}$$

Considering the case where the transverse wall is not allowed to bend locally out of plane, i.e. as if being restrained by an axially rigid diaphragm, the estimated displacement (type I component) along the height of the wall and the corresponding maximum displacement at the top due to flexure would be:

$$d_{f,I}(z) = \int_0^z \phi(\zeta)(z-\zeta)\,d\zeta = \frac{qz^2}{24EI_{plan}}\left(6H^2 - 4Hz + z^2\right), \tag{4.13}$$

$$\Delta_{f,I} = d_{f,I}(H) = \frac{qH^4}{8EI_{plan}} \tag{4.14}$$

In Eq. (4.14) the moment of inertia I_{plan} of the composite plan of the structure (comprising both longitudinal and transverse walls) is defined by:

$$I_{plan} = \frac{(b+t)(a+t)^3}{12} - \frac{(b-t)(a-t)^3}{12} \tag{4.15}$$

The local increase of the shear compliance of the walls at the level of window openings was disregarded in obtaining Δ_s from Eq. (4.10). Note that the shear force resultant, $V(z)$ only depends on the level of the cross section examined, defined by coordinate z, regardless of the presence of openings. However, the average shear stress, $\tau(z)$, is amplified locally at the level of openings due to the reduced area of the wall supporting the shear force. The local increase in the average shear stress value is:

$$\tau_{add}(z) = \frac{V(z)}{(1-p_o)A_w} - \frac{V(z)}{A_w} = \frac{V(z)}{A_w} \cdot \frac{p_o}{1-p_o} \quad z \in [z_1, z_2] \tag{4.16}$$

where p_o is the percentage of the wall plan area A_w (including both longitudinal and transverse walls) occupied by the openings and z_1, z_2 are the lower and upper levels of the opening respectively. The corresponding additional shear strain occurring between levels z_1 and z_2 is,

$$\gamma_{s,add}(z) = \frac{V(z)}{A_w G_w} \cdot \frac{p_o}{1-p_o} = \frac{q(H-z)}{A_w G_w} \cdot \frac{p_o}{1-p_o}, \quad z \in [z_1, z_2] \tag{4.17}$$

which causes an increase in horizontal displacement at every level $z \geq z_1$:

$$d_{s,add}(z) = \int_{z_1}^{z} \gamma_{s,add}(\zeta)\,\mathrm{d}\zeta = \begin{cases} \dfrac{qp_o}{A_w G_w (1-p_o)}(z-z_1)\left[H - 0.5(z+z_1)\right], & \text{if } z \in [z_1, z_2] \\ \dfrac{qp_o}{A_w G_w (1-p_o)}(z_2-z_1)\left[H - 0.5(z+z_1)\right], & \text{if } z \in [z_2, H] \end{cases} \tag{4.18}$$

The added displacement at the top now becomes

$$\Delta_{s,add} = d_{s,add}(H) = \frac{qp_o}{A_w G_w (1-p_o)}(z_2-z_1)\left[H - 0.5(z_2+z_1)\right] \tag{4.19}$$

If more than one groups of openings at different levels of z_1, z_2 are to be examined, further $\Delta_{s,add}$ terms will need to be added, one for each group.

4.2.4 Contributions to Lateral Drift from Out-of-Plane Flexure of the Transverse Walls – Type II Components

The final term needed to complete the deformation analysis is owing to the out-of-plane flexure of the transverse walls (type II component). Each transverse wall is modeled by a rectangular plate supported on three out of four edges and uniformly loaded. One edge (the bottom connecting to the foundation) is considered clamped. The other two adjacent edges (where the transverse wall is supported by the longitudinal ones) are partially restrained against rotation about the z axis. If the two partially clamped edges are taken to the limit of simple supports (no rotational restraint), then the analytical solutions by Timoshenko & Woinowsky-Krieger [page 210, Table 39, (1987)] for the

deformation shape due to uniform loading are applicable. By incorporating an empirical factor to take into account the effect of partial clamping then, the maximum displacement at the middle of the free edge (midcrest point) under uniform load $q_x = \rho_w g t$, becomes:

$$\Delta_{f,II} = a_1 a_2 \frac{\rho_w g t H^4}{D_{plate}} \tag{4.20}$$

where

$$D_{plate} = \frac{E_w t^3}{12(1-\nu^2)} \tag{4.21}$$

and a_1, a_2 are coefficients that depend on the aspect ratio H/b of the wall. a_1 may be estimated analytically as the limit of summation of the terms of an infinite series provided by Timoshenko & Krieger. Alternatively, by performing nonlinear regression of the results for the aspect ratio H/b ranging between 0 and 3 (which is the range of practical interest for the types of structures considered) the following expression is obtained (depicted in Fig. 4.3(a)):

$$a_1 = 0.0130\left[0.143 + (H/b)^{2.93}\right]^{-1.16} \tag{4.22}$$

Multiplier a_2 is approximated roughly by a linear function for the same range of values for the aspect ratio. It is meant to reproduce the effect where a relatively tall wall ($H > b$) will see its midcrest displacement reduced by a greater percentage due to the partial clamping of the vertical edges. Some guidance in choosing its value is provided through additional solutions in Timoshenko & Krieger (1987) for the limit case where all three edges are clamped (Fig. 4.3b):

$$a_2 = 1 - 0.2H/b \tag{4.23}$$

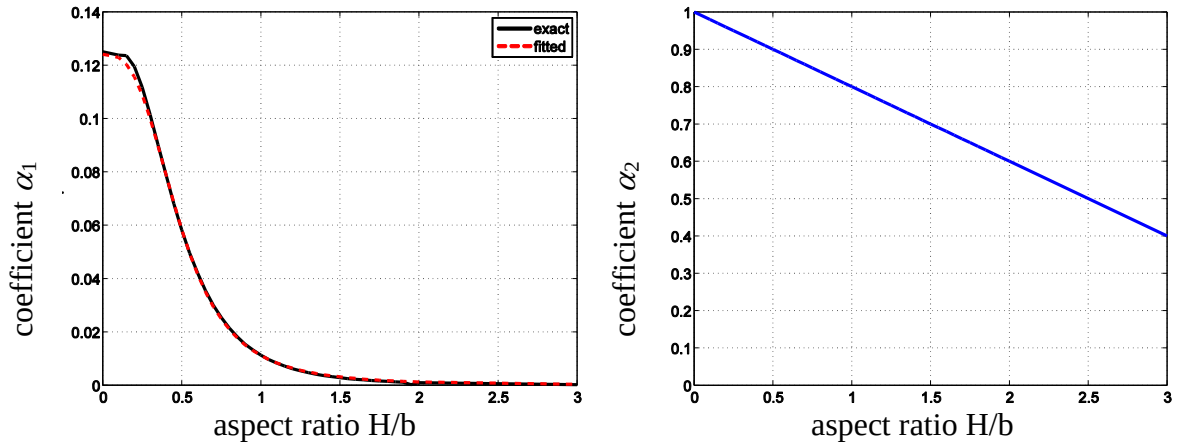

Figure 4.3: The coefficients used in determining type II flexural deformation at the transverse wall midcrest: (a) Regression of the a_1 coefficient via Eq (4.22), (b) a_2 coefficient by Eq. (4.23).

4.2.5 Effect of Diaphragms in Moderating Out-of-Plane Deformation

The presence of a diaphragm affects the shape of lateral translation of the structure by (a)

restraining the type I flexural deformation of walls parallel to the seismic action, and (b) reducing the out-of-plane (type II) flexural deformation of transverse walls. Both effects are represented by empirical reduction factors, namely $\lambda_{f,I}$ and $\lambda_{f,II}$ that define what percentage of the (unrestrained) flexural deformations $\Delta_{f,I}$ and $\Delta_{f,II}$ participates in the total midcrest displacement.

The bending stiffness of diaphragms relative to the walls is what determines the contribution of the type I flexural deformation to the control-node (midcrest of transverse wall) displacement. Factor $\lambda_{f,II}$ is similarly a direct function of the axial (extensional) stiffness of the diaphragm. The nature of the function connecting the parameters of interest may only be found for specific cases by numerical methods (e.g., FE analysis). Simpler approximations can also be employed, as shown in the Appendix.

4.3 Total Displacement at Mid-Crest and Translational Mode Shape

The peak lateral displacement is expected to occur at the mid-crest of the transverse wall owing to the local amplification effected by the out-of-plane bending of transverse walls unsupported at the crest. Type I displacements prescribe the translation, in the direction of the earthquake, of the walls parallel to the load and thus, of the corner supports of the transverse walls. They comprise the shear deformation of the walls with their openings and the flexural deformation of type I:

$$\Delta_I = \Delta_s + \Sigma\Delta_{s,add} + \lambda_{f,I}\Delta_{f,I} \tag{4.24}$$

The transverse walls displace in the direction of the earthquake by out of plane action: the additional deflection occurring at mid-span relative to their corner supports due to Type II deformations is:

$$\Delta_{II} = \lambda_{f,II}\Delta_{f,II} \tag{4.25}$$

The total mid-crest displacement is:

$$\Delta_{tot} = \Delta_I + \Delta_{II} = \Delta_s + \Sigma\Delta_{s,add} + \lambda_{f,I}\Delta_{f,I} + \lambda_{f,II}\Delta_{f,II} \tag{4.26}$$

The contribution of each component of deformation to the shape of lateral translation of the entire structure is obtained by normalizing the terms of the above equation with the total displacement at mid-crest, Δ_{tot}.: the resulting normalized displacement pattern at that point assumes the value of 1.0 and thus, the associated point may serve as the control node in determining the performance point on the pushover curve of the structure, from an ESDOF type analysis (ATC 41 (2007), EC-8 (2004)). For each mechanism of deformation the following participation factors in the final shape are defined:

$$\delta_I = \frac{\Delta_I}{\Delta_{tot}};\ \delta_{II} = \delta_{f,II} = \frac{\lambda_{f,II}\Delta_{f,II}}{\Delta_{tot}};\ \delta_s = \frac{\Delta_s}{\Delta_{tot}};\ \delta_{s,add} = \frac{\Sigma\Delta_{s,add}}{\Delta_{tot}};\ \delta_{f,I} = \frac{\lambda_{f,I}\Delta_{f,II}}{\Delta_{tot}} \tag{4.27}$$

so that $\delta_I + \delta_{II} = (\delta_s + \delta_{s,add} + \delta_{f,I}) + \delta_{f,II} = \mathbf{1}$.

Each participation factor is used to scale the respective deformation functions in the total translational shape of peak response. For type I components the functional forms are defined from Eqs. (4.9), (4.13) and (4.19), as follows:

$$\begin{aligned}\Phi_I(z) &= \Phi_s(z) + \Phi_{s,add}(z) + \Phi_{f,I}(z) \\ &= \delta_s \frac{z(2H-z)}{H^2} + \delta_{s,add} \frac{\Sigma d_{s,add}(z)}{\Sigma \Delta_{s,add}} + \delta_{f,I} \frac{z^2}{3H^4}\left(6H^2 - 4Hz + z^2\right)\end{aligned} \tag{4.28}$$

Note that the last two terms in the right hand side of Eq. (4.28) are typically dwarfed by the shear deformation of the wall without openings. To further simplify this approximation, these two terms are lumped into the first (shear deformation component) by replacing the participation coefficient δ_s with δ_I (Eq. 4.29).

$$\Phi_I(z) \approx \delta_I \frac{z(2H-z)}{H^2} \tag{4.29}$$

While the neglected contributions may be important locally, as they are amplifying point-wise values of strains and curvatures, they are of little significance in estimating the global equivalent SDOF properties: Typically, δ_s will account for more than 80% of the total type I deformation. Thus, Eq. 4.29 will be ideal in practical estimation of the ESDOF system period and participation factor, whereas Eq. 4.28 may be used to obtain local deformation demands from global estimates.

The type II flexural deformation shape of the wall is a more complicated function, which, for the sake of simplicity is represented in an approximate way in the present study. Thus, at any given distance from the base, *z*, relative outwards displacements across the width of the building, *b*, follow a function that ranges between a sine and a cosine shape, depending on the value of a constant, *c*:

$$\Phi_{f,II}(y) = \frac{\sin(c\pi y/b - p_c) + \sin(p_c)}{1 + \sin(p_c)}, \quad where \quad p_c = (c-1)\pi/2 \tag{4.30}$$

The significance of this assumption pertains to the degree of clamping at the vertical supports of transverse walls as implied by the lateral deflected shape of the plan of a simple rectangular structure depicted in the mode shapes of Fig. 4.4(a) or (b). Thus, parameter *c* takes on values between 1 and 2 thereby transforming the function of Eq. (4.30) from a half-sine shape (appropriate for modeling out-of-plane deflection of a wall pinned at the ends) to a full cosine shape (for modeling a wall with fully clamped ends) to represent different degrees of fixity along the vertical edges of the transverse wall.

The partial clamping is best represented by a value of *c* = 1.5, which is adopted for the local shape in order to define *local* failure criteria. Based on extensive parametric studies with the above expression, there is little to be gained for the global ESDOF system properties by using the more complex expressions associated with this value of *c*. Thus the simpler and analytically more tractable sinusoidal shape of *c* = 1 is preferred instead, when extracting the *global* ESDOF system properties. Variation along the height z is provided by a cubic polynomial that resembles the shape of shear deformation found earlier. Altogether, the type II relative displacement shape of the transverse wall which determines the additional lateral translation of points in the transverse walls relative to the wall edges (whose displacements in the translational shape were already defined by Eq. (4.30)),

becomes:

$$\Phi_{II}(y,z)=\Phi_{f,II}(y,z)=\delta_t\frac{z^2(2H-z)}{H^3}\frac{\sin(1.5\pi y/b-0.25\pi)+\sqrt{2}/2}{1+\sqrt{2}/2}$$
$$\cong\delta_t\frac{z^2(2H-z)}{H^3}\sin\frac{\pi y}{b},\qquad y\in[0,b],\quad z\in[0,H] \tag{4.31}$$

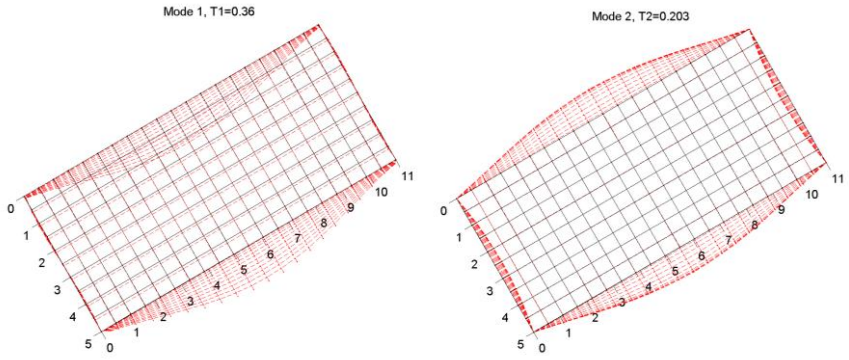

Figure 4.4. (a), (b) Plan-view of the first two eigenmodes for a rectangular-plan masonry structure with flexible diaphragms (*H* = 6m, *a* = 5m, *b* = 11m, *t* = 0.60m).

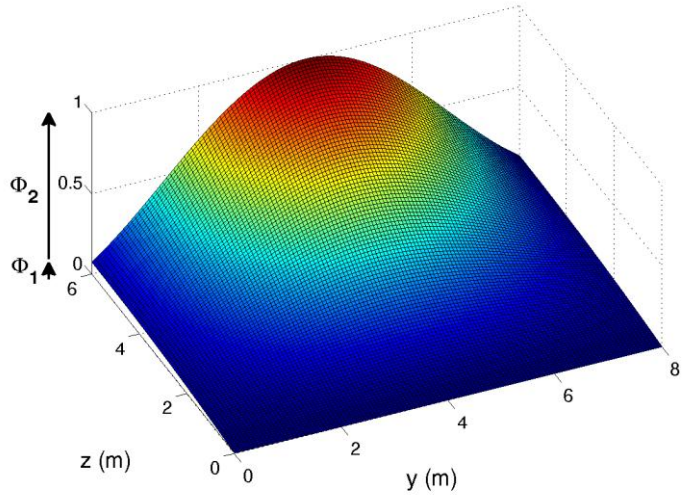

Figure 4.5. The mode shape assumed by Equation (4.32) for the total deformation of the transverse wall for *H* = 6m, *a* = 8m, *b* = 8m, *t* = 0.625m. As shown by the arrows, the Φ_I component determines the displacement at the corners, but Φ_{II} clearly dominates at midcrest.

For the longitudinal walls, only type *I* deformation is possible, thus only $\Phi_I(z)$ is needed to describe their distribution pattern. For the transverse walls (and story or roof diaphragms, assuming no separation has occurred), both types of deformation are present. Thus, their total shape is obtained from the added contributions of Eq. 4.29 and 4.31:

$$\Phi_t(y,z)=\Phi_I(z)+\Phi_{II}(y,z) \tag{4.32}$$

The total deformation for the any level of seismic loading and for any part of the structure

may now be estimated by multiplying the appropriate type I or type I+II shape functions with the corresponding seismic displacement demand Δ_{tot} estimated for the control node from the displacement design spectra (Fig. 4.5).

4.4 Masonry Material Behavior

The stress-strain behavior of a masonry element under plane stress is idealized as shown in Fig. 4.6(a). The ascending branch is assumed linear up to the point of apparent yielding, whereas the length of the plateau depends on the inherent ductility of the blocks and mortar but also on the manner of construction (timber-lace or not). The nominal shear strength of a masonry element, f_v, is estimated as a weighted product of compressive strength of building block strength f_{bc} and joint mortar compressive strength (Eurocode 6, (2005)), f_{mc}: $f_{m,y}=1.25kf_{bc}^{0.7}f_{mc}^{0.3}$ (stress terms in MPa, with k in the range of 0.35 to 0.55). The range of values of the parameters listed above may vary, but the mean strength is estimated as 0.5MPa with a standard deviation of 0.15MPa. Note that the code recommended values for the shear distortion upon *yielding* of the masonry wall (yielding here is used to identify the onset of friction-sliding behavior along mortar joints after the occurrence of diagonal cracking) is in the range of 0.15%, whereas the shear strain ductility ranges, reaching values as high as 3 in cases of timber laced masonry (KANEPE 2010). The design code model for shear strength rides on a Mohr-Coulomb type of idealization of the behavior of stone masonry, according with which, the cracking shear strength, $v_{w,y}$, of unreinforced masonry is expressed in terms of the inherent stone-binder cohesion, σ_z is the normal compressive stress clamping the potential sliding plane, and μ is the apparent frictional coefficient.

$$v_{w,y} = c_b + \mu \cdot \sigma_z \tag{4.33}$$

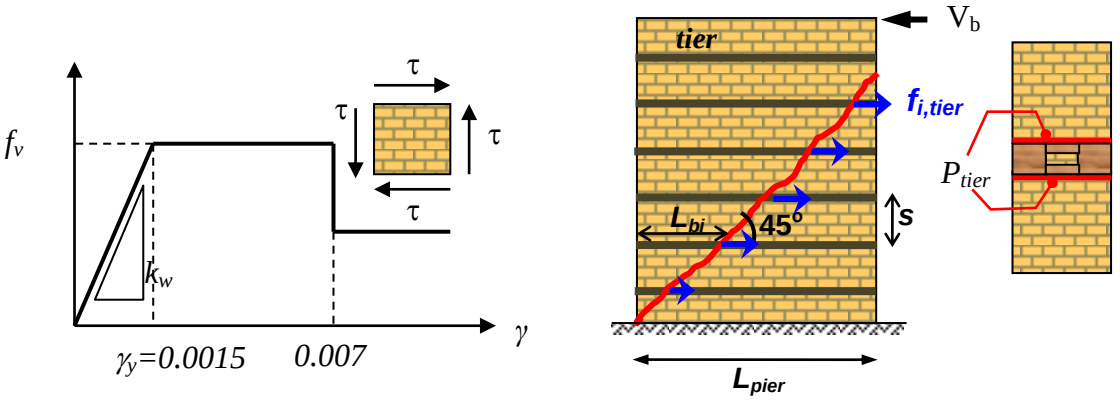

Figure 4.4. Behavioral Models: (a) Code-recommended resistance curve for masonry wall element, (b) Model illustrating the contribution of timber laces

In obtaining the code relationship the frictional component of shear strength has been neglected on the assumption that normal stresses owing to overbearing loads are very small; this simplifies Equation (4.33) to a Tresca-type failure criterion. The cohesion c_b may alternatively be taken as the weighted product of tensile (f_{wt}') and compressive (f_{wc}') strengths of the weaker component of the composite masonry (i.e., of the mortar): $c=0.5(f_{wt}'\ f_{wc}')^{0.5}$ (where f_{wt}' is approximated as $0.1f_{wc}'$); this approach yields commensurate results with those given earlier (conservatively around 0.5MPa). The contribution of tiers in this strength model is estimated by the

total force, V_b, sustained by the number of tier elements (n_{tier}) that intersect a 45° plane of failure after diagonal cracking ($n_{tier}=a/s_{tier}$ where s_{tier} the spacing of tiers in height and a the dimension of the building parallel to the earthquake, Fig. 4.6(b), Tastani et al., (2009)):

$$V_b = \sum_{i_{tier}=1}^{n_{tier}} A_{tier}\, f_{i,tier} \tag{4.34}$$

Parameters A_{tier} and $f_{i,tier}$ are the area and axial stress of the material that acts as tier reinforcement, which is equal to u_bxP_{tier}x$L_{b,i}$, where u_b is the bond stress at the mortar – timber interface (taken for simplicity equal to the tensile strength of the masonry wall, f_{wt}'), P_{tier} is the contact perimeter of the cross section of the timber tier element with masonry and $L_{b,i}$ the *minimum* available contact length of tier with the wall, measured to the left or to the right of the diagonal cracking plane.

4.5 Basic ESDOF System Parameters

Deriving the properties of the associated equivalent, or generalized single degree of freedom system (ESDOF) that represents the overall building behavior in spectral coordinates has been the motivating objective for this paper. Thus, the definition of the shape of lateral translation was a necessary intermediate step in the process of estimation of the essential dynamic properties of the ESDOF, namely, the associated mass (mobilized by the response shape), period, excitation coefficient and the corresponding mass participation factor.

The total mass of the system may be found as the sum of the wall masses, the roof mass m_{rf} and any gravity and service loads present on the N_{st} building floors. With reference to the building plan of Fig. 4.2, having a wall mass density ρ_w, and typical floor mass m_{st} (comprising a distributed mass of ρ_{rf} and ρ_{st} per unit area of roof and floor, respectively, and a live load of q), the total system mass becomes:

$$m_{tot} = m_w H + m_{rf} + m_{st} \tag{4.33}$$

where

$$m_w = 2\rho_w t(a+b) \qquad m_{rf} = \rho_{rf}(a+t)(b+t) \qquad m_{st} = (\rho_{st} + 0.3q/g)(a+t)(b+t)$$

The generalized mass of the ESDOF is obtained using the translational shape of vibration as follows (Clough and Penzien 1976):

$$\begin{aligned} m &= \int\int \overline{m}(y,z)\left[\Phi_t(y,z)\right]^2 dz\,dy \\ &= 2\int_0^H \rho_w a t \Phi_I^2(z)dz + 2\int_0^H\int_0^b \rho_w t \Phi_{II}^2(y,z)dy\,dz + \sum_{j=1}^{N_{st}} \frac{m_j}{b}\int_0^b \Phi_{II}^2\left(y, \frac{H}{\kappa_j}\right)dy \end{aligned} \tag{4.34}$$

where H/κ_j represents the z coordinate where diaphragm j (or equivalently mass m_j) is located. Thus, by analytic integration:

$$m = \frac{16}{15}\rho_w t H a \delta_I^2 + \frac{\rho_w t H b}{105}\left(112\delta_I^2 + \frac{308}{\pi}\delta_I \delta_{II} + 29\delta_{II}^2\right) + \sum_{j=1}^{N} m_j \left(\frac{2\kappa_j - 1}{\kappa_j^2}\right)^2 \cdot \left(\delta_I^2 + \frac{4\delta_I \delta_{II}}{\kappa_j \pi} + \frac{\delta_{II}^2}{2\kappa_j^2}\right) \tag{4.35}$$

For example, for a typical two story house, where the mid-story is located at mid-height (at $H/2$) using $m_1=m_{st}$, $\kappa_1=2$ and $m_2=m_{rf}$, $\kappa_2=1$ simplifies the above expression to:

$$m = \frac{16}{15}\rho_w t H a \delta_I^2 + \frac{\rho_w t H b}{105}\left(112\delta_I^2 + \frac{308}{\pi}\delta_I \delta_{II} + 29\delta_{II}^2\right) + m_{rf}\left(\delta_I^2 + \frac{4}{\pi}\delta_I \delta_{II} + \frac{1}{2}\delta_{II}^2\right) + m_{st}\frac{9}{16}\left(\delta_I^2 + \frac{2}{\pi}\delta_I \delta_{II} + \frac{1}{8}\delta_{II}^2\right) \tag{4.36c}$$

The generalized stiffness of the ESDOF system is estimated following the same concept (Clough and Penzien 1976); the integration is simplified significantly if the Poissons' effects in plate bending are neglected:

$$K \approx \int_0^H k_w \cdot 2at \cdot \left[\frac{d\Phi_I(z)}{dz}\right]^2 dz + 2\int_0^H\int_0^b E_w \frac{t^3}{12}\left[\frac{\partial^2 \Phi_{II}(y,z)}{\partial y^2} + \frac{\partial^2 \Phi_{II}(y,z)}{\partial z^2}\right]^2 dy\,dz = \frac{8a}{3H}k_w t \delta_I^2 + E_w t^3 \delta_{II}^2\left(\frac{b}{3H^3} + \frac{\pi^2}{45bH} + \frac{29\pi^4 H}{1260b^3}\right) \tag{4.37}$$

where $k_w = f_v / \gamma_y$ is the elastic slope of the shear force – shear strain diagram of masonry (units of stress). For example, the average shear stress-strain behavior for common stone masonry walls (without tiers) adopted by Eurocode 8-III (2005) is depicted in Fig. 4.6(a). The associated period of the system is calculated from:

$$T = 2\pi\sqrt{\frac{m}{K}} \tag{4.38}$$

The earthquake excitation factor, L_e representing the degree to which the assumed shape of translation is excited by the ground motion is defined by:

$$L_e = \int\int \overline{m}(y,z)\Phi_t(y,z)dzdy = 2\int_0^H \rho_w a t \Phi_I(z)dz + 2\int_0^H\int_0^b \rho_w t \Phi_{II}(y,z)dydz + \sum_{j=1}^{N_{st}} \frac{m_j}{b}\int_0^b \Phi_{II}\left(y, \frac{H}{\kappa_j}\right)dy \tag{4.39}$$

$$= \frac{4}{3}\rho_w t H \delta_I (a+b) + \frac{5}{3\pi}\rho_w t H b \delta_{II} + \sum_{j=1}^{N_{st}} m_j \frac{2\kappa_j - 1}{\kappa_j^2}\left(\delta_I + \frac{2\delta_{II}}{\pi\kappa_j}\right)$$

For the special case of the two story house examined previously:

$$L_e = \frac{4}{3}\rho_w tH\delta_I (a+b) + \frac{5}{3\pi}\rho_w tHb\delta_{II} + m_{rf}\left(\delta_I + \frac{2\delta_{II}}{\pi}\right) + m_{st}\frac{3}{4}\left(\delta_I + \frac{\delta_{II}}{\pi}\right) \quad (4.40)$$

Furthermore, the effective mass mobilized by the deflected shape, *m** and the associated participation factor *Γ* may now be estimated as (Clough and Penzien, 1976):

$$\Gamma = \frac{L_e}{m}, \quad m^* = \frac{(L_e)^2}{m} \quad (4.41)$$

Based on the above calculations, the generalized effective mass for the translational shape considered is found to be in the order of 45-84% depending on the building dimensions; its magnitude underlines the fundamental difference between lumped systems (where the usual value is over 75% of total mass) from the distributed mass systems such as the one examined herein. The larger the values of *a* and *H* are, as compared to *b*, the higher the effective mass. Since the critical direction of ground excitation for a rectangular building is when it strikes orthogonal to the longer wall, it may be said that in general $b \geq a$, thus, the effective mass will generally be low. Still, the proposed displacement pattern actually represents a much higher percentage of the system's response, as the next significant mode has practically the same period, only the out-of-plane walls bend in opposite directions (as illustrated in Fig. 4.4(a) and (b)). Thus, the proposed shape sufficiently assesses the system behavior and it enables rapid transformation from global to localized seismic demands, and relatively accurate calculations on the seismic vulnerability of a large group of similar buildings. Note that the above expressions can be easily modified to incorporate additional structural components contributing to the mass and stiffness of the structure. For example, interior walls oriented in the direction of the earthquake contribute to mass and stiffness while reducing the unsupported length of transverse walls (their contribution is added on to that of the parallel exterior walls by increasing proportionately the equivalent wall thickness and subdividing the transverse span to b/2 in both the mass and stiffness calculations). Interior walls oriented orthogonal to the earthquake contribute to the mass in the same manner as the other transverse walls (i.e., their contribution is accounted for by increasing proportionately the equivalent transverse wall thickness in the mass equations only).

4.6 Performance Evaluation via Nonlinear Static Procedures

The estimated period of the structure is needed in order to evaluate the demand in terms of total acceleration (i.e. base shear) and relative displacement at the control node of the structure, from the acceleration spectrum of the design hazard (e.g. the Code prescribed total acceleration spectrum). Therefore, from the associated spectral acceleration and spectral displacement values, $S_a(T)$ and $S_d(T)$ at period *T* the required behavior factor, *q* may be obtained as follows:

$$q = \frac{\Gamma \cdot m \cdot S_a(T)}{V_{by}} = L_e \cdot \frac{S_a(T)}{V_{by}} \quad (4.42)$$

The corresponding control node displacement D_{target} is,

$$D_{target} = \Gamma \cdot C_1 \cdot S_a(T) \cdot \frac{T^2}{4\pi^2} = \Gamma \cdot C_1 \cdot S_d(T) \tag{4.43}$$

where C_1 is the inelastic displacement ratio at a strength reduction factor of q, which for the low period range as befits the types of structures considered: $C_1 = \mu_\Delta / q$, where the required displacement ductility demand, μ_Δ is estimated from:

$$\mu_\Delta = 1 + (q-1) \cdot \frac{T_2}{T} \quad (for\ the\ EC8\text{ - }I\ type\ I\ spectrum)\ or,$$
$$\mu_\Delta = \frac{q^2 + 1}{2} \quad (according\ with\ the\ equal\ energy\ assumption) \tag{4.44}$$

The displacement demand throughout the structure is obtained from the product $D_{target} * \Phi_t(x,y,z)$; spatial derivatives of this result provide the localized deformation demands (shear distortion angles, relative drift ratios, curvature of walls in out of plane bending). In the following sections these values are then compared with the corresponding deformation capacities to assess the potential for failure.

4.7 Capacity Curve Definition

With no loss of generality it is assumed that the response of the structure to a constant horizontal acceleration (pushover load for distributed parameter systems) is described by an equivalent elastic perfectly plastic pushover curve that terminates at an displacement capacity of Δ_u (blue line in Fig. 4.7). Thus, only two points of base shear versus roof drift are needed to define the structural behavior, namely nominal yield and ultimate failure. Obviously, this means that several aspects of masonry behaviour are neglected, e.g., the influence of cracking development that introduces a gradual reduction of stiffness in the ascending branch up to yield, and any residual strength that may be available after the ultimate displacement is reached (red curve in Fig. 4.7). Still, the above assumptions are considered acceptable in view of the considerable uncertainty surrounding masonry.

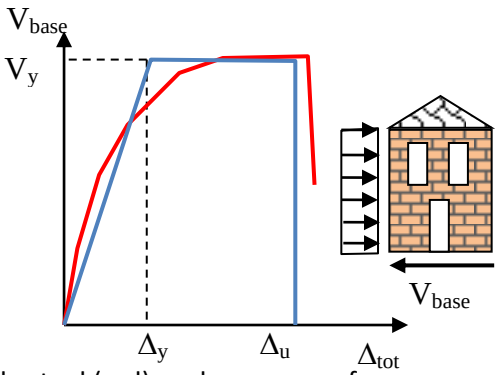

Figure 4.7. Idealized (blue) and actual (red) pushover curve for masonry structure.

The pursuit for determination of the performance point is tied to the control node displacement which acts as a multiplication factor on the normalized translational displacement shape of the structure in order to completely determine its displacement (curvature, strain) profile. This is in essence akin to a displacement-based pushover analysis (e.g., Moehle (2002), Pinho-

Antoniou (2005), Thermou et al. (2007)) in contrast to the typical force-based pushover where the load pattern/profile is constant, with the load factor acting as the multiplier, while the displacement profile changes as the structure is loaded. The advantage of a displacement-based approach is that it essentially dispenses with the need for a nonlinear static analysis as everything is determined by the control node displacement and the constant displacement pattern. Thus, in order to estimate the base shear for each given value of the midcrest displacement, all that is needed is the relationship between these two variables which is implicitly conveyed in the normalized displacement shape.

According to Fig. 4.6(a) it has been assumed that walls develop elastic material behaviour up to the occurrence of a nominal yield point. If it is temporarily assumed that this point is associated with yielding of the walls in direct shear, it follows that the shear strength f_v of the material is reached at a given level z in [0,H]. If $A(z)$ is the wall shear area at this level (comprising the cross sectional area of walls parallel to the plane of action), then the yield shear at this level is

$$V'_y(z) = f_v A(z) \tag{4.42}$$

The corresponding value of the horizontal load to cause this level of shear can be found by dividing the above value by $H - z$, i.e., the loaded height of the wall above level z. Since the loading is uniform, multiplying this critical load value by H provides the shear force at level z = 0, or the corresponding yield base shear, assuming failure occurs at z:

$$V'_{by}(z) = f_v A(z) \frac{H}{H - z} \tag{4.43}$$

The actual base shear at yield is the minimum of V_{by}(z), over all values of z. Although seemingly tedious, for typical square or rectangular openings, it suffices to check only the values for z at the base of the building (z=0) and at the lowest level of each row of openings.

The corresponding control node displacement Δ'_y due to shear failure at nominal yielding may be found by enforcing nominal deformation limits on the displacement shape determined in the preceding. For example for the walls yielding in shear this is the top displacement for which the displacement shape results in a critical shear strain value equal to the milestone number of 0.0015 listed in the horizontal axis of Fig. 4.6(a). This establishes the baseline elastic behaviour of the structure. If subsequent checks for "yielding" due to other mechanisms of failure (pertaining to Immediate Occupancy - LS1 - criteria) return a lower control node displacement, Δ_y, then the yield base shear V_{by} is re-adjusted by simple linear interpolation along this elastic baseline. (For example alternative modes of failure that could precede shear yielding refer to cracking of the transverse walls bending out of plane either at midspan or along the vertical corners due to excessive axial tension). Thus, formally:

$$V_{by} = \frac{\Delta_y}{\Delta'_y} \cdot \min_{0 \le z \le H} V'_{by}(z) \tag{4.44}$$

The ultimate displacement is determined by Life-Safety (LS2) performance criteria.

Several acceptance criteria and associated limit-states may be recalled in assessing a masonry structure even when response is considered in simple translation as is proposed in the

present study. These may be expressed in terms of force or displacement/deformation. The objective in each case is to quantify a limiting value of strain or curvature that may be associated with failure. This limiting value may be related to control node displacement through the deformation shape which enables implementation of the demand-to-capacity check. Three main failure scenarios are presented in the following.

4.8 Shear Failure of Walls

This failure criterion will be evaluated by checking the wall shear strain against the limiting shear strain of γ_{lim}. For this, the shear strain components in type I mode of deformation are considered (being invariable with the transverse coordinate, *y*) as the first derivative of the corresponding displacement shape.

$$\Phi'_{I,s}(z) = \frac{\partial(\Phi_s + \Phi_{s,add})(z)}{\partial z} = 2\delta_s \frac{H-z}{H^2} + \delta_{s,add} \frac{\Sigma\gamma_{s,add}(z)}{\Sigma\Delta_{s,add}} \tag{4.45}$$

Typically, the additional strain produced by an opening is localized exactly at the levels where the opening is (in contrast to the displacement which influences the entire structure above the opening) (Eq. (4.29)). Thus, the sum implied above may contain only one or two terms at each value of *z*, depending on the openings' configuration. This strain estimate corresponds to a control node displacement of 1.0 (equal to the displacement shape maximum). By simple analogy, the minimum value of the midcrest displacement $\Delta_{\gamma,lim}$ corresponding to the attainment of a critical value of shear strain equal to γ_{lim} can be estimated as:

$$\Delta_{\gamma,lim} = \frac{\gamma_{lim}}{max\Phi'_{I,s}(z)} \tag{4.46}$$

The highest values of shear strain occur at the ground level and at the lowest extremity of each row of openings. Thus, the evaluation of the above equation is much simplified.

4.8.1 Type II (out-of-plane) failure of transverse walls

In response to type-II deformation of the transverse walls, the limited tensile strength of masonry results in the appearance of cracking and ultimately failure. To check for this condition, the curvatures ϕ of the transverse wall are estimated using Eq. (4.31) for type II deformations:

$$\phi_{zz} = \frac{\partial^2\Phi_t(y,z)}{\partial z^2} = \frac{2\delta_{II}(2H-3z)}{H^3} \cdot \frac{2\sin(1.5\pi y/b - 0.25\pi) + \sqrt{2}}{2+\sqrt{2}} - \frac{2\delta_I}{H^2} \tag{4.50}$$

$$\phi_{yy} = \frac{\partial^2\Phi_t(y,z)}{\partial y^2} = -\frac{9\pi^2\delta_{II}}{2(2+\sqrt{2})b^2H^3} \cdot z^2(2H-z) \cdot \sin(1.5\pi y/b - 0.25\pi) \tag{4.51}$$

$$\phi_{yz} = \phi_{zy} = \frac{\partial^2\Phi_t(y,z)}{\partial y \partial z} = \frac{3\pi\delta_{II}}{(2+\sqrt{2})bH^3} \cdot z(4H-3z) \cdot \cos(1.5\pi y/b - 0.25\pi) \tag{4.52}$$

Using the above expressions, the principal values of the curvatures ϕ_1, ϕ_2 are obtained :

$$\phi_{1,2} = \frac{\phi_{yy} + \phi_{zz}}{2} \pm \sqrt{\left(\frac{\phi_{yy} - \phi_{zz}}{2}\right)^2 + \phi_{yz}^2} \tag{4.47}$$

The maximum values of curvature, ϕ_1 and ϕ_2 identify maximum tension strains either on the inside or on the exterior façade of the transversal walls. In absolute terms, ϕ_2 attains its maximum at the mid-crest and along the vertical supports of the wall at the corners of the building. For lower building heights, the maximum tension on the outside façade initially stays on the midline of the wall, and then starts shifting towards both lower corners, indicating an inverted-Y yield line, according to classical plate theory (Fig. 4.8a).

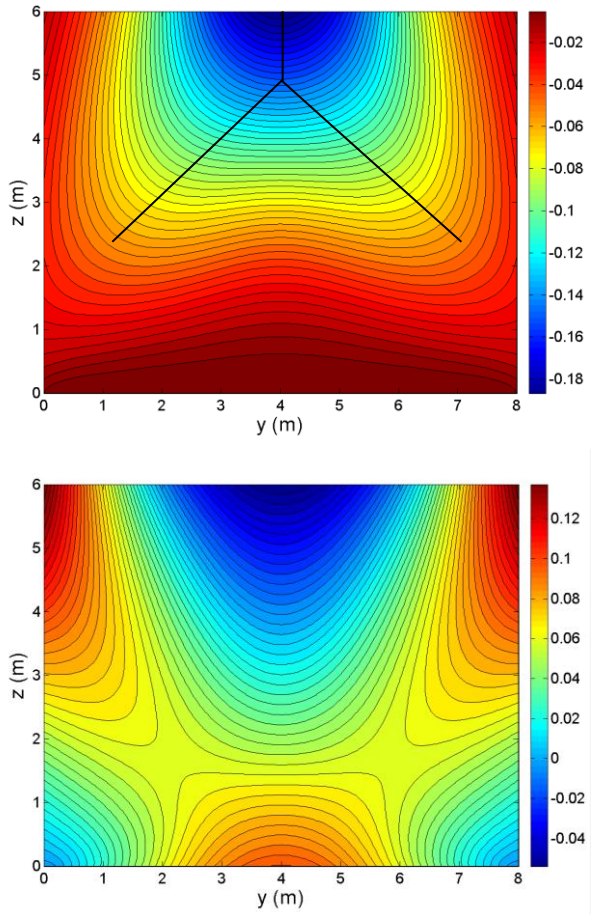

Figure 4.8. Type-II out-of-plane deformation of transverse wall for H = 5.6m, a = 8m, b = 8m, t = 0.625m: (a) minimum (tension on exterior façade) and (b) maximum (tension on interior façade) principal curvature contours. The ridges in the tension stresses indicate the expected inverted-Y yield line mechanism.

Given that cracking progresses from top to bottom, failure may be defined by the appearance of tension cracks along the top p fraction of the height. For the critical top half of the wall, ϕ_{yy} completely dominates ϕ_2. Thus, Eq. (4.52) can become a proxy for ϕ_2. For a control node displacement of $\Delta_{\varphi,lim}$ the failure condition is written as $\phi_{yy}(y, z)\cdot\Delta_{\varphi,\text{lim}} = \phi_{\text{lim}}$ for $y = b/2$, $z = (1 - p)H$, where $p \in [0,1]$. Solving for $\Delta_{\phi,lim}$, the result is:

$$\Delta_{\phi,lim} = \phi_{lim} \frac{2(2+\sqrt{2})b^2}{9\pi^2(1-p)^2(1+p)\delta_{f,II}} \tag{4.48}$$

Selecting an appropriate value for the limiting curvature ϕ_{lim} and the percentage p of the cracked path associated with a given performance level are important. For walls without tiers the cracking strain of masonry divided by the distance to the neutral axis may be used, i.e., $\varphi_{cr}=2(0.1f_c^{'}/E_w t)$. In the presence of tiers, the walls possess flexural ductility. Exceeding φ_{cr} may still result in cracking, however, actual failure is now associated with a higher ultimate curvature φ_u. The influence of any openings on the transverse wall can be accounted for by appropriately modifying p. For example, if it is requested that p = 50% of the wall height needs to reach φ_{lim}, then the height of any openings in the top 50% of the transverse wall (especially if close to its midline) can be used to directly reduce the required p.

4.8.2 Type I flexural failure of walls

The type 1 flexural component of deformation may induce failure of the longitudinal walls akin to typical beam bending. Their curvature along the vertical direction, using the more accurate shape proposed, is:

$$\frac{d^2\Phi_{f,I}(z)}{dz^2} = 4\delta_{f,I}\frac{(H-z)^2}{H^4} \tag{4.49}$$

This is maximized at ground level (z=0), and equal to $4\delta_{f,I}/H^2$. Assuming a typical linear distribution of strain along the horizontal dimension (length a) of the longitudinal wall and given a critical strain of ε_{wu}, it is requested that no more than a p percentage of the wall length has exceeded it. This corresponds to a simple limit on the length of the flexural crack that may appear in the long-wall and it is achieved at a curvature value of $\varepsilon_{wu}/(pa)$. As the above estimate of curvature corresponds to a unit control node displacement, by simple analogy the limiting value of mid-crest displacement is:

$$\Delta_{\varepsilon,lim} = \frac{\varepsilon_{wu}/(pa)}{max[d^2\Phi_{f,I}(z)/dz^2]} = \frac{\varepsilon_{wu}H^2}{4pa\delta_{f,I}} \tag{4.50}$$

4.8.3 Failure at wall corners

Failure at corners due to axial tension (Fig. 3.1): The absolute value of the tension force over a strip of 1m height where the longitudinal wall is pulled apart from the transverse walls is:

$$N_{f2}(z) = \Delta_{N,t}\cdot E_w I\left.\frac{\partial^3\Phi_t(y,z)}{\partial y^3}\right|_{y=0} = \frac{27\pi^3\delta_{II}\Delta_{N,t}}{8(1+\sqrt{2})b^3H^3}\cdot z^2(2H-z) \tag{4.51}$$

where $I = t^3*(1m)/12$ refers to the moment of inertia of a 1m wide horizontal strip of the longitudinal wall deforming out of plane (type II deformation) and $\Delta_{N,t}$ is the control node displacement when this mode of failure controls. Dividing by the area of the 1m strip (t·1m) yields the axial stress that needs to be resisted to prevent cracking, starting from the top of the building and extending down to the

value of z where the limiting tensile stress f_{wt} is last exceeded. If the length of such a crack is required to remain less than pH, then, setting $z = H\,(1 - p)$ and solving for $\Delta_{N,t}$, the value of the associated displacement at the control node may be estimated:

$$\Delta_{N,t} = \frac{32(1+\sqrt{2})b^3}{9E_w t^2 \pi^3 \delta_{II}(1-p^2)(1-p)} \cdot f_{wt} \tag{4.52}$$

4.9 Example Application

Application of the methodology is demonstrated here on a simple unreinforced masonry model structure which was tested under simulated ground motions on a shake table by Bothara et al. (2009). The building model was built at a scale of 1:2 (Fig. 4.9). The specimen had 0.11m thick masonry walls, a rectangular floor plan of 2.88m x 1.92m and was a two storey structure with a first floor height of 1.34m, a second floor of 1.14m and a roof gable rising by 0.815m (the geometric scale to a real building prototype was 1:2). Masonry prism strengths were as follows: f_{wc}=16.2 MPa, $\varepsilon_{wc,max}$=0.0035, E_w=6.1 GPa, v_{wy}=0.93MPa (Eq. 4.33), f_{wt}=0.42 MPa. Shear modulus of the homogenized material G, was taken equal to 1000MPa (the ratio of an assumed shear strength of 1MPa at a cracking shear distortion of 0.1%), whereas the Poisson's ratio was taken ν=0.25. The specific weight γ_w of clay bricks (single brick) was taken 20kN/m^3, whereas for ceramic roof tiles the unit-area weight was taken γ_r=1.5kN/m^2 including roof trusses and sheathing. Additional masses were added at the gable walls, at the floor level and at the eaves level as follows: (a) for testing in the longitudinal direction added mass per gable was 0.04 tonne, 2.1 tonne at the floor level and 2.02 tonne at the eaves, (b) for testing in the transverse direction, 2.1 tonne masses at the floor level and an equal amount at the eaves level respectively.

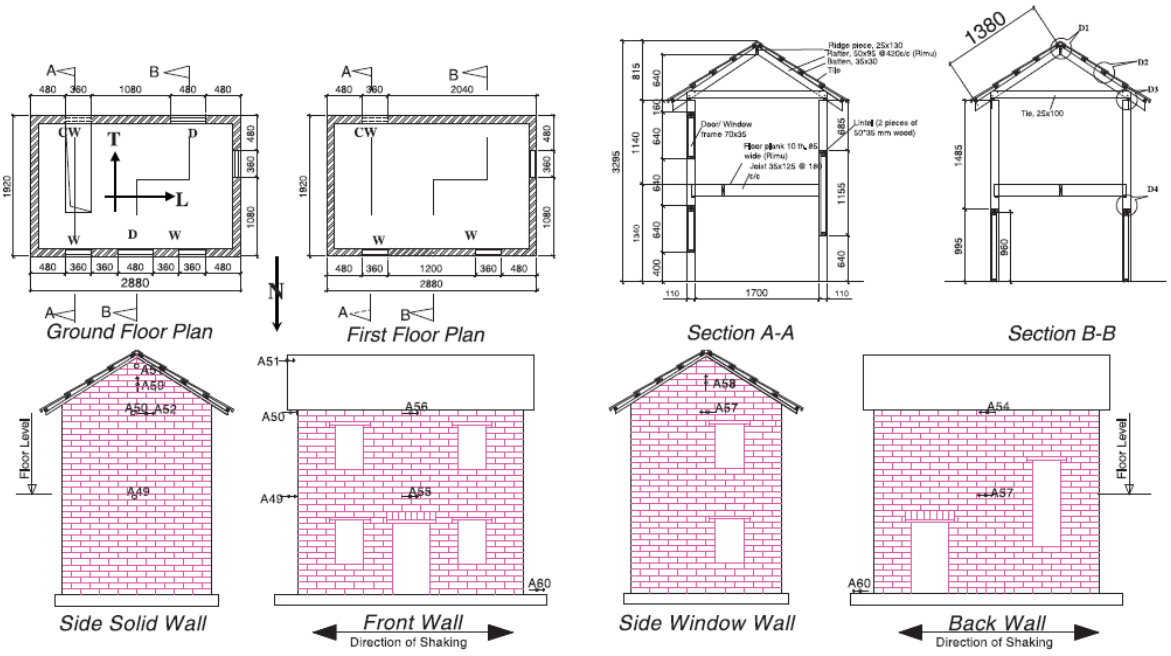

Figure 4.9: Plan and elevation of the Specimen Structure: The direction to North (N) refers to the specimen orientation above: during this testing, longitudinal direction coincided with E-W. The Elevations show the locations of accelerometers when the model was tested longitudinally. From Bothara et al. (2010).

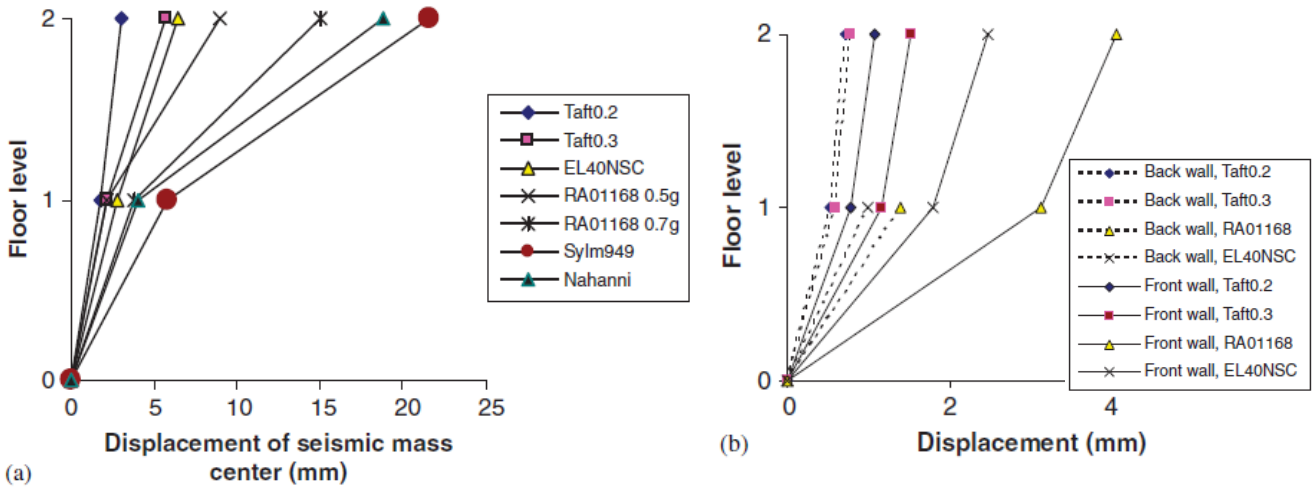

Figure 4.10: Displacement profiles of the structure when subjected (a) to transversal (N-S) and (b) longitudinal (E-W) shakings. From Bothara et al. (2010)

4.9.1 Calculation of response shape for earthquake in the longitudinal direction:

Based on the model developed in the present work, for motion in the longitudinal direction of the building it follows from Eq. (4.10) that

- $\Delta_s = qx(2.5m)^2/2/1000MPa/[(2.77m+1.81m)x2x0.11m] = 0.0031q$,
- from Eq. (4.15), $I = [(2.88^3x1.92m^4) - (2.66^3x1.7m^4)]/12 = 1.55m^4$,
- from Eq. (4.14), $\Delta_{f,I} = qx(2.5m)^4/8/[6100MPa\ x1.55\ m^4)] = 0.000558q$,
- and from Eq. (4.19) $\Delta_{s,add,1} = 0.000376q$ (for p_o=25%, z_1=0.4m, z_2=1.04m) for the openings in the ground floor and $\Delta_{s,add,2} = 0.000056q$ (for p_o=15%, z_1=1.68m, z_2=2.32m) for the openings in first floor; last, for H/b = 2.5/1.92 = 1.3, from Fig. (4.3), $a_1 = 0.005$, $a_2 = 0.75$;
- from Eq. (4.21) $D_{plate} = 6100x10^3kN/m^2x0.11^3m^3/12/(1-0.25^2) = 721.7$ kN-m;
- $\Delta_{f,II} = 0.005x0.75x20kN/m^3x0.11x2.5^4/D_{plate} = 0.446$ mm.
- For an average estimate of q, calculate total weight: W = [(2x0.04 +2.1 +2.02)x9.81 + 20x(2.77+1.81)x2x0.11x2.5 + 20x0.5x1.81x0.815x0.11x2 + 2.88x1.92x1.5] = 103.12 kN (mass = 10.5 tn),
- thus q=W/H = 103.12kN/2.5m = 41.24kN/m = 41.24 N/mm.
- Therefore, Δ_{tot} = (0.0031+0.000558+0.000376+0.000056) x 41.24 + 0.446mm = 0.168mm +0.44mm = 0.6mm. Thus, from Eq. (4.27) δ_I=0.168/0.6 = 0.28, δ_{II}=0.44/0.6=0.72.
- From Eq. (4.29) it follows, $\Phi_I(z)=0.28z(2x2.5-z)/2.5^2$, and from Eq. (4.31), $\Phi_{II}(y,z)=0.72[z^2(2x2.5-z)\sin(\pi y/1.92)]/2.5^3$.

From Eq. (4.35) it follows that

- $m_w = 2$ x 20kN/m^3 x 0.11m x(2.88m + 1.92m) / 9.81m·s^{-2} = 2.15 tn/m, m_{rf} = (2 x 0.04 + 2.02)tn

+ [20 x 0.5 x 1.81 x 0.815 x 0.11 x 2 + 2.88 x 1.92 x 1.5] / 9.81m·s^{-2}=2.1+1.17=3.27 tn, and m_{st}=2.1 tn.

According to Eq. (4.36c) the generalized mass of the system is,

- m = (16/15) x (20/9.81) x 0.11 x 2.5 x 2.88 x 0.28^2 + [(20/9.81) x 0.11x 2.5 x1.92 x (112 x 0.28^2 + (308/3.14) x 0.28 x 0.72 + 29 x 0.72^2) /105] + (3.27) x (0.28^2 + (4/3.14) x 0.28 x 0.72 + 0.5 x 0.72^2) + 2.1 x (9/16) x (0.28^2 + (2/3.14) x 0.28 x 0.72 + (1/8) x 0.72^2)=2.84tn

whereas from Eq. (4.37) the generalized stiffness is,

- K= (8x2.88/3/2.5) x 1000x 10^{3}kN/m^{2}x 0.11x0.28^2 + 6100 x 10^{3}kN/m^2 x 0.11^3 x 0.72^2 x [(1.92/3/2.5^3) + (3.14^2/45/1.92/2.5) + (29 x 3.14^4 x 2.5/1260/1.92^3)] =30183.7kN/m

And the corresponding period (Eq. 4.38) is, T=2 x 3.14 x (m/K)$^{1/2}$=0.061 sec. This value correlates excellently with the reported value of T_{exp}=0.072 sec (=13.7 Hz) obtained from longitudinal white noise testing of the structure before cracking; note that period elongation was reported from repeated tests after subjecting the structure to a series of ground motions. At that stage the elongated period was T_{exp}=0.09 sec (=11Hz). This value is close to the analytical estimate obtained if the modulus of elasticity is halved in order to account for the effects of cracking (T=0.061x√2 = 0.086 sec).

From Eq. (4.40) the value of L_e is calculated as follows:

- L_e =(4/3)x(20/9.81)x 0.11x2.5x0.28x (2.88+1.92) + (5/3/3.14) x (20/9.81)x0.11x2.5x1.92x0.72 + 3.27x(0.28+(2/3.14)x0.72) + 2.1x(3/4)x(0.28+(0.72/3.14)) = 4.6334

And Γ from Eq. (4.41): Γ=4.6334/2.84 = 1.63 tn.

4.9.2 Response shape for earthquake in the transverse direction:

Again the proposed model is used to estimate the dynamic properties of the structure for motion in the transverse direction of the building as follows: from Eq. (4.10)

- Δ_s = qx(2.5m)^2/2/1000MPa/[(2.77m+1.81m)x2x0.11m] = 0.0031q,
- from Eq. (4.15) *I* = [(2.88x1.92^{3}m^4) - (2.66x1.7^{3}m^4)]/12 = 0.609m^4,
- from Eq. (4.14), $\Delta_{f,I}$ = qx(2.5m)^4/8/[6100MPa x0.609 m^4)] = 0.00131q,
- and from Eq. (4.19) $\Delta_{s,add,1}$ = 0.000376q (for p_o=25%, z_1=0.4m, z_2=1.04m) for the openings in the ground floor and $\Delta_{s,add,2}$ = 0.000056q (for p_o=15%, z_1=1.68m, z_2=2.32m) for the openings in first floor; last, for H/b = 2.5/2.88 = 0.86, from Fig. (4.3), a_1 = 0.0116, a_2 = 0.828;
- from Eq. (4.21) D_{plate} = 6100x10^{3}kN/m^{2}x0.11^{3}m^3 /12 /(1-0.25^2) = 721.7 kN-m; $\Delta_{f,II}$ = 0.0116x0.828x20kN/m^{3}x0.11x2.5^4 /D_{plate} = 1.143mm.
- For an average estimate of q, calculate total weight W = [(2.1tn+2.1tn)x9.81m·s^{-1} + 20x(2.77+1.81)x2x0.11x2.5 + 20x0.5x1.81x0.815x0.11x2 + 2.88x1.92x1.5] = 103.12 kN, thus q=W/H = 103.12kN/2.5m = 41.24kN/m = 41.24 N/mm.

Therefore,

- Δ_{tot} = (0.0031+0.00131+0.000376+0.000056) x 41.24 + 1.143mm =(0.199 + 1.143) mm = 1.34mm. Thus, from Eq. (4.27) δ_I=0.199/1.34 = 0.15, δ_{II}=1.143/1.34=0.85.

  From Eq. (4.29) it follows,

- $\Phi_I(z)=0.15\cdot z\cdot(2\cdot 2.5-z)/2.5^2$, and from Eq. (4.31), $\Phi_{II}(y,z)=0.85[z^2(2\cdot 2.5-z)\sin(\pi y/2.88)]/2.5^3$.

From the preceding section it was found that m_w = 2.15 tn/m, m_{rf} = 3.27 tn, and m_{st}=2.1 tn.

According to Eq. (4.36c) the generalized mass of the system is,

- m = (16/15) x (20/9.81) x 0.11 x 2.5 x 1.92 x 0.15^2 + [(20/9.81) x 0.11x 2.5 x2.88 x (112 x 0.15^2 + (308/3.14) x 0.15 x 0.85 + 29 x 0.85^2) /105] + (3.27) x [0.15^2 + (4/3.14) x 0.15 x 0.85 + 0.5 x 0.85^2] + 2.1 x (9/16) x [0.15^2 + (2/3.14) x 0.15 x 0.85 + (1/8) x 0.85^2]=2.59tn

whereas from Eq. (4.37) the generalized stiffness is,

- K= (8x1.92/3/2.5) x 1000x 10^3kN/m^2x 0.11x0.15^2 + 6100 x 10^3kN/m^2 x 0.11^3 x 0.85^2 x [(2.88/3/2.5^3) + (3.14^2/45/2.88/2.5) + (29 x 3.14^4 x 2.5/1260/2.88^3)] =6981.3kN/m.

The corresponding period in the transverse direction (Eq. 4.38) is, T=2 x 3.14 x $(m/K)^{1/2}$=0.12 sec. The reported value correlates adequately with the reported value of T_{exp}=0.102 sec (=9.8 Hz) obtained from white noise testing of the structure in the transverse direction before the application of ground motion shaking in that direction; again, period elongation was reported from repeated tests after subjecting the structure to a series of ground motions. In the end of tests the elongated period was T_{exp}=0.14 sec (=6.83 Hz). Again this value is sufficiently close to the analytical estimate if the modulus of elasticity is halved in order to account for the effects of cracking in the direction of shaking (T=0.12x√2 = 0.17 sec).

Again, from Eq. (4.40) the value of L_e is calculated as follows:

- L_e =(4/3)x(20/9.81)x 0.11x2.5x0.15x(2.88+1.92) + (5/3/3.14) x (20/9.81)x0.11x2.5x2.88x0.85 + 3.27x (0.15+ (2/3.14) x0.85) + 2.1x(3/4)x(0.15+(0.85/3.14)) = 4.109

And Γ from Eq. (4.41): Γ=4.109/2.59 = 1.58

4.10 Conclusions

The degree of complexity of computational approaches in assessing the seismic demands and capacities of traditional masonry is disproportionately more complex than the level of knowledge and uncertainty surrounding these structures and their properties. As an alternative, a simple mechanistic model is developed in the present paper that may serve to reproduce the global vibration characteristics while also employing a local shape to allow estimating typical local failures. In all cases, no complex structural analysis is needed whereas all estimations may be performed from parameterized expressions using spreadsheet calculations. Application of the model to a model structure with flexible diaphragms, which was tested on a shake table to strong ground motion

records it was found that the model successfully approximates the measured period, and period shift occurring due to cracking as well as the displacement patterns developing in the structure during the earthquakes including the associated drift demands. Assessment is now possible on a deformation-driven frame of reference, since the estimated deformation demands may be compared with simple criteria for deformation capacity of the URM structure.

4.11 Appendix

The contribution of the type 1 and type 2 flexural deformations of the walls to the global control node displacement of the system is moderated by two appropriate reduction factors, λ_{f1} and λ_{f2}. The best approach to estimated them would be via finite element simulations, yet, for the benefit of a simple approach, crude linear approximations may also be employed as follows.

Let $\lambda_{f1} = f(\lambda)$, where λ is the ratio of the bending stiffness of the diaphragm over the bending stiffness of the transverse walls:

$$\lambda = \frac{E_c I_{diaph}/a}{E_w I_{wall}/H} \tag{4.53}$$

where

$$I_{wall} = t_w^3 \cdot b/12, \qquad I_{diaph} = \begin{cases} t_s^3 \cdot b/12, & \text{if diaphragm} = \text{slab} \\ t_b^3 \cdot 2b_w/12, & \text{if diaphragm} = \text{perimeter beams} \end{cases} \tag{4.54}$$

A concrete slab of t_s thickness is often used as a retrofit measure at each story level, while a perimeter beam of a uniform cross sectional width b_w and depth t_b is a common retrofit measure at the crest. In this context it is assumed that the two perimeter beams at the crest partially restrain the flexural deformation of the longitudinal walls. Note that in this case the transverse wall length, b, affects the resulting values of λ in Eq. (24), while for a slab the term b cancels out.

The full restraining effect corresponding to $\vartheta_{f1} = 0$ can be represented by a slab with E_c = 25GPa, E_w = 5GPa, H = 3m, t_w = 0.6m t_s = 0.2m, or a stiffness ratio of λ = 0.2. Then, an appropriate linear function for ϑ_{f1} is defined, as follows

$$\lambda_{f1} = max(\mathbf{1} - \mathbf{5}\lambda,\ \mathbf{0}) \tag{4.55}$$

Factor λ_{f2} is a function of the axial (extensional) stiffness of the diaphragm, k_d. For the purposes of a simple approximation, a linear function is assumed, taking on the value of 1 for k_d = 0 (i.e., when the crest boundary is unrestrained in out-of-plane translation) and 0 when the diaphragm stiffness ratio exceeds a certain critical limit corresponding to the full restraining action of a concrete slab, set here at 60GN/m (which corresponds to full support of the crest boundary against out of plane displacement). Then

$$\lambda_{f2} = max\left(\mathbf{1} - \frac{k_d}{\mathbf{60}GN/m},\ \mathbf{0}\right) \tag{4.56}$$

To estimate k_d a slab can be treated like a deep beam of height "*a*" and span "*b*", where *a*, *b* are the plan dimensions of the structure. By solving this as a Timoshenko beam that includes both bending and shear deformations (Timoshenko, "Strength of Materials, Part I: Elementary theory and problems") we find its midpoint deformation *d* when subjected to a uniform load of $q \cdot b$. Then, a measure of the slab's stiffness at the wall midcrest can be obtained as

$$k_{d,slab} = \frac{qb}{d_{mid}} = \frac{384 E_c I_{slab,y}}{b^3 \left[1 + 4(1+\nu)(a/b)^2\right]}, \quad \text{where } I_{slab,y} = a^3 t_s / 12 \tag{4.57}$$

For a critical rigid slab assumed of t_s=0.2m, $a = b$ = 5m, using E_c = 25GPa and ν = 0.25 for concrete we get a value of about 25GN/m. If, instead, a simple perimeter beam is the highest stiffness element restraining the out-of-plane wall bending, a simple Bernoulli beam solution (neglecting shear deformation) can be used to find that two such beams (one on each transverse wall), assumed to be clamped on both ends, would have a total midpoint stiffness of

$$k_{d,beam} = \frac{qb}{d_{mid}} = \frac{2 \cdot 384 E_c I_{beam,y}}{b^3}, \quad \text{where } I_{beam,y} = t^3 t_b / 12 \tag{4.58}$$

CHAPTER 5 – CRITERIA FOR SEISMIC ASSESSMENT

Co-authored with F. Karantoni, Lecturer at U.Patras, Greece,

and M. Papadopoulos, Associate Prof. at DUTh, Greece

5.1 Scope: This chapter establishes a performance-based framework for seismic assessment and retrofit of traditional unreinforced masonry structures (TURM); both demand indices and acceptance criteria are geometric variables (drift ratios that quantify the intensity of out of plane differential translation and in plane shear distortion of masonry walls oriented transversally to and along the seismic action, respectively for in plane and out of plane deformation) related through derived expressions with the fundamental response of the building. This framework is particularly useful for setting retrofit priorities and for management of the collective seismic risk of historical settlement entities. A characteristic Balkan type of traditional building is used in the study as a model structure for illustration of concepts; the structure represents the construction methods and building characteristics of the historical town of Xanthi (Greece).

5.2 Background Regarding Timber- Laced Structures

Stone masonry construction has been used throughout the Balkans for building structures from time immemorial. A traditional unreinforced masonry (TURM) building type comprising timber-laced construction (TL), was the preferred structural system in several cities of Northern Greece up to about 60 years ago when it was displaced by reinf. concrete. This structural system, known by various local trade names, actually draws its origin from the ancient Minoan times; timber lacing is used as a metaphor in the Bible, "*where the strength of soul secured by faith at times of trial, is compared to the strength of houses imparted by timber lacing in the event of an earthquake"*. In Herculaneum, near Pompeii, samples of timber laced buildings that survived the volcanic eruption of 78 A.D. are still standing, considered by historians a low-cost type of construction dating from that ancient period, referred to as *opus craticium* in roman times (Langerbach 2002, Papadopoulos 2013) (Fig. 5.1a). This later became known as *fachwerk*, *chatmas*, or *half-timbered system* in the various parts of Europe and Asia where it was found (Fig. 5.1b, 1c).

Figure 5.1: (a) Timber-Laced Masonry House from Herculaneum dating 78 A.D.), (b) Timber Laced Wall (c) Stone masonry timber laced wall

With regards to the old-town of Xanthi the TURM-TL buildings comprise a vital portion of its historical fabric, identifying the city (Fig. 5.2). Primary construction materials are stone (natural blocks, usually in the foundation and in the lower floors, and man-made solid clay-bricks in the upper levels) and timber (such as timber structural elements, floor ties, timber lacing elements, etc.), often tied in strategic locations with iron clamps and ties to improve member connectivity. The structural system combines a stiff load-bearing timber-laced stone-masonry wall system for the lower floor, with the upper floor made of an infilled timber frame, particularly in the southern or south-eastern sides of the building. The load bearing structure comprises stone masonry foundation with connecting mortar; in some cases, to improve the redundancy of the foundation particularly in compliant soils, a supporting substrate layer made of treated timber is provided under the foundation.

Figure 5.2: Typical Samples of traditional houses in the historical center of the city of Xanthi.

Load bearing walls in the first floor including the major interior divisions are made of stone masonry with lime-type connecting mortar and carefully tied timber-laces. Frequently, the connections between timber laces reveal many techniques borrowed from the local ship-making industry. Secondary interior dividing walls were made of light timber-woven gages coated with a lime-based mortar (mud-based mortar was used in poorer dwellings), usually reinforced with straw

or animal hair; this is also evident in ancient monuments, but its use is found throughout southern Europe and Asia. In construction of a traditional house these three structural forms were used selectively, combined in an overall structural system and expanded in space following well-defined rules depending on their weight, load-carrying capacity, and stiffness so as to optimize distribution of mass, stiffness and deformation compliance. Energy dissipation through internal friction is a characteristic mechanism for all three structural forms described (laced masonry, infilled timber frames and timber-woven walls), extending over a large range of deformation capacity prior to failure. This type of behavior to seismic loads is enhanced by the partial diaphragm action of the floor system, to a degree that depends on the robustness of its structure and the manner of its connection or attachment to the load bearing walls. In many of these buildings the roof timber truss is elastic and does not contribute by diaphragm action to the structure.

5.3 A Sample Structure Representative of the Building Population

In the framework of a comprehensive preservation strategy, a decisive step is the thorough identification of the internal force path implicit in the formation of the structural system: this is useful not only both for assessment of the deficiencies accumulated by deterioration due to ageing and systemic inadequacies, but also for evaluation of the effectiveness of alternative options for intervention and restoration. Here, simulation through Finite Element modeling may enable insightful interpretation of the global building workings and load transfer. (The relevance of this type of analysis may be diminished at a local level owing to the inherent uncertainties with regards the accuracy of modeling of member-to-member interaction, connectivity between structural components, and the actual mechanical properties of the constituent materials and material phases.)

Computer-aided modeling for seismic assessment of a typical historical structural system used in construction of urban residences up to the early 1900's is used in the present chapter as a tool in order to gain understanding into the structural function of three different traditional building structures taken from the core of the old-town of Xanthi in Thrace, N.E. Greece. There is a particular interest in verification of the potential utility of computer modeling in all phases of engineered preservation technologies of such structures, including assessment, restoration, rehabilitation and reuse, by enabling improved understanding of the structural function of the system of construction, but also in guiding the retrofit strategy through informed targeting of the retrofit objectives. By definition, when referring to preservation and restoration of structures that convey a historical value for the community, a certain type of compromise must be negotiated between the need to preserve the structure as a surviving heritage exhibit, and the need to secure the safety of its inhabitants against loss of life or property in the event of a significant earthquake.

After assembling an extensive database that record the local characteristics of the TURM-TL building population of the city of Xanthi (Papadopoulos 2013), a representative sample with geometric and construction characteristics that correspond qualitatively to the median of the values and details of the database was developed to be used as an object of study of the available assessment procedures in this class of buildings (Fig. 5.3). The building consists of timber-laced stone masonry with lacing at regular intervals throughout the exterior walls of the lower floor and the northern side of the second floor (Fig. 5.3(d)). It is a typical middle-class traditional house with a

morphology that combines the typical masonry-trade characteristics and the neoclassical elements that were often included due to the European influences imported by the local tobacco merchants. The south side of the buildings usually consists of a timber-laced frame that is set out (protrudes) in the corner relative to the supporting masonry walls of the first floor in a so-called “bay-window” or “erker” or “sahneshi” formation (for example, Fig. 5.2b). The way the protruding part of the structure is supported is as follows: a horizontal beam running parallel to the first-floor exterior masonry wall is supported on diagonal timber braces defines the lower end of the bay. The diagonal braces are fixed in one of the horizontal laces of the lower floor masonry wall; first storey floor beams supported on the exterior masonry wall extend outwards up to the end of the bay and are supported on the perimeter beam described above. The timber-laced infilled frame walls of the protrusion are supported on the perimeter beam and floor. Interior divisions both in the first and second floors comprise timber infilled frames which are integrally functioning with the overall structure to secure its characteristic resilient earthquake behavior.

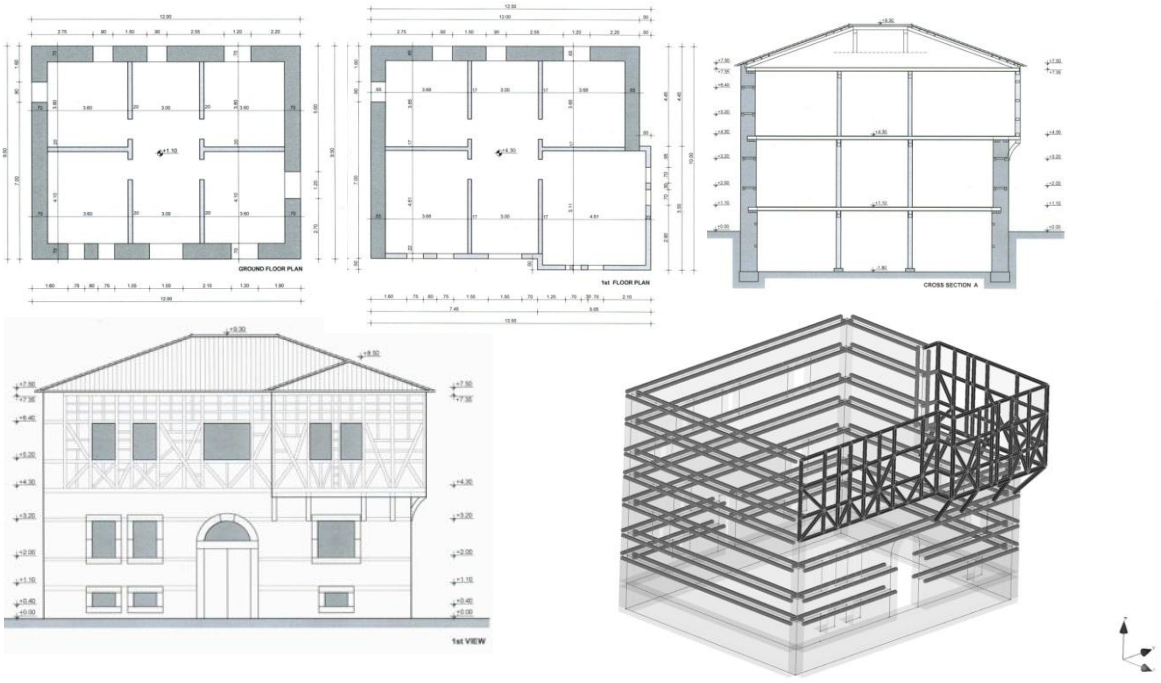

Figure 5.3: Representative sample building from the historical city core of Xanthi. (a) Plan view of first floor, (b) Plan view of upper floor, (c) Building cross section, (d) Front view, (e) Arrangement of timber laces

To evaluate the anticipated seismic response of the structure a 3-d finite element model was assembled for linear elastic analysis (Fig. 5.4); shell elements were used to model the perimeter walls including the upper-floor south-east facing bay. Interior walls were not considered for simplicity (as recommended by EC8-III, secondary elements may be neglected in the model). Beam elements were used to model the timber-laced frame, connecting nodes of the underlying shell mesh in a manner that mimicked the geometry of the frame (Fig. 5.3(d)). Type-I earthquake spectrum as prescribed in EC8-I was used to represent the seismic hazard, with a pga of a_g = 0.16g (coord. to the left) which is the design acceleration level for the greater region according to the Hellenic Nat. Annex to EC8-I.

5.3.1 Properties of the Model Structure

The building has an orthogonal plan arrangement, 8.8m × 11.3 m in the x, y-directions. The foundation comprises 0.85 m thick walls extending 0.5m below grade in the basement which is a -1.8m from street level; perimeter walls are 0.75m thick, timber laced with embedded timber laces about 0.1m thick, extending over the entire perimeter and spaced at 0.8m height-wise. Interior divisions are infilled timber frames of about 0.2m thickness. Basement height is 2.9 m (clear height is 2.72m). The first floor is raised at +1.1m from street level, having a total height of 3.2m (clear height of 3.02m), whereas the floor diaphragm thickness (comprising beams and floor planks) is 0.18m. The upper floor at +4.3m from ground level has a total height of 3.0m (clear height of 2.82m, and a floor thickness of 0.18m. Perimeter masonry walls are 0.65m thick, timber laced over the entire perimeter spaced at 0.8m in height. Interior divisions are infilled timber frames -0.17 m thick, whereas the southern and eastern exterior timber-frames including the range over the bay are 0.22m thick. The timber roof is at +9.30m, comprising timber trusses, roof cover and byzantine-type roof tiles. The compressive strength of the stone masonry walls is taken equal to f_w=3.0 MPa, and the assumed effective modulus (50% reduced from the nominal elastic value to account for cracking) is, E_{eff} = 1500MPa. Effective cracking strength of the masonry, f_{tw}, is taken about a tenth of f_w (=0.3MPa). Specific weight of the masonry walls is taken 22 kN/m^3, whereas timber used throughout the structure is classified as C14 (specific weight of 5.5 kN/m^3).

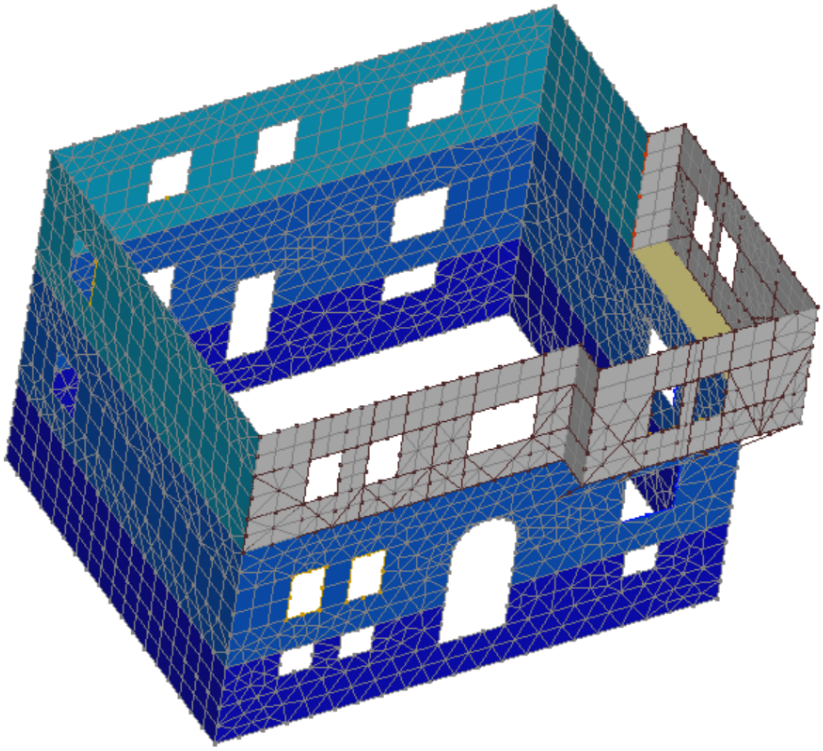

Figure 5.4: Finite Element Idealization of the TURM-TL Model Structure

5.4 Seismic Assessment of TURM-TL Buildings Through Modeling

According with EC8-III which sets the framework for assessment and retrofit of all type of existing structures, the various alternative methods which have been proposed in order to estimate demand for conventional reinforced concrete buildings, theoretically are also applicable to also apply to URM

buildings including the traditional types. Thus, (a) the simple equivalent single degree of freedom representation where demand is obtained directly from the spectrum (see appendix B in EC8-I), (b) the linear lateral force analysis procedure (static), (c) the modal response spectrum analysis (linear, with CQC or SRSS type modal response combination), (d) the non-linear static (pushover) analysis and (e) the non-linear time history dynamic analysis are all considered applicable in this domain.

It is relevant to underline at this point the significant differences between frame structures for which the above methods have been extensively proof-tested and URM structures: the former are marked by lumped masses at the floor levels (discrete system), whereas the latter have distributed mass throughout the structure (distributed or continuous system). By default this difference raises the level of difficulty in required modeling of URM as compared with RC structures even while in the elastic range of response (shell elements in a spatial mesh are needed), whereas all points of contact between different materials should be represented with nonlinear gap/spring elements in order to reflect the localized compliance. The result is that the level of confidence in the results is disproportionately lower than the effort required in conducting the analysis particularly with (d) and (e). Furthermore, with regards to option (c) which leads to combination of modal maxima in order to estimate "design" values, it is also relevant to note that contrary to what is seen in lumped systems, where the fundamental mode is usually the translational mode, engaging very large fractions of mass participation (over 75%), several tens to hundreds of modes need be considered when applying the same procedures in distributed systems such as URM structures before a tolerable amount of mass may be excited (less than 65%), whereas it is very difficult to identify the fundamental translational mode from among the multitude of modes estimated, which can be relating to the vibration of a subordinate component (such as a spandrel or an intermediate wall, see Fig. 5.5). In this light both the CQC and SRSS approaches yield excessively conservative values the irrelevance of which can lead to excessive interventions if used as benchmark for acceptance criteria, since no building would actually be able to sustain the levels of the iconic demands thus estimated (Fig. 5.5d, Table 5.1); most remarkable is that the estimated values for the displacements exceed by a factor of 2 the value associated with the estimated translational period of the structure, corresponding to the displacement value that would be developed by a structure with a period of at least 1 sec.

5.5 Assessment Response Indices

Systematic seismic assessment and upgrading of traditional masonry buildings to levels comparable with modern requirements for seismic resistance of residential structures requires analytical methods that will identify possible damage localization. Here, damage is identified by the amount of deformation occurring in the various components of the structure; in structural components deformation is measured by the relative displacement, or preferably, by the relative drift ratio between successive points of reference. Relative drift ratio (θ) is the displacement difference that occurs between successive points, normalized by their distance; being a non-dimensional parameter it may be used in direct comparison to material deformation capacity at milestone points of response (cracking, rupture, collapse) both in plan and height-wise.

TURM buildings typically have flexible diaphragms and as such, are particularly vulnerable to out of plane bending of walls oriented orthogonal to the earthquake action. For this problem,

relative drift in plan - θ_{plan}, refers to the relative displacement of the point with peak outwards deflection as compared to the wall corner. Similarly, *relative drift* (in height) measures the rotation of the structure at the point of peak lateral response from the vertical axis: θ_v is defined by the ratio of relative displacement occurring between two reference points located at different heights (z_1 and z_2) on the same vertical line, divided by their distance, (z_1-z_2). θ_v is owing primarily to the shear distortion of walls oriented parallel to the ground motion, (θ_{sh}), as well as to the out of plane flexural action of walls oriented in the orthogonal direction (θ_{fl}). All these assessment parameters are geometric quantities. The magnitude and localization of these during seismic response, at least the peak values which are of interest in practical design, are implicitly contained in the normalized deflected shape that the structure assumes at peak displacement under the design earthquake.

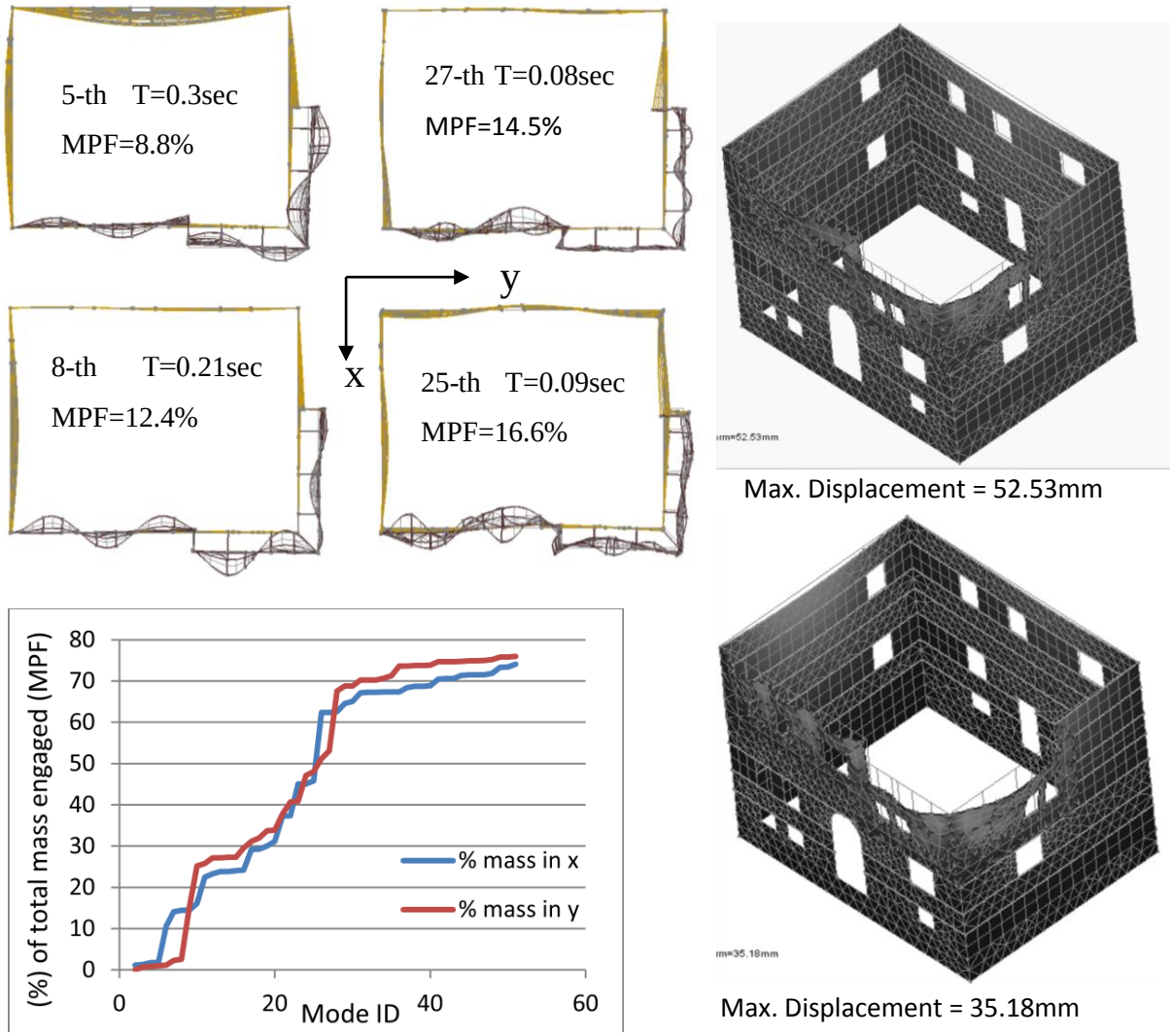

Figure 5.5: (a)-(d) Plan view of various modes and corresponding mass participation factors (MPF). (e), (f) Displacement values estimated from modal CQC for combined gravity loads and Earthquake action along x and y. (g) Percent of total mass engaged in vibration as a function of the total number of modes considered.

5.6 Essential Elements of a Seismic Assessment Method for TURM-TL Buildings

In the context of an equivalent single degree of freedom formulation (ESDOF) used routinely according to design and assessment codes (EC8-I, EC8-II, 2005) for estimating dynamic response, the generalized properties of the structure are obtained with reference to the shape of the fundamental mode of lateral translation; thus, if $\Phi(x,z)$ is the normalized deflected shape of a structure undergoing a ground motion in the y-direction, then the peak displacements at any point in the structure may be calculated from the product of the spectral displacement of the ESDOF, times the coordinate of the fundamental mode shape at the point considered, as $u(x,z)=\Phi(x,z)S_d(T)$, where T is the associated period of the structure when it vibrates free in the mode $\Phi(x,z)$ (obtained from generalized properties based on standard procedures, Clough and Penzien 1993).

Several analytical alternatives have been proposed for estimating the translational mode shape, $\Phi(x,z)$, the complexity of which is beyond the scope of the structures considered in the present chapter (see for example the work by Vamvatsikos and Pantazopoulou 2010, summarized in Chapter 4 of this report). A universal procedure opted for by most engineers is to conduct a computer analysis using a finite element idealization of the structure and classical numerical calculation of eigenvalues / eigenvectors. This approach is fraught with the difficulties detailed earlier in this section. Furthermore, because of the great uncertainty regarding the material properties and the degree of restraint provided at connections between different materials, results obtained ought to be considered primarily in a qualitative light. As a rule of thumb, assessment of TURM structures should be conducted on seismic response demand indices that are relatively insensitive to the accuracy of the estimation of period and damping, and should secure some conservatism in the process. Considerations adopted in the present study are as follows:

- (a) Because TURM buildings rarely exceed 7-8 m in height, typically having flexible diaphragms and roof beams, they usually belong in the plateau range of the acceleration spectrum (i.e. their fundamental translational period does not exceed 0.4-0.5 sec) – a finding that is confirmed by detailed finite element studies. Thus, for the needs of practical assessment, demand for the entire class of these buildings is linked to the values at the end of the plateau region of the design spectrum (i.e., assuming $T=T_C$, where, Type I spectrum of EC8 is considered for representation of the seismic hazard with a_g=0.16g and S=1.0 for the location). Thus, assessment is performed for the following set of response values assumed to occur at the top of the building when it is considered to vibrate in lateral translation in the event of the design earthquake:

$$T_B \le T \le T_C : \quad S_e = a_g \cdot S \cdot \eta \cdot \beta_o / q \qquad (5.1a)$$

$$S_d(T) = a_g \cdot S \cdot \eta \cdot \beta_o \cdot \frac{T_C^2}{4\pi^2} \cdot \left(\frac{\mu}{q}\right) \approx 0.025 a_g \cdot \beta_o \cdot S \cdot \eta \cdot T_C^2 \cdot \left(\frac{q^2+1}{2q}\right) \qquad (5.1b)$$

For T_C=0.5sec, β_o=2.5 and damping ratio ξ=5% ($\eta=\sqrt{10/(5+100\xi)}$ =1 for ξ=5%) the above set of expressions yield $S_e=0.4g=3.9m/s^2$, $S_d=0.025m$.

- (b) In conventional modal analysis, S_e and S_d calculated in the preceding need be multiplied by the coefficient of excitation of the structural system considered (term Γ, see EC8-I 2004, Appendix B), the

value of which depends on the shape of lateral translation assumed for the generalized ESDOF system; whereas for lumped systems this may be in the range of 1.2-1.3, in distributed systems this may well exceed that value of 2 depending on the assumed mode shape.

- (c) For a distributed mass / distributed stiffness system, it was stated that most computer analysis programs produce a multitude of eigenvectors each engaging a small or even insignificant fraction of the total mass in dynamic excitation. To overcome this difficulty, the shape of the fundamental translational vibration, *Φ(x,z)* or *Φ(y,z)* may be best estimated from a pushover analysis rather than from the solution of the eigen-analysis; according with Clough and Penzien (1993), in estimating the fundamental translational mode of free vibration it is noted that the displacements result from the application of the inertia forces acting on mass, which in turn are proportional to the distributed mass and the associated accelerations, which are obtained as the second time derivative of displacement.

Thus, the fundamental translational shape *Φ(x,z)* (or *Φ(y,z)*) is the displacement profile resulting from the application of a static load *p(x,z)* (or *p(y,z)*), proportional to *m(x,z)*Φ(x,z)* (or *m(y,z)*Φ(y,z)*, respectively). If the perimeter wall thickness is approximately constant, the distributed mass is proportional to the weight of the walls per unit area of wall surface. Results of sufficient accuracy, according with the iterative procedure of Rayleigh, will be obtained even if the applied distributed load is not exactly proportional to the exact mode. A common approach is to calculate the lateral deflection *u(x,z)* (or *v(y,z)*) for the structural system when it is loaded by its self-weight acting in the horizontal direction (as a first approximation); if a more refined result is sought, then the applied load could be the self-weight multiplied by the height coordinate *z/H* (where *H* the height of the structure).

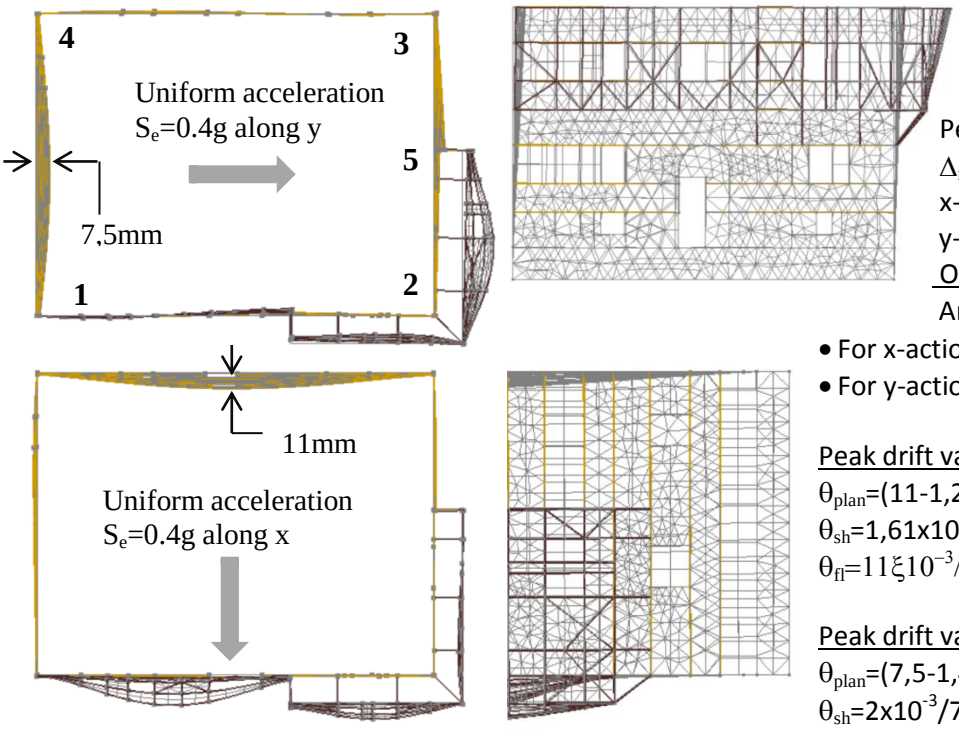

Peak roof displacements, $\Delta_{max:}$ For action along:
x-dir: 22,07mm
y-dir: 17,65mm

Optional Safety factor:
Amplify results by S_d/Δ_{max}

- For x-action: 0,025/0,022 = 1,13
- For y-action: 0,025/0,0176 = 1,4

Peak drift values: Action in x:
θ_{plan}=(11-1,28)x10^{-3}/(11.3/2)=**0.17%**
θ_{sh}=1,61x10^{-3}/7,5=0,02%
θ_{fl}=11ξ10^{-3}/7,5=**0,14%**

Peak drift values: Action in y:
θ_{plan}=(7,5-1,46)x10^{-3}/(8,8/2)=0.13%
θ_{sh}=2x10^{-3}/7,5=**0,026%**
θ_{fl}=7,5x10^{-3}/7,5=0,1%

Figure 5.6: Deformed structure under uniform acceler. according to the proposed method. Critical is action in x

The fundamental mode of translational vibration is then estimated by normalizing the displacement profile with respect the maximum displacement coordinate in the direction of interest (i.e., $\Phi(x,z)=u(x,z)/u_{max}$). It is interesting to note that when using this particular shape for calculating the response, pass participation is very high (above 90%) whereas the coefficient Γ converges to 1 in this case.

The results of the procedure outlined in the preceding are illustrated in Fig. 5.5, which depicts the deformed shape of the structure when loaded with mass proportional loads in the *x* and *y* directions, respectively, and corresponding lateral displacement profile, for definition of the θ_{plan} and θ_v distributions for the estimated S_d value (*22.03 mm* at the most displaced point of the crest).

Evidently the procedure described provides a much more transparent picture of the state of the structure and identifies easily the tendency for localization of deformation (points of anticipated damage) for the purposes of assessment, whereas avoiding the implications of overestimation of demands caused by superposition of modal maxima. To illustrate this point, results obtained for displacements and moments from the two approaches, i.e. (complete quadratic combination of modal maxima, and the static procedure proposed) are listed in the following table for the vertical lines at the corners of the building's plan, *1, 2, 3, 4, 5,* identified in Fig. 5.6(a). Cells in bold identify points where the values of the moments are large and at the same time, critically different between the two methods. Note that the values of cracking moments (per unit width of wall strip) for the masonry walls range between the values of *7 kN-m/m* in the upper floor to *16 kN-m/m* at the base. Thus, cracking will evidently occur, and if q the ratio of peak moment to the above cracking strength values, estimated here in the range of *q=3* for motion in the x-direction, it follows that the peak elastic drift values estimated in the note of Fig. 5.6 should be multiplied by a factor of $(3^2+1)/(2\cdot3)=1,67$ (see Eq. 5.1(b)), thus, the corresponding peak drift values (for motion in the x-direction) are, $\theta_{plan}=0.17\%\cdot1,67 = 0,29\%$, $\theta_{sh}=0,02\%\cdot1,67=0,035\%$ and $\theta_{fl}=0,14\%\cdot1,67=0,24\%$.

5.7 Acceptance Criteria in terms of Deformation - Concluding Remarks

Deformation measures calculated above can be used to determine the performance level (characterization of damage level) attained by the structure in response to the design earthquake. Considering that cracking rotations (drift ratios) in masonry elements are in the order of *0.15%*, the above values for drift demands correspond to ductility levels of two in the masonry walls ($2\approx0.29\%/0.15\%$) – this demand level in within the ductility capacity of the timber laced masonry wall, illustrating the resilience and favourable earthquake response prescribed by the timber-laced mode of construction of these traditional buildings. The level of demand is much higher locally in the bay region, however, this part of the structure is particularly ductile and resilient due to the timber connections.

The procedure described for assessment of TURM-TL structures is a displacement-based method that eliminates the over-conservatism of combination of modal maxima, enabling identification and quantification of the locations of potential damage in this class of historical structures. Note that through the F.E. evaluation of the alternative types of analysis it was demonstrated that applying a uniform field of accelerations in the direction of the ground motion yields dependable estimations for the shape of lateral deformations – much more so than the modal

superposition approaches, which, owing to the close spacing of several modes in this class of continuous systems, results in excessively conservative estimations.

Table 5.1: Summary of calculated results from the two methods: *G+E$_x$* represents values from static analysis for gravity loads and uniform lateral acceleration equal to the value at Spectral Plateau. Modal superposition represents the result of CQC on modal maxima.

			G+E$_x$ / Modal Superposition				G+E$_y$ / Modal Superposition			
edge	z (m)	node	u (mm)	v (mm)	M$_x$ (kNm/m)	M$_y$ (kNm/m)	u (mm)	v (mm)	M$_x$ (kNm/m)	M$_y$ (kNm/m)
1	7.5	157	1,19/0,7	-0,33/1.4	0,13/0,82	0,94/4,26	0,03/0,53	2,0/2,44	-0,07/1,3	-0,13/6,72
	5.8	108	1,03/0,5	-0,19/0,76	0,08/0,15	0,35/0.64	0,04/0,4	1,42/1,38	-0,03/0,13	-0,13/0,54
	4.3	107	0,87/0,44	-0,12/0,39	22,6/22,7	2,33/9,67	0,01/0,31	1,0/0,75	-37,7/44,4	-12,94/18,4
	2.6	99	0,62/0,3	-0,04/0,2	11,77/10,3	2,6/2,3	0/0,2	0,66/0,41	-16,4/16,5	-1,97/3,78
	1.1	59	0,36/0,16	-0,01/0,09	3,9/3,63	1,74/1,5	0/0,11	0,33/0,18	-5,85/5,25	-0,66/1,62
	0	385	0/0,06	0/0,03	-2,26/1,76	0,02/1,55	0/0,04	0,11/0,05	-1,18/1,87	-4,33/3,14
2	4.3	166	0,86/0,36	0,21/0,23	-0,03/0,67	0,02/0,4	0/0,3	0,82/0,49	0,06/0,68	0,04/0,34
	2.6	539	0,60/0,23	0,11/0,16	-1,45/0,97	-0,3/3,86	0/0,18	0,59/0,33	-0,13/1,18	1,12/4,1
	1.1	50	0,34/0,12	0,05/0,08	0,55/2,33	0,56/0,57	0,01/0,09	0,32/0,16	1,94/2,34	-0,63/0,84
	0	387	0/0,05	0/0,03	-2,85/1,5	0,21/0,5	0/0,04	0,12/0,06	-1,11/1,75	1,09/0,96
3	7.5	154	1,61/0,89	-0,21/0,62	33,5/38,87	1,7/4,66	-0,28/0,63	1,45/0,81	-20,8/26,23	-0,9/3,28
	5.8	886	1,31/0,64	-0,18/0,48	32,7/27,26	6,17/5,3	-0,19/0,45	1,27/0,66	-15,95/16,5	-2,17/3,44
	4.3	116	1,0/0,44	-0,13/0,38	**33,43/24,2**	7,32/5,4	-0,11/0,32	1,08/0,54	-14,80/13,5	-4,0/3,32
	2.6	858	0,65/0,26	-0,08/0,25	-20,7/14,7	-4,06/2,2	-0,05/0,19	0,78/0,37	9,08/9	0,40/1,95
	1.1	47	0,34/0,12	-0,04/0,13	7,4/5,67	2,39/1,94	-0,02/01,0	0,42/0,2	-3,33/4,02	-2,13/1,44
	0	388	0/0,05	0/0,05	-1,38/2,6	1,57/1,46	-0,01/0,04	0,15/0,07	0,17/1,97	-0,15/0,96
4	7.5	147	1,28/0,74	0,02/0,52	31,65/33,13	3,29/4,8	0,13/0,51	1,46/0,87	**25,95/52,7**	1,55/5,25
	5.8	29	1,12/0,6	0,02/0,44	25,87/20,7	5,16/4,2	0,12/0,43	1,27/0,71	**21,21/34,4**	3,41/7,06
	4.3	109	0,93/0,46	0,01/0,36	-27,15/19	-5,83/4,24	0,07/0,33	0,89/0,57	**-15,21/31,0**	-2,37/4,93
	2.6	876	0,64/0,3	0,01/0,25	-14,81/10	-2,72/1,73	0,06/0,21	0,76/0,37	-11,72/14,2	-0,78/2,88
	1.1	40	0,32/0,14	0,0/0,13	-5,76/4	-2,22/1,59	0,03/0,1	0,42/0,19	-5,69/5,91	-1,36/1,58
	0	389	0/0,05	0/0,05	-1,68/1,97	-2,25/1,1	0,01/0,04	0,16/0,07	-1,16/2,23	1,64/1,03
5	7.5	158	1,57/0,84	1,19/8,26	0/0	0/0	-0,27/0,6	6,09/6,7	0/0	0/0
	5.8	326	1,26/0,61	0,53/5,65	0,44/1,0	0,17/6,83	-0,17/0,44	4,64/4,5	-0,52/0,61	4,84/5,2
	4.3	121	0,86/0,36	0,03/3,34	**-33,4/76,3**	**-34,5/52,9**	0/0,3	3,11/2,6	**40,27/46,7**	**-24,4/47,26**
	2.6	1262	0,60/0,24	-0,02/1,70	3,98/12,71	1,7/11,87	-0,02/0,18	1,87/1,4	-8,34/8,4	-2,46/10,84
	1.1	1190	0,32/0,12	-0,02/0,7	1,38/3,14	-0,34/8,56	0/0,09	0,88/0,6	-1,76/2,24	3,32/6,7
	0	1165	0/0,05	0/0,19	0.46/1,51	-0.25/13,8	0/0,04	0,26/0,17	2,17/1,47	15,28/11,6

It is important to recall that conservatism in the context of historical constructions is not necessarily a desirable attribute: here it is sought to rehabilitate the structure using non-invasive, reversible interventions. Thus, overestimating the demands can be catastrophic for the monument as it will invariably lead to over-strengthening and, inevitably, to the use of excessively invasive measures.

The chapter also shows that it is indeed possible, using simple analytical approaches, to estimate the seismic resistance of URM structures despite the complexity these structures present to conventional analysis due to the continuity and spatial development of the load bearing parts of the structure.

REFERENCES

ACORD-CP http://www.itech-soft.com/en/acordCP/acordCP.htm

Bothara J, Dhakal R., and J. Mander, (2010). "Seismic performance of an unreinforced masonry building: An experimental Investigation", Earthquake Engrg. Struct. Dyn., **39**:45-68.

Çaktı E., Oliveira C., Lemos J., Saygılı Ö., Görk S., and Zengin E. (2013). "Earthquake Behavior of Historical Minarets in Istanbul", CDROM Proceedings, COMPDYN 2013, (Eds: Papadrakakis, Papadopoulos and Plevris), Kos Island, Greece, 12-14 June.

Ceci A.M., Contento A., Fanale L., Galeota D., Gattulli V., Lepidi M., Potenza F. (2010). "Structural performance of the historic and modern buildings of the University of L'Aquila during the seismic events of April 2009", Engineering Structures, DOI: 10.1016/j.engstruct.2009.12.023.

CEN. EN 1998-1 Eurocode 8: Design of Structures for Earthquake Resistance - Part 1: General Rules, Seismic Actions and Rules for Buildings, European Committee for Standardization, Brussels, 2004.

CEN. EN 1996-1-1 Eurocode 6: Design of Masonry Structures - Part 1-1: General Rules for Reinforced and Unreinforced Masonry Structures, European Committee for Standardization, Brussels, 2005.

CEN. EN 1998-3 Eurocode 8: Design of Structures for Earthquake Resistance - Part 3: Assessment and retrofitting of Buildings, European Committee for Standardization, Brussels, 2005

FEMA 310. 1998. *Handbook for Seismic Evaluation of Buildings*. Federal Emergency Management Agency, American Society of Civil Engineers (ed.).

Chopra AK. *Dynamics of Structures: Theory and Applications to Earthquake Engineering*. Prentice-Hall: Englewood Cliffs, NJ, 1995.

Clough RW, Penzien J. *Dynamics of Structures.* Mc Graw Hill: New York, 1975.

Cornell CA, Krawinkler H. Progress and challenges in seismic performance assessment, *PEER Center News* 2000; **3**(2). URL http://peer.berkeley.edu/news/2000spring/index.html, [Oct 2009].

D'Ayala D, Spence R, Oliveira C, Pomonis A. Earthquake Loss Estimation for Europe's Historic Town Centres. *Earthquake Spectra* 1997; **14**(4):773–793.

D'Ayala D, Speranza E. Definition of collapse mechanisms and seismic vulnerability of historic masonry buildings. *Earthquake Spectra* 2003; **19**(3):479–509.

Elnashai, A. 2001. Advanced inelastic (static) pushover analysis for earthquake applications. *Structural Engineering and Mechanics*, Technopress, Korea, **12**(1):51-69

Gülkan P., Sozen M.A. 1999. Procedure for determining seismic vulnerability of building structures. *ACI Structural Journal* 96(3): 336-342.

Günay S. and Mosalam K., (2010). "Structural Engineering Reconnaissance of the April 6, 2009, Abruzzo, Italy, Earthquake, and Lessons Learned", *PEER 2010/105*, April 2010, 62pp.

International Charter for the Conservation and Restoration of Monuments and Sites, Decisions and Resolutions, Document 1, *II. International Congress of the Architects and Technicians of Historic Monuments*, Venice, 1964. (http://www.international.icomos.org/e_charte.htm)

ITSAK, *Institute of Technical Seismology and Earthquake Resistant Structures*, Thessaloniki, Greece.

Karantoni F.V., M.N. Fardis, (1992) "Computed versus observed seismic response and damage of masonry buildings". ASCE Journal of Structural Engineering 118:7, 1804-1821.

Karantoni F.V., M. Papadopoulos and S. Pantazopoulou, *Criteria Guiding Seismic Assessment Strategies of Traditional Masonry Buildings*, Second Conference on Smart Monitoring, Assessment and Rehabilitation of Civil Structures (2SMAR), Istanbul, 2013.

Kontari Th. M., *Seismic Assessment of Neoclassical Buildings through Computer Simulation*, MASc thesis, Depart. Of Civil Engineering Demokritus University of Thrace, Xanthi, Greece, 2011 (*in greek*).

Lagomarsino S, Penna A, Galasco A, Cattari S. TREMURI program: Seismic Analyses of 3D Masonry Buildings, Release 2.0, University of Genoa, Italy; 2012 [mailto: tremuri@gmail.com].

Lagomarsino S., A. Penna, A. Galasco, S. Cattari, (2013). "TREMURI program: An equivalent frame model for the nonlinear seismic analysis of masonry buildings", Engineering Structures **56**(2013):1787–1799, Elsevier.

Langenbach R (2002), "Survivors in the midst of devastation, Traditional Timber and Masonry Construction in Seismic Areas", *Conference Proceedings, 7th US National Conference on Earthquake Engineering,* Boston, Massachusetts, July 21-25.

Lemos J.V. (1998). Discrete element modeling of the seismic behaviour of stone masonry arches. In: G. N. Pande, J. Middleton, B. Kralj (eds.) *Proc. of the Fourth International Symposium on Computer Methods in Structural Masonry*. London.

Lourenço, P. B., 2001. Analysis of historical constructions: From thrust-lines to advanced simulations. *Historical Constructions,* pp. 91-116.

Lourenço, P. J. B. B., 1996. *Computational strategies for masonry structures.* PhD Thesis: Delft University Press.

Lourenco, P. B., Milani, G., Tralli, A., and Zucchini, A., (2007). "Analysis of masonry structures: review of and recent trends in homogenization techniques, Can. J. of Civil Engineering, **34**:1443-1457.

Lourenço, P. J. B. B., 2011. *SAHC SA2 Document - A note on other non-linear material models.* Universidade do Minho - Guimaraes, s.n.

National Service for Management of Earthquake Damages in Northern Greece (Υ.Α.Σ.Β.Ε.), *Restoration of the damages caused to the General Hellenic Consulate due to earthquake,* Ministry of public works, Thessaloniki, Greece, 1979.

Papadopoulos M.L., S. J. Pantazopoulou (2011). Simulation for Seismic Assessment of Traditional Houses in the Historical Core of the City of Xanthi before and after Non-Invasive Structural Interventions, *CD-ROM Proceedings* of the III ECCOMAS Thematic Conference on Computational Methods in Structural Dynamics and Earthquake Engineering, Corfu, Greece, 26–28 May 2011, M. Papadrakakis, M. Fragiadakis, V. Plevris (eds.)

Papadopoulos, M., "Seismic Assessment of Traditional Houses in the Balkans – Case Studies in Xanthi", *J. of Civil Engineering and Science*, (in print), http://www.ij-ces.org/, 2013.

Papadopoulos M., H. Cotta, T. Gounaridou, *The history of the school of the "Hellenic high school"of Thessaloniki*, Municipality of Thessaloniki, Thessaloniki, Greece, 2001 (in Greek).

Paraskeva, Th. and A. J. Kappos. 2010. Further development of a multimodal pushover analysis procedure for seismic assessment of bridges. *Earthquake Engineering and Structural Dynamics*, **39**(2): 211–222, J. Wiley & Sons, USA.

Pardalopoulos S.J., M. Th. Kontari, S. J. Pantazopoulou, (2013). Analytical Procedure for Seismic Assessment of Masonry Buildings With Historical Value, Proceedings, COMPDYN 2013, 4th ECCOMAS Thematic Conference on Computational Methods in Structural Dynamics and Earthquake Engineering, M. Papadrakakis, N.D.Lagaros, V. Plevris (eds.), Kos Island, Greece, 12–14 June 2013

Pardalopoulos S.J., S. J. Pantazopoulou, *Seismic Assessment of 19th Century Heritage building Through Simulation*, COMPDYN 2011 – Computational Methods in Structural Dynamics and Earthquake Engineering, M. Papadrakakis, M. Fragiadakis, V. Plevris (eds.), Corfu, 2011.

Pardalopoulos, S. J. Pantazopoulou, *Spatial Displacement Patterns of R.C. Buildings Under Seismic Loads*, Computational Methods in Earthquake Engineering, Computational Methods in Applied Sciences 21, M. Papadrakakis et al., Springer, pp. 123-145, 2011.

Pardalopoulos S.J., *Seismic Design of Natural Gas Pipeline Networks Attached in Existing and New Constructions*, PhD Thesis, Demokritus University of Thrace, Xanthi, Greece, 2012.

Royal Decree - 10/31-12-1945. On the Design Loads of Structural Works, (in Greek).

Roca, P., Cervera, M., Gariup, G. & Pelà, L., 2010. Structural Analysis of Masonry Historical Constructions. Classical and Advanced Approaches. *Arch Comput Methods Eng,* **17:** p. 299–325.

SAP2000, Computers and Structures, Inc., University Avenue, Berkeley, California 94704, USA.

Simsir CC, Aschheim MA, Abrams DP. Out-of-plane dynamic response of unreinforced masonry bearing walls attached to flexible diaphragms. *Proceedings of the 13th World Conference on Earthquake Engineering*, Vancouver, B.C., 2004, Paper No. 2045.

Scheibmeir, E. (2012). Nonlinear Seismic Analysis of a Masonry Arch Bridge. MSc Thesis, Universitat Politècnica de Catalunya, July, Erasmus Mundus Programme.

STADATA. 3Muri Program, Release 5.0.4; 2012 [www.3muri.com].

Tanrikulu AK, Mengi Y, McNiven HD. The nonlinear response of unreinforced masonry buildings to earthquake excitation. *Earthquake Engineering and Structural Dynamics* 1992; **21**(11):965–985.

Tastani S, Papadopoulos M, Pantazopoulou S. Seismic response of traditional masonry buildings: parametric study and evaluation. *Proceedings of the 1st International Conference on Protection of Historical Buildings,* Rome, Italy, 2009.

Timoshenko S, Woinowsky-Krieger S. *Theory of Plates and Shells.* McGraw-Hill: New York, 1987.

Tassios T.P. and Vassilopoulou I. 2002. Shear transfer capacity along a r.c. crack, under cyclic loading. *Rolf Eligehausen zum 60. Geburtstag, Befestigungstechnik Bewehrungstechnik und*.

Tastani S.P., Pantazopoulou S.J. 2008. Detailing procedures for seismic rehabilitation of reinforced concrete members with fiber reinforced polymers. *Elsevier Engineering Structures* 30:450–461.

Thermou G.E., S. J. Pantazopoulou, A. S. Elnashai, *Global Interventions for Seismic Upgrading of Substandard RC Buildings*, ASCE Journal of Structural Engineering, ASCE, 138(3): pp. 387-401, 2012.

Thermou G.E., S. J. Pantazopoulou, *Assessment Indices for the Seismic Vulnerability of Existing R.C. Buildings*, Earthquake engineering and Structural Dynamics, DOI: 10.1002/eqe.1028, Wiley InterScience, 2010.

TNO DIANA BV, 2010. DIANA – User's Manual, Delft: s.n.

Tomazevic Miha. 2006. Series on Innovation in structures and construction, Vol. 1:Earthquake-resistant design of masonry buildings, A.S. Elnashai and P.J. Dowling (eds.), Imperial College Press.

Vamvatsikos, D. and S. J. Pantazopoulou, “Simplified Vulnerability Assessment of Historical City Cores – the Example of the Old City of Xanthi”, *CD-ROM Proceedings*, 9th U.S. and 10th Canadian Conference on Earthquake Engineering, Toronto, Canada, July 2010.

Vintzileou E. The effect of timber ties on the behaviour of historic masonry. *ASCE Journal of Structural Engineering* 2008; **134**(6):961–972.

Vintzileou E., Zagkotsis A., Repapis C., Zeris Ch. 2007. Seismic behaviour of the historical structural system of the island of Lefkada, Greece. *Elsevier Construction and Building Materials* 21:225–236.

Vitruvius, On Architecture*,* pp.147-175 Vol. I, Books I-V, Athens, Plethron, 1996.

Wolfgang Müller-Wiener (1995), *Architecture in Ancient Greece, pp.*70-101, University Studio Press, Thessaloniki.

Zucchini, A. P. L., 2007. Mechanics of masonry in compression: Results from a homogenisation approach. *Computers and Structures,* Volume 85, p. 193–204.